DEVELOPMENT OF A LOW POWER ULTRASONIC DATA ACQUISITION AND IMAGING SYSTEM.

Presented by

YONAEL GORFU

In the fulfilment of the requirement
for the degree of
Doctor of Philosophy
of the University of Strathclyde.

Department of Electronic
and Electrical Engineering

June 1988 Glasgow

TABLE OF CONTENTS

CHAPTER 6

IMAGE FORMATION AND PROCESSING

CHAPTER 7

CONCLUSION

ABSTRACT

The theoretical and practical development of a low power ultrasonic data acquisition and imaging system designed for peak power limited applications is presented. The system drastically reduces transducer excitation levels used in conventional ultrasonic detection systems (from a few hundred volts to less than 5 volts) without sacrificing signal to noise ratio by utilising dual Golay code matched filtering. A new, entirely digital hardware approach is adopted in the implementation to achieve high processing speed, accuracy and versatility. A new, comprehensive theoretical appraisal of such a discrete time system is conducted and the hardware developed based on the concepts discussed is described together with experimental verification of its performance. A system that is free of most forms of coherent and non-coherent contaminating noise is shown to be practically feasible. Additionally, an implementation technique for combining both signal to noise ratio and resolution enhancement is proposed and experimentally verified.

Practical, array based imaging and image processing strategies are developed. Finally, real images of various weakly reflecting targets are presented to demonstrate the performance of the entire low power imaging unit. It is believed that this comprehensive and practical demonstration of a low power and high signal to noise ratio ultrasonic imaging system will help to significantly widen the application areas of ultrasonic testing.

CHAPTER 1

CHAPTER 1

INTRODUCTION

1.1 BACKGROUND

The use of ultrasonic testing methods has now progressed to such a stage that good quality cross sectional images of hidden defects or body organs may be obtained. Piezoelectric devices used for the transmission and reception of ultrasound have been accurately modelled [31,32] resulting in improved, simulation study based system design. Various signal processing and hardware design strategies are also being investigated to tackle outstanding problems which still prevent a wider utilisation of ultrasonic testing (for example, see [13,24,36]).

One outstanding problem in ultrasonic detection is that associated with poor signal to noise ratio in the acquired data. This often arises as a result of the high attenuation of ultrasound in certain media, poor coupling between sensor and test specimen, limitations imposed in peak transmission power levels and the existence of various forms of coherent and non-coherent noise in receivers [13]. There are also problems with image resolution which is often determined by the temporal and spatial characteristics of the piezoelectric devices used for transmission and reception [36]. Other practical problems include the design and repeatable manufacture of transducer arrays for high frequency imaging applications

and probes with spatially invariant responses [32,36].

The present work developed as a result of a medical imaging project which necessitated investigation of ways of minimising peak transmission power while at the same time maintaining or improving signal to noise ratio. In searching for such techniques, it was observed that at present there is a lack of a self contained data acquisition and imaging strategy for use in all peak power limited applications where environmental conditions severely restrict system performance. The thesis covers the systematic development of an imaging system for such applications. This chapter introduces the fundamental concepts which relate to the core of the work and outlines the aims, contributions and organisation of the thesis.

Ultrasonic imaging

Ultrasonic imaging is now widely used for non-destructive evaluation of materials and mechanical structures as well as non-invasive medical diagnosis. The ultrasonic imaging technique which is of interest in the present investigation and which, in general, is most widely used falls in the general category of pulse-echo ranging. The basic process may be described as follows.

Firstly, a high amplitude voltage excitation function (usually in the order of a few hundred volts) is applied to a piezoelectric transducer. The device responds by emitting a short duration mechanical wave which propagates and is reflected by the target to be imaged.

The reflected signal is then reconverted to a voltage, often by the same transducer used for transmission. The time delay between the transmission and reception gives information of the distance of the object. This method of acquiring ultrasonic data is known as the 'pulse-echo' method and the echo data acquired over a period of time is conventionally referred to as the 'A-scan'. Now, if such pulse-echo data acquisition of A-scans is repeated from several known positions of the transducer, the time of flight delays from various points on the reflector to each transducer position will permit the exact location and sizing of the reflector, which may then be displayed in a suitable two dimensional format.

To avoid the need to mechanically manipulate (or scan) transducers, electronically scanned arrays have been developed. These essentially consist of several piezoelectric devices arranged in known geometrical configurations. They could be used in the mode mentioned above where each transmits and receives sequentially and the pulse-echo time of flight information of each is used to locate the reflector. Alternatively, their excitations could be suitably phased so that a combined mechanical wavefront that insonifies a particular angle or point in space is created (known as transmission steering and focussing). The steering and focussing may also be performed on reception by appropriately delaying and summing the received data.

The array configuration most widely used for imaging purposes is a linear one whereby several thin and tall piezoelectric transducers (referred to as the array elements) are aligned side by side on a heavy backing material. Arrays could also be constructed from a single piezoelectric ceramic by using appropriate electrode patterns to define the individual elements (known as monolithic arrays) [30].

Although such array based ultrasonic imaging is finding increasing application, some major hardware related problems still persist. These include the following.

(a) Many applications involve highly attenuating media making it imperative for imaging systems to utilise high transmission power intensity levels in order to get images with reasonable signal to noise ratios. Parallel to this there is often the conflicting requirement of minimising transmission power to intrinsically safe levels in applications such as biomedicine and non-destructive evaluation in explosive environments [1,3]. Hence, to widen the application areas, there is a need to devise practical low power ultrasonic data acquisition and imaging techniques.

(b) Even where there is no power limitation imposed by the application environment, the hardware associated with high voltage excitation is often bulky, complex and expensive. There is a need for simplified, versatile and cost

effective hardware.

(c) The performance of an imaging system also largely depends on the performance of the sensor array. For good image resolution, array elements should have uniform, short duration (broadband) responses. The construction of high frequency transducer arrays with such properties still remains difficult.

The points raised in (a) and (b) constitute the major problem areas addressed in this work.

Correlation and pulse compression

Another concept closely related to the core of the work and repeatedly raised throughout the thesis is correlation. Correlation is a mathematical operation commonly used to establish the degree of similarity between two signals. Or generally termed, it is a comparison process. In time domain, the correlation operation involves multiplication, time shifting (or delay) and integration. Mathematically, the correlation (cross correlation) of two periodic signals (functions of time) $f_1(t)$ and $f_2(t)$ may be expressed as follows.

$$f_{12}(\tau) = \lim_{T \to \infty} \frac{1}{T} \int_{-T/2}^{T/2} f_1(t).f_2(t+\tau)\, dt \qquad \ldots 1.1$$

Where, τ represents a time delay.

If the time scale and amplitude are quantised into discrete steps, the correlation operation may be re-expressed as,

$$f_{12}(n) = \sum_{k=-\infty}^{\infty} f_1(k).f_2(n+k) \qquad \ldots 1.2$$

Where, the indices k and n are the sampled versions of t and τ given in eqn. 1.1.

Thus, if the two functions f_1 and f_2 are identical the correlation operation would have a maximum at zero shift (n=0), as all overlapping samples would be identical.

If two identical wide bandwidth but long duration signals are cross correlated, the result would be a wide band but very short duration pulse, with the peak occurring at zero shift. Such derivation of a short duration pulse by correlating long duration waveforms is commonly referred to as pulse compression [17]. Pulse compression is used in radar and sonar to increase transmission energy and maintain resolution [17,12]. In such applications, the process involves the transmission of a wide band and long duration (hence high energy) signal and pulse compressing the returning signal by correlating it with a stored replica of the transmitted one. Such correlation based reception is also referred to as matched filtering.

An optimal adaptation of matched filtering techniques for practical ultrasonic applications also constitutes part of the present investigation.

1.2 AIMS AND CONTRIBUTIONS OF THESIS

The aim of the present work is the theoretical study and development of an optimised, low power ultrasonic data acquisition, processing and imaging system for application in peak power limited non-destructive evaluation and medical imaging. The main aims are summarised as follows.

(a) To select and devise a suitable, general technique for the construction of such a system.

(b) To establish a sufficient theoretical background for optimised, simulation based design.

(c) To develop and test a dedicated hardware for the purpose of low power, array based ultrasonic imaging.

(d) Investigate any possible further applications of the selected strategy.

Based on these aims, an imaging system which utilises correlation based transmission and reception has been developed.

It is considered that this work has been successful and that a number of important contributions to the general field of ultrasonic data acquisition and imaging have developed. These are summarised as follows.

(A) The thesis demonstrates a complete theoretical and practical development of a self contained special purpose ultrasonic system for peak power limited applications. This involved the original design, development and practical implementation of a fast and versatile ultrasonic imaging system which operates at less than

5 volts, in contrast to existing systems utilising excitation levels which are greater than 100 volts. Hence, a solution for intrinsically safe instrumentation in low signal to noise ratio situations has been offered, which may possibly widen the scope of ultrasonic non-destructive evaluation, in addition to safe biomedical applications.

(B) The work establishes a detailed theoretical basis for the development of a practical, real time ultrasonic digital correlation based system and has demonstrated the use of correlation reception for ultrasonic imaging.

(C) During the course of the work, alternative correlation based signal processing strategies for improved ultrasonic reception were investigated. These included techniques for fast cancellation of any form of coherent noise and the generation of pseudo-random sequences from conventional probes for improved pulse compression. It is anticipated that such techniques will have important practical consequences for acoustic imaging in general.

(D) Practical imaging and image processing strategies have been developed for a wide range of ultrasonic applications.

(E) A number of important practical contributions have also been made within the details of developing the hardware system. These included novel techniques for differential transmission and reception, the use of TTL line drivers for probe excitation and the utilisation of dedicated digital correlators for ultrasonic pulse

compression.

1.3 ORGANISATION OF THESIS

The thesis is presented in seven Chapters. The first is the introduction outlining the underlying aims and objects of the project and thesis, while in the last chapter, the thesis is summarised and suggestions for further work are given. Chapters 2 to 6 attack the two main aspects of the problem; i.e. low power data acquisition and imaging.

Chapter 2 mainly contains a review of the problems involved in low power ultrasonic data acquisition, with a critical review of the main correlation (or matched filtering) based data acquisition system implementation methods. The techniques reported by others are outlined and their advantages and disadvantages discussed. The basic equations pertinent to the signal to noise ratio in such a system are also presented. Alternative analogue and digital implementation methods are proposed. Among the suggested alternatives the relative merits of a new digital hardware implementation technique are shown to be much better and an outline of the technique is given.

The third chapter deals with theoretical aspects particularly relevant to a digital implementation of the correlation scheme. A discrete time system representation is given together with the input/output relationships.

This is followed by a discussion of the main theoretical design considerations which include characteristics and parameter selection of the transducer excitation function (a form of pseudo-random binary sequences), selection of quantisation resolution and the derivation of the associated signal to noise ratio expressions. Additionally, new applications which utilise the inherent properties of the excitation function for purposes other than the standard signal to noise ratio enhancement are proposed.

In the fourth chapter, the data acquisition hardware constructed is described in detail. Experimental results are included to demonstrate its performance. These are compared with simulated results and an excellent matching of the two data sets is shown.

Chapter 5 looks at an alternative implementation which combines the signal to noise ratio enhancement of matched filtering with the resolution improvement of deconvolution methods. A pre-filtering approach is considered here. It is shown that the actual pseudo-random excitation function can be generated from a transducer, given apriori knowledge of the transducer impulse response.

The sixth chapter deals with imaging. The synthetic aperture method of image formation is proposed and reviewed. Its limitations such as sidelobes and aperture limitation are discussed and improvements are suggested.

Processing methods for the improvement of image quality are discussed and finally, sample experimental results obtained by the entire data acquisition/imaging unit are shown.

After the concluding chapter, the Appendix section looks at details of some software and hardware utilities which were crucial for the work and in which considerable time was spent to develop, but which however cannot directly fall into the central theme of the thesis so as to be given full treatment within the chapters. These include hardware specifications, a flow chart of the digital correlation simulation package, the set up program for the IBM DMA facility and a description of the construction of specialised transducer arrays. Parameters of probes and arrays used for experimental measurements are also given.

It has been attempted to keep most sketches and block diagrams within the text to facilitate text discussion. Photographs of real results and plots of simulated results have been placed at the end of the relevant chapters.

CHAPTER 2

THE SIGNAL TO NOISE RATIO PROBLEM IN ULTRASONIC DATA ACQUISITION AND METHODS OF IMPROVEMENT

2.1 INTRODUCTION

A major problem area investigated in this project is that associated with low signal to noise ratio (SNR) in the ultrasonic data acquisition process; of particular interest being applications involving highly attenuating media but requiring low operating power levels. In this chapter, the main causes of this problem and its possible solutions are discussed. A correlation based technique of SNR improvement is proposed as the best solution and major implementation techniques reported by others are reviewed. Some possible alternative analogue and digital implementation techniques are then proposed. In the discussion of alternative implementations, it is shown that existing methods have mainly involved analogue processing and that a fully digital hardware implementation would offer a number of significant advantages. Accordingly, a proposed configuration for such a digital processing scheme is outlined.

2.2 THE SIGNAL TO NOISE PROBLEM AND ITS CAUSES

There are various applications of ultrasonic non-destructive testing which require the use of low transmission power levels. Non-destructive evaluation (NDE) in explosive environments and medical imaging are typical examples where peak energising levels have to be

CHAPTER 2

maintained to low, intrinsically safe limits. A problem often encountered in ultrasonic data acquisition in such power limited applications is low SNR. Often, such applications involve highly attenuating media, and this coupled with the peak power limits gives rise to severe problems in signal detection. There are also applications where although there may not be any peak power limits, too much attenuation in the material under test and coupling problems due to surface roughness still result in poor signal detectability. In such situations, additional amplification on the receiving end merely results in a proportional enhancement of various forms of channel noise, thus leaving the signals still undetectable.

There are various sources of channel noise. One of these is wide band electrical noise generated in the receiver, which could be in the form of thermal noise, shot noise and flicker noise. These forms of noise are unavoidable but owing to their wide spectrum, their relative magnitudes with respect to the useful signal can be suppressed by various signal processing techniques. They may also be minimised by careful circuit design.[38]

Another source of channel noise is 'interference' or 'pick up', which usually consists of periodic signals in the vicinity of the detection system. Although it is difficult to suppress such interference sources once they occur, it is however possible to significantly minimise their occurrence by proper circuit layout, shielding, etc.

Small distributed reflectors known as clutter are also known to be sources of channel noise [7]. Like the electrical noise, these are unavoidable. However, due to the randomness of their distribution, their relative contribution can often be suppressed by averaging. As the clutter contribution may be coherent, spatial as well as time averaging may be used to minimise such noise.

Where the detection involves analogue to digital conversion, quantisation error is another source of noise. This is considered in more detail at a later stage. However, it can be mentioned here that quantisation noise is also assumed to have a random distribution and can be minimised by appropriately choosing the number and distribution of the quantisation levels.

Of all these, the electrical noise is considered to be the most significant cause of low signal to noise ratio in peak power limited ultrasonic applications.

The applications mentioned earlier generally operate in pulse echo mode;i.e. ultrasonic pulses of very short duration are derived from single transducers or multiple elements in an array and the returning echoes are then received, amplified and processed for display purposes. The transducer excitation function is usually a step or a very narrow pulse. This mode of operation shall be referred to as the 'conventional' technique in any discussion to follow.

In the conventional pulse echo mode of operation,

the SNR can be improved from the transmitting end by increasing the insonifying pulse amplitudes. Increasing the width could also increase the transmitted energy but it degrades the system resolution, and may affect the range as well as the repetition rate or speed. The resolution refers to the minimum unambiguously detectable target width or separation while the range refers to the minimum and maximum distances within which targets can be identified. In this mode, these factors are determined by the transducer impulse response and the transmitter pulse repetition rate respectively.

However, an arbitrary increase of the insonifying pulse amplitude is impossible, especially where the applications demand intrinsically safe operation. Direct filtering of the received and amplified signals is not necessarily helpful because as indicated earlier, receiver noise is generally wide band. Averaging over many readings is another approach. But in some cases this may require hundreds of transmit/receive cycles to achieve an acceptable signal to noise ratio, thus rendering the system too slow for on-line applications or where it may be required to enhance data from a multi element array.

It can therefore be concluded that in peak power limited applications, the SNR of a conventional system cannot be improved without degrading its performance with respect to speed as well as spatial sensitivity. The problem presented is then to develop an ultrasonic

detection system that:

(a) Provides a significant signal to noise ratio enhancement without increasing peak transmitted power.

(b) At least maintains the range, resolution and speed capabilities of a conventional pulse echo system.

2.3 CORRELATION BASED DATA ACQUISITION

A matched filter configuration of an ultrasonic detection system using correlation based transmission and reception has been proposed as the best approach towards solving the problem of low SNR (for example see [7]). Matched filtering is also implemented in radar and sonar for signal to noise ratio improvement (for example see [17]).

A matched filter is a filter whose impulse response is a mirror image of the desired signal, delayed by some interval. As the amplitude spectrum of its impulse response is the same as that of the signal, frequency components with little relative signal energy are strongly attenuated while those with high relative energy are not. It can be shown that the matched filter forms the cross correlation between the received signal corrupted by noise and a replica of the transmitted signal; the replica being incorporated in the matched filter via the frequency response function.[18]

A general correlation system may be configured as shown in Fig. 2.1.[6,12,13,15]

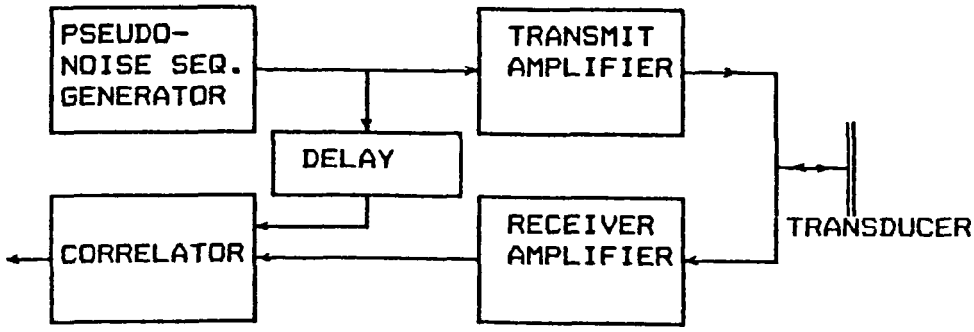

Fig. 2.1 Outline of a correlation based data acquisition system.

In a correlation based system, a wide band pseudo-random sequence is either directly applied to the transducer or is used to modulate an RF burst which is then applied to the transducer. On reception, the returning signals are cross correlated with a delayed replica of the original driving sequence, preceded by the appropriate demodulation where applicable. As the autocorrelation of such a sequence is a very narrow pulse, the output would possess similar resolution to a conventional pulse echo system. However, this arrangement makes it possible to get an increase in average transmitted power without infringing on peak power limits and thus makes it possible to achieve a faster signal to noise ratio enhancement. This is achieved from the transmitting end in both continuous wave and pulse echo modes of operation, and from the receiving end as well in pulse echo mode. The improvement on transmission is achieved due to the increase in the average transmitted power. The excitation sequence duration can be made as

large as required without affecting the system range and resolution. The spectra of the code sequences are bandlimited and exhibit reject zones in the pass band. Thus, a resulting filtering effect on reception and correlation also leads to an improvement of SNR. An additional advantage of this approach is that if the operation is in continuous mode there would be a significant improvement in range, due to the non-periodicity of the excitation waveform.

2.4 SIGNAL TO NOISE RATIOS IN A CORRELATION BASED SYSTEM

It has been shown that a correlation system can provide a theoretically unlimited signal to noise ratio enhancement and results having very large orders of signal to noise ratio enhancement have been reported.[13]

A general expression for the signal to noise ratio enhancement (SNRE) is given by,[12,13]

$$SNRE = k.B.T \qquad \ldots\ldots 2.1$$

Where, B is the -3 dB bandwidth of the received signal,

T is the correlator integration time and

k is a proportionality constant.

As the bandwidth is limited by the transducer, it would appear that the SNR can be arbitrarily increased by simply increasing the integration time, subject to hardware and speed constraints.

In the case where the voltage excitation is in the form of a pseudo-random binary sequence, eqn.2.1 may be

re-written as,[13,14]

$$SNRE = n.N.B.tw \qquad \ldots\ldots 2.2$$

Where, N is the number of bits in one transmit burst,

n is the number of bursts in a correlation cycle,

tw is the sequence bit width.

Accordingly an approximate expression for the SNR in receiver noise limited operation is given by,[13]

$$SNR = n.N.B.tw(Ps/Pn) \qquad \ldots\ldots 2.3$$

Where, Ps & Pn refer to signal power and noise power respectively.

When finite length pseudo-random binary sequences are used in conjunction with short integration times, due to a resulting incomplete pulse compression an additional source of interference known as 'self noise' or 'range sidelobes' is created. Instead of being just a narrow triangular pulse, the autocorrelation of the codes will also include sidelobes of lower amplitude. These give rise to 'false echoes'. It would, for example be difficult to differentiate between sidelobes from a large reflector and real echoes from a small one. This in effect degrades the resolution as well as signal to noise ratio. However, the problem of self noise can be solved by appropriate code selection. Where continuous wave mode of operation is possible, the use of m-sequences has been proposed. These are maximal length pseudo-random binary codes that can be generated by any finite length shift register [13]. For pulse echo mode, it has been shown that special

pseudo-random binary code pairs known as Golay codes cancel out range sidelobes in two transmit/receive cycles [14]. These pairs have autocorrelations with equal central peaks but opposing sidelobes, thus cancelling out the self noise on summation. These are described further in Chapter 3. It has also been noted that so called Quaternary E-codes have similar sidelobe cancellation properties while Barker codes of length 13 have minimum sidelobes, although their short length results in a limited SNRE [14].

In clutter limited operation, it has been shown that the clutter power can only be reduced by averaging over many readings. Readings from different position would be required to randomise the clutter contribution. The effect of clutter can be observed in the expression for SNR, which for no range sidelobes is of the form,[13]

$$SNR = \frac{Ps}{Pc + (Pn/n.N.B.tw)} \qquad .....2.4$$

Where, Pc is the interfering clutter noise power and the other variables are as described in eqns. 2.2 and 2.3.

It may thus be concluded that as long as the enhancement factor, n.N.B.tw, is greater than one, a correlation system would always have a better signal to noise ratio than a conventional pulse-echo system [13]. For example, correlating over a 32 bit Golay code pair of 166ns/bit would provide an SNRE of 10.6 (10 dB), if the transducer being used has a 1 MHz bandwidth. Integrating

over, say 16 pairs, would then give an enhancement of about 170 (22 dB), and so on.

2.5 IMPLEMENTATION TECHNIQUES

2.5.1 Transmission and Reception Aspects

Basically three transmit/receive techniques have been proposed.

The first employs an RF noise source to drive the transducer (for example, see [7]). This technique is used in continuous wave mode of operation and therefore requires separate transmitting and receiving transducers. An analogue delay is required to delay the reference signal. The configuration employed is outlined in Fig. 2.2.

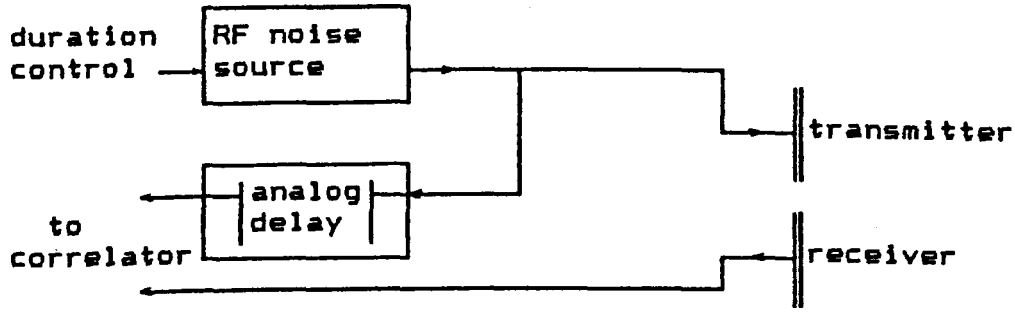

Fig. 2.2 Transmit/receive set up for a correlation system operating in continuous wave mode with RF noise excitation.

Echoes from particular targets may then be investigated by suitably adjusting the analogue delay line. Some problems in this approach can however be identified. The delay line consists of two transducers in a water tank, with a position control mechanism for

varying the separation distance. The transducers used in the delay line need to be as closely matched as possible to those used in the transmitter and receiver. This is difficult to achieve in practice. A second point to note is that the response in the delay line cannot be linear;i.e. variation of the separation distance does not only vary the delay but also the input/output response. The output for a given input would be different for various separations due to the variations in the diffracted field profile as well as due to variations in attenuation with distance. Even if exactly matching transducers are used and the delay line non-linearity is negligible, this approach would still have a lower resolution than a conventional transmit/receive system. This is because the reference to the correlator is also bandlimited by the delay line transducers. The best output would be the correlation of the transmit/receive impulse response of the transmitter and that of the delay line transducers. If, for example, all the transducers are identical, this arrangement degrades the resolution by a factor of two. Last but not least, the need to use separate transmitting and receiving transducers is a restricting factor, especially where array applications are concerned. An unnecessary geometrical restriction would be introduced in the design.

In continuous wave mode of operation, m-sequences have also been used [6,12]. The use of binary sequences

makes it possible to discard the analogue delay line and instead to use more accurately controllable digital delay techniques. In the particular example shown in Fig. 2.3 two identical m-sequence generators are used [6]. One is applied to the transducer while the other generates an identical reference sequence after a programmable delay.

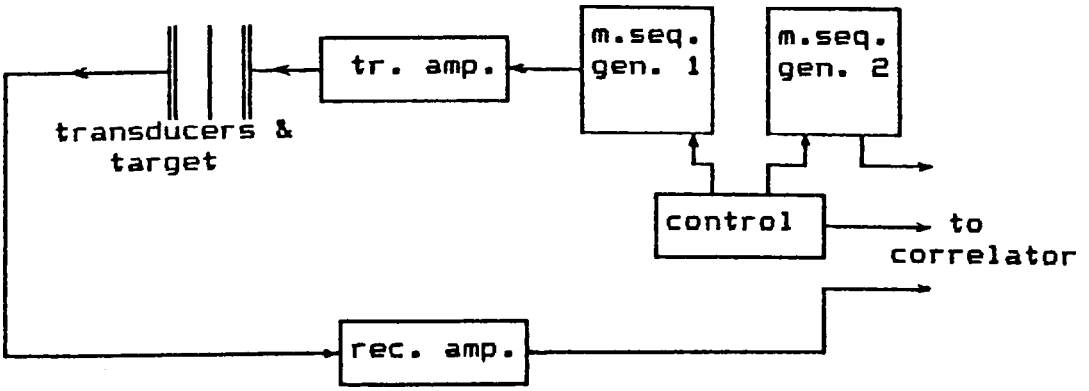

Fig. 2.3 Transmit/receive set up of a correlation system operating in continuous wave mode with m-sequence excitation.

The transmitting transducer is driven directly by a bipolar version of the sequence and the reception side only consists of a wideband amplifier. The only drawback in this approach is the continuous wave mode limitation of having to use separate transmitting and receiving transducers.

A third technique extends the one mentioned above and uses an m-sequence phase modulated RF [12]. The RF carrier has the same frequency as the transducer centre frequency. It has been noted that this is the most efficient method of transmission [13]. All the applied energy is effectively used since the transducer would have

no filtering effect. It is certainly more effective than directly applying the sequences. Noting that the spectra of such codes generally possess a much wider bandwidth than that of low MHz transducers illustrates this fact. It may also be noted that the code spectra exhibit uniformly distributed low energy regions.

The receiver used in the modulated RF method employs conventional synchronous detection with in phase and quadrature phase channels [12]. The outputs of the two channels are then fed into separate correlators. Although this method enables a more efficient transmission, it requires a lot more hardware than the directly sequenced case.

Another proposed approach is pulse echo version of direct sequencing [13]. The basic structure is shown in Fig. 2.4.

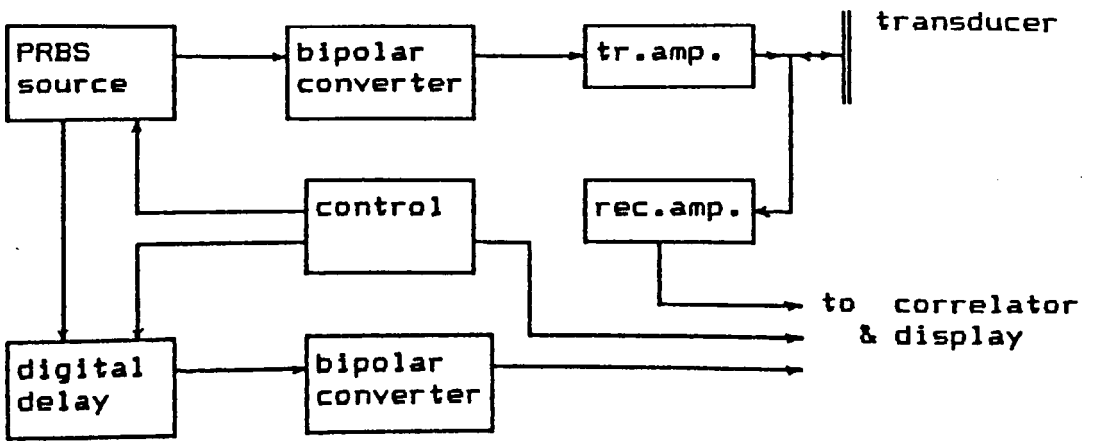

Fig. 2.4 Transmit/receive set up of a correlation system operating in pulse echo mode with directly sequenced PRBS.

This technique, which uses a single transducer for both transmission and reception was first demonstrated with m-sequences, in conjunction with multiple averaging for sidelobe reduction [13]. Later on it was used with paired Golay codes and a single transmit receive cycle [14].

2.5.2 Correlation Synthesis

(a) Analogue correlation

The correlation sections of the transmit receive approaches mentioned earlier have been implemented in essentially identical ways. All are basically analogue; incorporating analogue multipliers and integrators in the form of operational amplifiers and low pass filters.

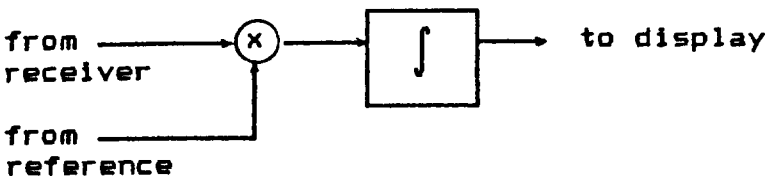

Fig. 2.5 Analogue correlation

The main advantage of such an analogue approach is that it is free from digital noise, which could be in the form of errors due to sampling, quantisation or interference from the system clock. Some disadvantages should also be considered. Such an arrangement is essentially a time integrating correlator, giving one point correlation at a time. This requires a relatively large integration time to form a complete correlation of two waveforms [4].

Low pass filters, when used for this application

were found to be not readily applicable for self noise cancellation since the start and end of an integration interval is not controlled [14].

Stability in long integration times has also been mentioned as a limiting factor [14].

Lastly, while not being susceptible to artificially generated but predictable noise as in a digital system, a purely analogue correlation circuit is susceptible to random noise, just as would originate in a receiver.

(b) Other approaches

A partially digital correlation approach has been tried by clipping the reference and received signals to binary levels and passing them through an exclusive OR logic for binary multiplication before going on to an integrator [7]. This is outlined in Fig. 2.6. This approach maintains phase information but loses amplitude information. Also, since all amplitude levels are quantised to only two levels, noise samples of relatively low levels may also be amplified to comparable levels as the useful signal.

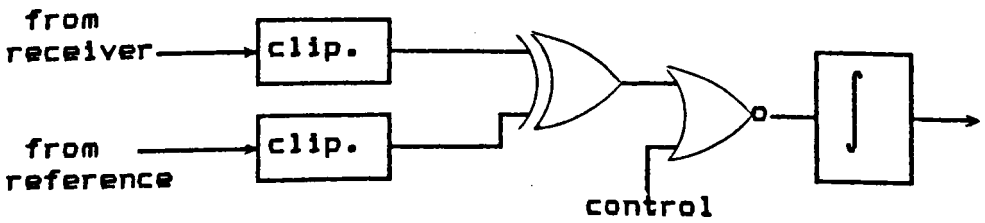

Fig. 2.6 Semi-digital correlation

In the m-sequence phase modulated case [12], the in phase and quadrature phase require two separate analogue correlation sections which are followed by amplitude squaring units and a final summer. This is shown in Fig. 2.7.

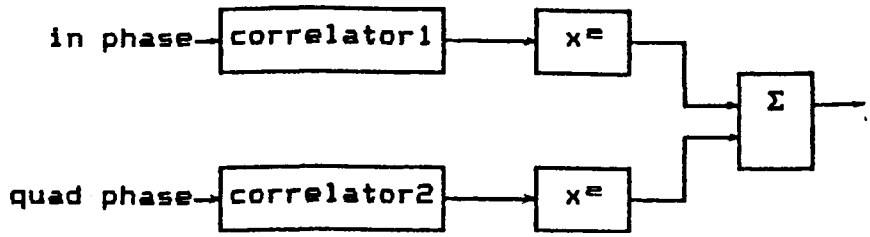

Fig. 2.7 Correlation section for technique using m-sequence phase modulated RF excitation.

As with the transmit/receive section, the hardware in the correlation part of this technique is quite involved [12].

(c) Alternatives

The relatively slower speed of time integrating correlators can be improved by using charge transfer devices with multiple sample handling capability. Although these devices operate with sampled data, they maintain the analogue amplitude levels of the samples and with a sufficiently high sampling rate, they could give the same accuracy as a purely analogue correlator. They will, however, be faster depending on the number of samples they can handle. Charge transfer devices could come in the form of delay lines or even dedicated convolvers and correlators. For example, tapped delay lines can be

configured to perform analogue/analogue or analogue/binary correlation as outlined in Fig. 2.8. The entire reference can be stored in one line while the received signal is passed through another with multiplication occurring at regularly spaced taps and the products being summed at the same time.

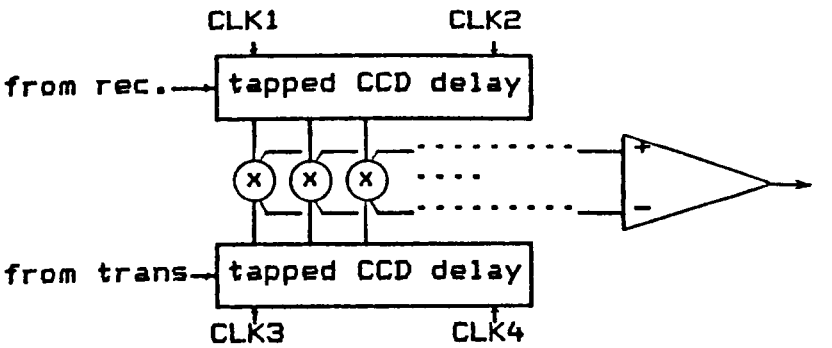

Fig. 2.8 Correlation set up using tapped CCD delay lines

Where, CLK1-CLK4 are independent clocks for shifting data into or out of the receiver and delay lines.

The problems associated with this approach are the following.

1. Tapped delay lines or dedicated correlators with sufficiently high sampling rates are not available.
2. A large bank of multipliers would be required if used as shown above.
3. As both the reference and received signals are maintained in analogue form, they will be susceptible to system noise just as the analogue approaches mentioned earlier.
4. Such devices often require complex clocking and control circuitry.

A second alternative would be using surface acoustic wave (SAW) devices. These could be in the form of dispersive delay lines, transversal filters and memory correlators. However, the current state of the technology is such that these devices,

1. Have very wide bandwidth.
2. Operate only in very high frequency regions (10 MHz to 1 GHz).
3. Are expensive and require complex support modules.

Therefore, SAW devices are currently not readily implementable for ultrasonic pulse compression operating in the region of a few MHz, although they have been successfully used for similar applications in radar signal processing and other spread spectrum communication.

A third alternative would be to use digital correlation. There are two possible approaches. Where speed is not important, the A-scans from the receiver can be digitised, stored, and the correlation performed by software only. Being totally off-line, such a technique would allow easy adjustment of various factors such as integration time, type and length of pseudo-random code, delay and point of observation, etc. A second possibility in a digital approach is on-line hardware correlation using dedicated correlators. Such devices with up to 20 MHz sampling rates are currently available. This approach has several advantages not available in the previously mentioned techniques. These are,

1. Simplicity in interfacing, cascading or expansion.
2. Flexibility for pre and post processing of data.
3. Immunity to additional system noise in the correlation stage.
4. Very high speed due to high sampling rate and multiple sample processing.

A typical digital correlator using N bit digitisation would be configured as shown in Fig. 2.9.

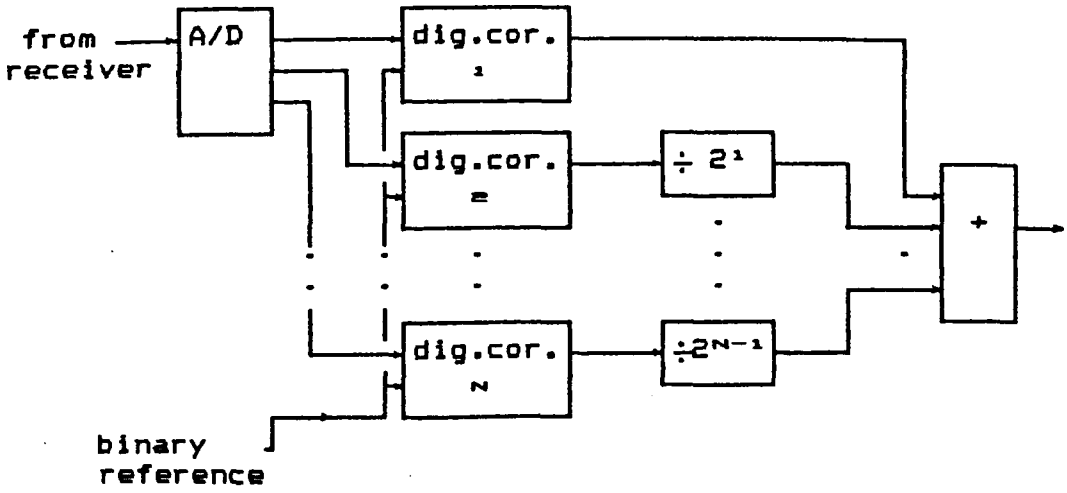

Fig. 2.9 Correlation using dedicated digital devices.

The disadvantages in a digital approach are,

1. quantisation noise is introduced (in both cases).
2. in the second case the need to use as many correlators as the number of digitisation bits may be expensive.

Mainly due to the high speed requirements of the intended application, as well as the other mentioned advantages of a digital implementation, the digital hardware correlation approach has been selected as a

solution for the peak power limitation and resulting signal to noise problem in the ultrasonic data acquisition stage.

2.6 CONCLUSION

In this chapter, the utilisation of correlation based data acquisition has been proposed as a means of meeting the conflicting requirements of having to use low energising levels and maintaining acceptable signal to noise ratios. The main causes of poor signal to noise ratio in peak power limited applications have been reviewed and electronic noise within the amplifying stages has been identified as the chief cause. Standard mathematical expressions pertaining to the SNRE offered by the correlation approach have been presented. It has been shown that the SNRE is a function of the system bandwidth and correlator integration time.

Mainly analogue processing based implementation techniques reported by others have been reviewed. Although immune from the artificially generated noise that occurs in a digital system, it has been noted that the reported analogue techniques suffer from several inherent disadvantages, outstanding of which are lack of accurate control, susceptibility to electronic noise and problems with integrator stability.

Possible alternative implementations based on charge coupled or surface acoustic wave devices (CCD and SAW) have been proposed. However, it has been argued that

although possibly novel for this application, such methods are currently not readily implementable due to the lack of devices for the required speed and operating frequencies and due to the fact that being essentially analogue, these techniques may not constitute a significant improvement over the other implementations reported earlier.

A purely digital hardware implementation has also been proposed as another alternative. A close examination of its relative advantages reveals that this method best meets the requirements of the intended application (low power imaging); the main requirements being very high speed, accurate control, ease for expansion and interface and immunity to unquantifiable errors. It is often mentioned that analogue methods are free of artificially generated digital noise. But looking at it from a slightly different point of view, it seems that this is unavoidable anyway. Even if higher frequency CCD's or lower frequency SAW's are available, or even if the the other analogue methods discussed earlier are used, digitisation is still imperative at some stage if the data is to be used for any meaningful knowledge based assessment. Thus, although not directly on the reception stage, quantisation noise will still be introduced.

Hence, it is concluded that the digital hardware method is the best choice for implementing the correlation scheme. Based on this method, a fast and versatile data acquisition and processing unit has been constructed.

Subsequent chapters describe the theoretical and hardware implementation details of this unit.

CHAPTER 3

CHAPTER 3

A THEORETICAL DESIGN APPRAISAL OF THE DIGITAL CORRELATOR

3.1 INTRODUCTION

This chapter attempts to evaluate the major theoretical and design considerations particularly relevant to a fully digital implementation of the correlation approach. It begins with a discussion on the overall system configuration and input/output relationships. This is followed by a detailed discussion on the properties and selection of the excitation pseudo-random binary sequence (PRBS). Additional, possible new applications of the particular selected PRBS are proposed and discussed. Finally, effects of quantisation and relevant selection considerations are reviewed.

3.2 SYSTEM CONFIGURATION

In this section, a block diagram representation of the discrete correlation system is outlined. The corresponding input and output relationships and signal to noise ratio are then discussed.

The main events occurring in a digital correlation system for ultrasonic applications may be summarised as follows.

i. The application of a suitable code sequence to the transducer.

ii. The received signal is then amplified. Random

electronic noise is introduced at this stage.

iii. The amplified signal is sampled and quantised, introducing a quantisation noise error.

iv. The delayed code and digitised signals are cross correlated.

Thus, the system input is the driving code while the correlated result constitutes the output. The transducer response, target characteristics, amplification and the different noise components would be factors that modify the amplitude and phase of the signal. The overall process is illustrated by the block diagram shown in Fig. 3.1.

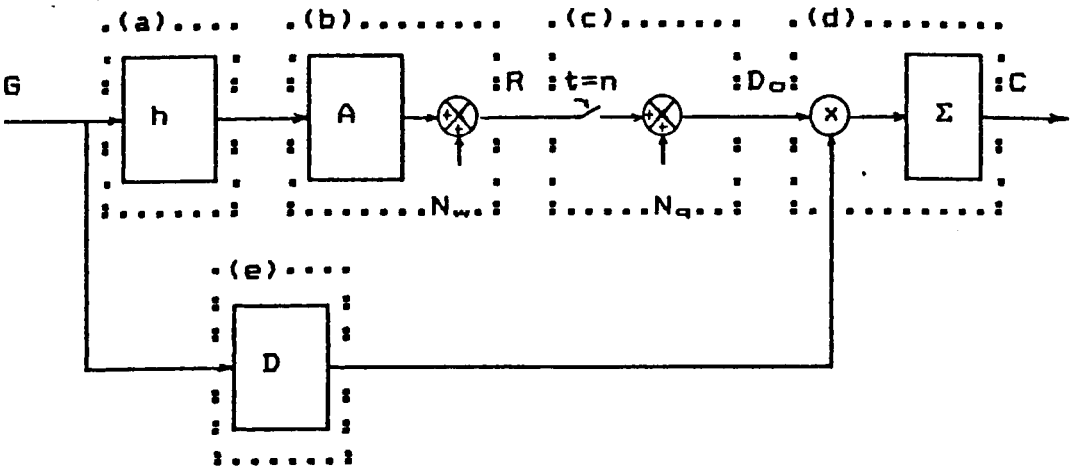

Fig. 3.1 System block diagram representation

(a) represents the transmit/receive impulse response of the transducer, it also includes the target impulse response.

(b) represents the electronic amplification stage. Random electronic noise (N_w) is introduced at this stage.

(c) represents the digitisation process. Quantisation noise (N_q) is introduced here as a result of rounding off the signal samples to a finite number of levels.

(d) is the correlation stage.

(e) is a delay equivalent to the signal transmit/receive time of flight and the propagation delay in the receiver and digitiser.

Also,

G represents the driving and reference code.

R represents the output of a receiver with linear gain A.

D_o is the digitised output.

C is the correlated output.

The random electronic noise (N_w) is assumed to arise from intrinsic noise sources within the amplifying stages. As such, it is white and uncorrelated with the signal. The quantisation noise (N_q) can also be assumed to be random in nature, as a quantised signal could have possessed any amplitude in the range between two quantisation levels. However, its overall power magnitude and distribution depend on the amplitude probability density function of the signal to be coded [5].

The input and output relationships of the system can thus be described as follows:

The discrete time input to the correlator, D_o, is given by,

$$D_o(n) = G(n) * h(n) + N_w(n) + N_q(n) \qquad \ldots.3.1$$

Where, * denotes convolution, and n is the sample number. Thus, for an m-sample correlation stage,

$$C(n) = \sum_{k=1}^{m} G(k).G(k+n) * h(k+n) + \sum_{k=1}^{m} G(k).N_{wq}(k+n)$$

$$= \sum_{k=1}^{m} R_{GG}(k) * h(k+n) + \sum_{k=1}^{m} G(k).N_{wq}(k+n) \quad ....3.2$$

Where, R_{GG} denotes the autocorrelation of the driving sequence, G, and N_{wq} is the sum of the noise voltages N_w and N_q.

Thus, if G is sufficiently wideband, R_{GG} will approach a delta function and the component $\Sigma G(k).N_{wq}(k+n)$ will tend to zero. Consequently, the correlated output will approximate closely to the transducer impulse response modified by the appropriate target characteristics.

In situations where channel noise is negligible, the best output of a digital correlator would be given by,

$$C(n) = A_0.h(k+n) + \sum_{k=1}^{m} G(k).N_q(k+n) \quad .....3.3$$

Where, A_0 is an amplitude scaling factor.

A much generalised configuration would be to represent the system as a matched filter with impulse response G as shown in Fig.3.2. The input is also G but bandlimited by the transducer response and contaminated by additive channel and quantisation noise. The output will be similar to eqn. 3.2.

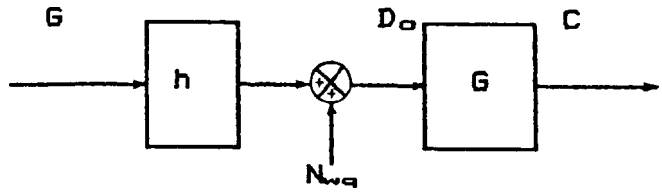

Fig. 3.2 System represented as a matched filter

From eqn. 3.2, it may be observed that the output SNR also depends on the degree of correlation between G and Nwq, unlike conventional pulse echo systems where any additive noise would be directly superimposed on the signal. This also contributes to the SNRE, as noise components not correlated with G are filtered out. This is in addition to the inherent SNRE due to the transmission and reception of more energy.

Finally, letting x_i represent signal voltage samples in conventional pulse echo operation and N_{wi} and N_{qi} represent noise voltage samples, the signal and noise powers can be summarised as follows.

$$\text{Signal power} = (1/m) \sum_{i=1}^{m} x_i^2 = \sigma_x^2 \qquad .....3.4$$

$$\text{Noise power} = (1/m) \sum_{i=1}^{m} [N_{wi} + N_{qi}]^2 \qquad .....3.5$$

$$= (1/m) \sum_{i=1}^{m} N_{wi}^2 + (2/m) \sum_{i=1}^{m} N_{qi}.N_{wi} + (1/m) \sum_{i=1}^{m} N_{qi}^2 \qquad ..3.6$$

$$\approx \sigma_w^2 + \sigma_q^2$$

σ_w^2 and σ_q^2 are the external additive noise and quantisation noise powers respectively. As stated earlier, these noise components are assumed to be random and

uncorrelated so that the middle term in eqn. 3.6 goes to zero for large m. Then, assuming that the operation outlined in Fig. 3.1 is free from coherent clutter and self noise, a general expression for the signal to noise ratio may be given by,

$$SNR(dB) = 10.\log\left|\frac{nNBtw(\sigma_x^2)}{\sigma_w^2 + \sigma_q^2}\right| \qquad .....3.7$$

Where, σ_x^2 is the signal power in a conventional pulse echo system.

$nNBtw(\sigma_x^2)$ is the signal power in a correlation system.

3.3 EXCITATION PRBS: GOLAY CODES

It is proposed to use a directly sequenced PRBS as the excitation and reference function of the system. In particular, complementary Golay codes are chosen to completely avoid self noise effects that would arise in systems using any general PRBS. This section discusses self noise and its influence and outlines the main properties of Golay codes. Although Golay codes have been chosen here primarily to eliminate restrictions arising due to self noise, it is shown that they possess additional advantages which may be exploited for ultrasonic applications.

3.3.1 Self Noise

Self noise occurs as a result of incomplete pulse compression in the correlation receiver. In the mathematics of stochastic processes, it is the error term in a finite length approximation of an infinitely long process [13]. In addition to the limitation imposed by the transducer response, the dynamic range and resolution of a correlation system may be further limited by the presence of self noise. Fig. 3.3 illustrates the simulated autocorrelation of a 64 bit pseudo- random binary sequence.

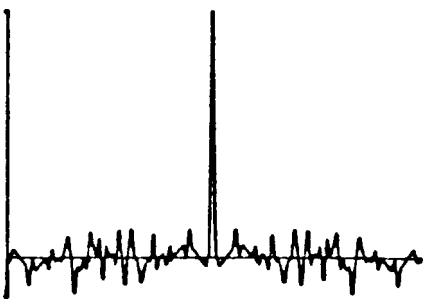

Fig. 3.3 Autocorrelation of a 64 bit PRBS

The artefacts created by incomplete pulse compression are clearly evident. The peak amplitude of the self noise relative to the correlation peak is bounded by,[14]

$$A_M < [n.N.B.t_w]^{-1/2} \qquad \ldots\ldots 3.8$$

Where, n,N,B,tw are as described in eqn. 2.2.

It is thus apparent that the relative amplitude of the self noise can only be reduced by increasing the sequence length. A prohibitively long sequence in turn

degrades the system speed and compromises the minimum detectable range in a single transducer pulse-echo operation (the closest target distance has to be greater than the product $v.N.t_w/2$, where v is the speed of ultrasound in the propagation medium). For example, to achieve a 10 % sidelobe level using a single sequence and a system of 1 MHz bandwidth, the sequence length has to be 0.1 ms, and the closest target distance from the transducer would have to be 7.5 cm in water and 30 cm in steel.

Restrictions arising from self noise may be avoided by the use of Golay code pseudo-random sequence pairs which provide sidelobe cancellation at the expense of dual transmission [14]. These codes have auto-correlations with equal peaks at zero shift and opposing sidelobes. Summation of the respective autocorrelation functions thus provides sidelobe cancellation. This is illustrated in Fig. 3.4 which shows the auto-correlations of two 32 bit complementary Golay codes and their sum.

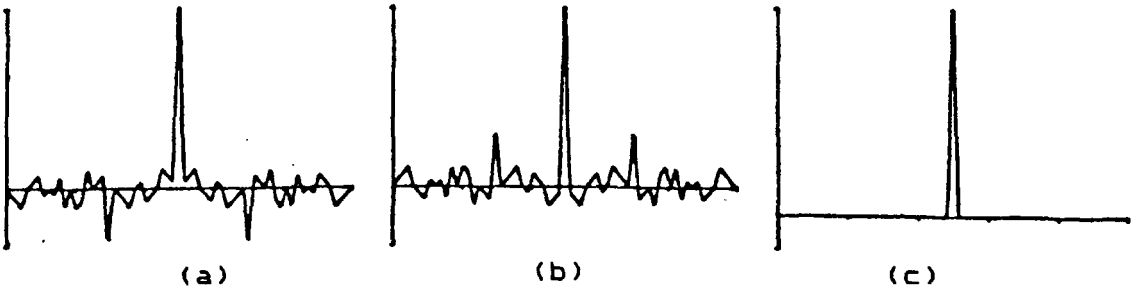

Fig. 3.4 Autocorrelations of a Golay code pair and their sum

It is thus possible to select the appropriate code length by only considering other unavoidable factors like speed and SNRE, without the additional complication of self noise generation. It should be emphasised that the choice of Golay codes over other binary sequences is justified by this total absence of sidelobes, thus allowing optimisation of other parameters.

3.3.2 Properties and Synthesis of Golay Codes

A complete discussion regarding the synthesis and properties of such codes may be found in reference [8]. The main properties are summarised below. A brief discussion on the synthesis of longer codes is also included.

(a) Definition and general properties

A set of complementary series is defined as a pair of equally long, finite sequences of two kinds of elements which have the property that the number of like elements with any one given separation in the first series is equal to the number of unlike elements with the same given separation in the other series. The 'elements' are the numbers in the sequence. For example, the two series (1,0,1,1) and (0,0,0,1) are complementary as they have respectively 2 pairs of unlike and 2 pairs of like adjacent elements, 1 pair of like and 1 pair of unlike adjacent elements, 1 like and 1 unlike pair with a separation of 1, 1 like and 1 unlike pair with a separation of 2, etc., for all possible combinations. The

basic property of complementary series may also be expressed in autocorrelative terms. If the elements of the series have values of +V and -V, the sum of the two autocorrelation functions will be zero everywhere except the centre term.

Consider the two series, A and B with elements a_i and b_i.

$$A = \{a_1, a_2, a_3, \ldots\ldots, a_{n-1}, a_n\} \qquad \ldots\ldots 3.9a$$

$$B = \{b_1, b_2, b_3, \ldots\ldots, b_{m-1}, b_m\} \qquad \ldots\ldots 3.9b$$

If e and f represent the autocorrelation functions of A and B;i.e.

$$e_j = \sum_{i=1}^{n-j} a_i a_{i+j} \qquad \ldots\ldots 3.10a$$

$$f_j = \sum_{i=1}^{n-j} b_i b_{i+j} \qquad \ldots\ldots 3.10b$$

Then,

$$e_j + f_j = 0 \quad j \neq 0$$

$$= 2n \quad j=0 \qquad \ldots\ldots 3.11$$

It is useful to define some terms at this stage. For convenience, the elements of the series will be represented by 1's or 0's. These are used to represent the two kinds of elements and do not have a numerical significance. In conventional terminology, pairs of like elements in a set (1,1 or 0,0) are referred to as even pairs and unlike ones (0,1 or 1,0) are referred to as odd pairs. When all elements of a set are replaced by the element of the other kind, the elements and the set are said to be 'altered' and are usually denoted by a prime.

For example, if a set D=(1,0,1,1) is altered, the altered set will be D'=(0,1,0,0). As far as the elements are concerned, the 'altering' process may be considered as a modulo 2 addition. Thus for an element, a (represented by 1 or 0), the altered element will be $a' \equiv a+1$ (modulo 2). A set is said to be 'reversed' if the order of its elements is reversed. For example, if set D given above is reversed, the new set will be D_R=(1,1,0,1). Finally, the 'parity' of a pair of elements is defined to be the sum of the elements modulo 2.[8]

Summary of main properties

1. The number of elements in two complementary series must be equal. Otherwise the pair with the longest separation in the longer sequence will not have a corresponding match in the shorter sequence. Thus, for the pair A and B described in eqn. 3.9, the lengths n and m should be equal.

2. The series are interchangeable. Substituting the elements of A by those of B and vice versa will not change the complementary property of the two sets.

3. One or both series may be reversed. The order of a pair does not affect the parity of that pair. Hence, the number of even and odd pairs in each series is not affected by a reversal of the order, maintaining the complementary property. The reverse of set A is $A_R=(a_n, a_{n-1}, \ldots, a_2, a_1)$.

4. One or both series may be altered as defined above. As

the parity of a pair is not affected by the alteration of both elements in a pair the complementary property is maintained. The altered version of set A will be $A'=(a_1', a_2', \ldots, a_{n-1}', a_n')$.

5. Alternate elements in each series may be altered. This process does not affect the parity of even spaced pairs. But the parity of odd spaced pairs is changed in both sequences. Due to the interchangeability discussed in (2), this does not affect the complementary property.

Using properties (2) to (5) discussed above 2^4 complementary pairs may be generated from a single pair.[8]

(b) Synthesis of higher order codes

It is known that the particular class of PRBS known as m-sequences can be easily generated by shift registers connected with the appropriate feedback. Golay codes cannot be generated in such fashion. However, a set of algorithms have been developed for generating longer codes and their complements from shorter ones [8]. The codes thus synthesised can then be stored and read out as required.

A summary of the main methods is given below. If required, their proof may be found in the indicated reference.

Consider the series, A and B, given in eqn 3.9 as well as a second complementary pair, C and D, with length m and elements c_i and d_i respectively.

1. The series G_1 and G_2 formed by appending the complementary series A and B and appending the series A and B' will be complementary.

$G_1 = AB = \{a_1, a_2, \ldots, a_{n-1}, a_n, b_1, b_2, \ldots, b_{n-1}, b_n\}$ ..3.12a

$G_2 = AB' = \{a_1, a_2, \ldots, a_{n-1}, a_n, b_1', b_2', \ldots, b_{n-1}', b_n'\}$ .3.12b

2. The series H_1 and H_2 obtained by interleaving the elements of A and B, and those of A and B' will be complementary.

$$H_1 = \{a_1, b_1, a_2, b_2, \ldots\ldots, a_{n-1}, b_{n-1}, a_n, b_n\} \quad \ldots 3.13a$$

$$H_2 = \{a_1, b_1', a_2, b_2', \ldots, a_{n-1}, b_{n-1}', a_n, b_n'\} \quad \ldots 3.13b$$

3. The series I_1 and I_2 given by,

$$I_1 = A^{c1} A^{c2} \ldots\ldots A^{cm} B^{d1} B^{d2} \ldots\ldots B^{dm} \quad \ldots 3.14a$$

$$I_2 = A^{dm} \ldots\ldots A^{d2} A^{d1} B^{cm'} \ldots\ldots B^{c2'} B^{c1'} \quad \ldots 3.14b$$

where the parity of the exponent determines whether the A or B subseries is altered (odd exponent) or not (even exponent), will be complementary.

4. The interleaved series,

$$J_1 = A^{c1} B^{d1} A^{c2} B^{d2} \ldots\ldots A^{cm} B^{dm} \quad \ldots 3.15a$$

$$J_2 = A^{dm} B^{cm'} \ldots\ldots A^{d2} B^{c2'} A^{d1} B^{c1'} \quad \ldots 3.15b$$

are also complementary. The effect of the exponents is as described in 3 above.

To generate the required sequences for the present system, the first algorithm was successively applied starting from the elementary two bit series given by,

$A = \{1,0\}$ and $B = \{1,1\}$.

It may be observed that these two sets satisfy all the criteria for being a complementary series pair. Thus,

using method 1, a 4 bit complementary pair, C and D, can be generated from A and B;i.e.

C = ⟨1,0,1,1⟩ and D = ⟨1,0,0,0⟩

C and D are then used to generate an 8 bit pair, which in turn may be used to generate a 16 bit pair, and so on until the required length of sequence (32 or 64) is reached. Then, if required, the properties discussed in (a) can be used to form different combinations.

3.3.3 Additional Advantages of Complementary Coding in Ultrasonic Systems

In the course of this project, it has been observed that the complementary nature of Golay codes can be exploited to produce a system,

(a) that also suppresses correlated non-common mode noise, in addition to random common mode noise.

(b) that could be configured to detect only moving targets.

As far as the author is aware, the use of Golay codes for these applications has not been reported by others to date.

(a) Non-common mode system noise cancellation

A correlation system provides a high SNRE by increasing the signal energy and suppressing uncorrelated random noise. Correlated noise can also be reduced if it is common mode by the use of a suitable amplifier configuration such as differential amplification. However,

the system can suffer a degradation of its SNR performance if there is a significant amount of correlated system noise that is not common mode. The complementary property of Golay codes can be utilised to neatly circumvent this problem. Consider a correlation system using one kind of code G_A (as in Fig. 3.1). In order to suppress common mode noise at the input stage, a standard configuration would be a differential arrangement as shown below in Figs. 3.5a and 3.5b. G_A and $-G_A$ refer to the applied code and its negative. The 'negative' of a code is derived by altering the signs of all the elements in the original sequence from positive to negative or vice versa.

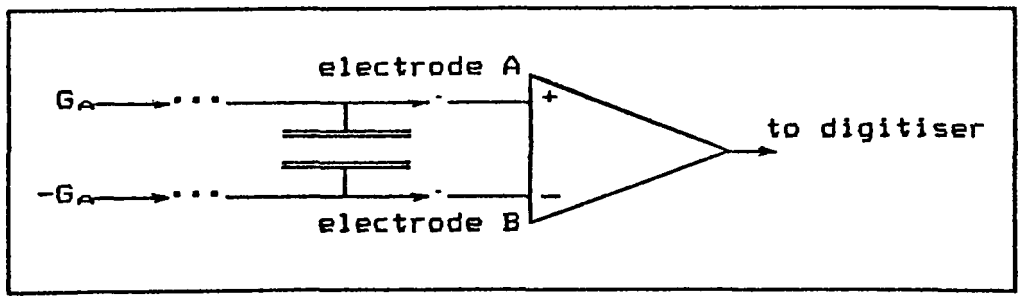

Fig 3.5a Differential amplification, circuit outline

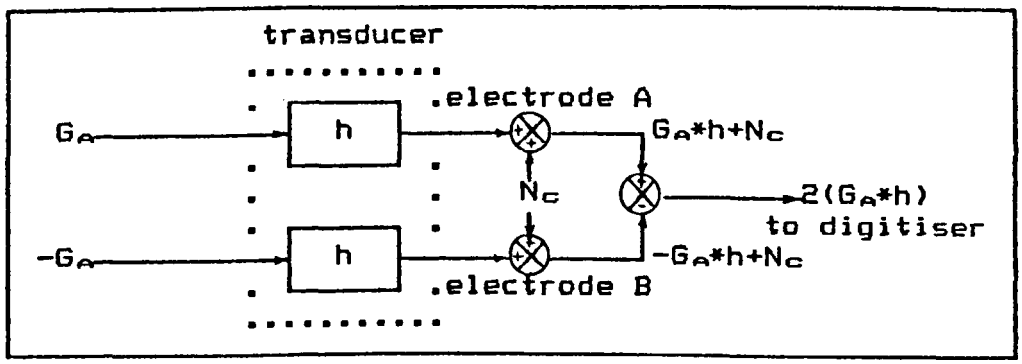

Fig. 3.5b Differential detection, system outline

This configuration of taking the difference of the signals from the transducer electrodes rejects noise common to both sides. This could be in the form of uncorrelated random noise or correlated but common mode noise.

The process shown in Fig. 3.5b may be described by:

$$G_A * h + N_C - (-G_A * h + N_C) \Longrightarrow 2(G_A * h) \quad ...3.16$$

However, if the noise is not common mode, i.e. if one line has noise $+N_C$ while the noise on the other is $-N_C$, it will be impossible to remove it using a single excitation function. The process would look as follows:

$$G_A * h + N_C - (-G_A * h - N_C) \Longrightarrow 2(G_A * h + N_C) \quad ...3.17$$

This results in a final correlated output of the form,

$$2([G_A * h + N_C]) . G_A = A_O h + N \quad ...3.18$$

Where, $A_O = 2(G_A . G_A)$

and $N = 2(N_C . G_A)$

The symbols '*' and '.' represent convolution and correlation operations respectively.

With Golay codes, this problem can be overcome by adding an extra transmission cycle with inverted transmitted and reference codes. Using the same arrangement and a complementary code pair G_A and G_B, with their negatives $-G_A$ and $-G_B$, the inversion property is utilised, i.e. the fact that inverting codes does not affect their complementary property. Thus, if G_A and G_B are complementary $\pm G_A$ and $\pm G_B$ will be complementary

regardless of the sign. If we then let N_{CA} represent non-common mode correlated noise appearing during the transmission of code G_A and N_{CB} represent the non-common mode noise component appearing during the transmission of code G_B, then the correlation output for each transmit/receive cycle will appear as shown below. Again one should refer to Fig. 3.5b, but keeping in mind that with Golay codes a transmit/receive cycle involves firing two bursts. A summing unit is also required after the correlation operation to add up the score of each transmission cycle.

1st code, 1st transmission -- $2(G_A * h + N_{CA}) \cdot G_A$ ..3.19a

2nd code, 1st transmission -- $2(G_B * h + N_{CB}) \cdot G_B$ ..3.19b

1st code, 2nd transmission -- $2(-G_A * h + N_{CA}) \cdot -G_A$ ..3.19c

2nd code, 2nd transmission -- $2(-G_B * h + N_{CB}) \cdot -G_B$ ..3.19d

summed result -- $4A_0 h$ and no noise ..3.20

This result is very significant. It means that it is possible, at least theoretically, to have a detection system that is free of any interference, common mode or otherwise; the only possible compromising factor being component precision. Difficulty in suppressing non-common mode system clock noise getting into the receiver stage is one major problem faced in the digital system implementation. But with this cancellation technique, it should no more be so. The same can be said about scan limitation due to main bang during excitation. Implementation of this method in the hardware system has

actually resulted in a significant reduction in clock noise as well as other non-common mode artefacts such as main bang and multiplexer switching effects that are not cancelled at the differential amplification stage. A demonstration of the improvement achieved may be found in Chapter 4.

(b) Moving target only detection

This comes from the same approach used above. If in transmitting and correlating the second code pair (eqns. 3.19c and 3.19d), the reference is not inverted, the outputs of the two transmissions will be exactly out of phase. Therefore, no output signal can be obtained from echoes returning from stationary objects (except for the noise term, which is not cancelled in this case). For a noise free system the process looks as follows.

1st code, 1st transmission -- $2(G_A * h).G_A$ ..3.21a

2nd code, 1st transmission -- $2(G_B * h).G_B$ ..3.21b

1st code, 2nd transmission -- $2(-G_A * h).G_A$ ..3.21c

2nd code, 2nd transmission -- $2(-G_B * h).G_B$ ..3.21d

summed result -- cancels out

The system will then only detect targets which move and cause phase mismatch during reception. Although not pursued any further here, this may have many useful applications. It may, for example, be possible to interpret the amplitude and phase information of the output signal into measures of parameters such as target velocity, flow rate, etc. As echoes from stationary

reflectors are inherently filtered out and do not affect the output, a system using this method may indeed be a powerful tool for such measurement applications. Imaging of flow vessels and on-line monitoring or imaging of periodically moving targets may also be possible novel applications.

3.4 CODE SIZE SELECTION CONSIDERATIONS

The size of the applied Golay code sequence must be carefully selected to satisfy various design constraints. The selection involves the optimisation of the three main parameters which characterise the code size. These are as shown in Fig. 3.6,

i. The bit width t_w,

ii. The number of bits in a sequence N, and lastly

iii. The overall sequence duration $N.t_w$.

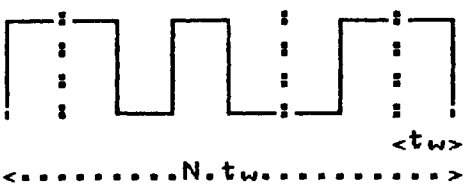

Fig. 3.6 An 8 bit Golay code showing code duration parameters.

This section outlines the main design considerations and proposes an optimum range of code size for the proposed ultrasonic system.

The bit width, t_w, determines the code bandwidth and the nature of excitation. It also influences the system SNR and speed. The number of bits, N, influences the

performance when moving targets are to be encountered and also determines the SNR and speed. Finally, the overall duration, $N.t_w$, determines the operational speed. So, it is required to study the selection of code duration from the point of view of system bandwidth and excitation, SNR and the speed performance which includes moving target detection and overall operational speed.

3.4.1 Bandwidth and Excitation

(a) Bandwidth requirement

The amplitude power spectrum of the triangular pulse derived in auto-correlating and summing the Golay codes exhibits a typical low pass characteristics of the form shown in Fig. 3.7, while a typical transducer response would be of the form shown in Fig. 3.8.

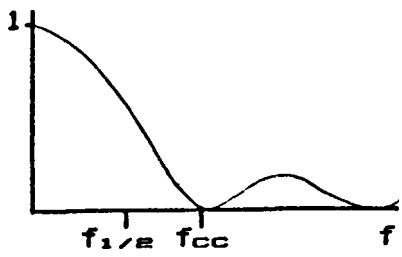

Fig.3.7 Autocorrelated codes frequency response.

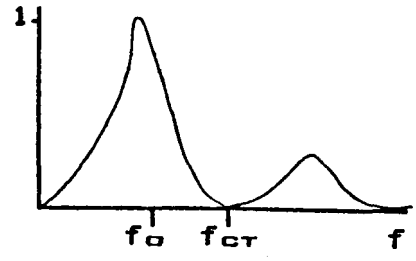

Fig.3.8 Transducer frequency response.

As the final output is a multiplication of these two responses, for efficient excitation and to obtain a resolution which is only limited by the transducer, the upper cutoff of the code response (f_{cc}) must be well above

that of the main transducer response (f_{cT}).

For a given code bit width t_w, the frequencies f_{cc} and $f_{1/2}$ can be expressed by:

$$f_{cc} = 1/t_w \qquad \text{.....3.22}$$

$$f_{1/2} \approx 0.4\ f_{cc} \qquad \text{.....3.23}$$

Transducers used for most ultrasonic applications have centre frequencies in the 1-5 MHz range. If these possess a half power bandwidth of 1 to 3 MHz, to fully excite the transducer, the excitation half power frequency $f_{1/2}$ has to be in the range 2-8 MHz with a cutoff (f_{cc}) of 5-20 MHz. This would require a bit width t_w in the range 50-200ns.

(b) Excitation

An additional factor to consider in the bit width selection is capacitive loading and distortion effects that may occur in the actual driving circuit. For proper correlation and self noise cancellation, the error in amplitude and duration of the codes applied to the transducer must be kept at a minimum. To ensure this, in addition to using drivers with very low output resistance, the selected code bit width must be sufficiently large so that the percentage distortion due to rise time etc. is minimised. Thus, if we are to employ a driver with 25 Ω output resistance, and a transducer with 1 nF static capacitance, it would take 30 ns for the output to reach 0.707 of its peak (Fig. 3.9).

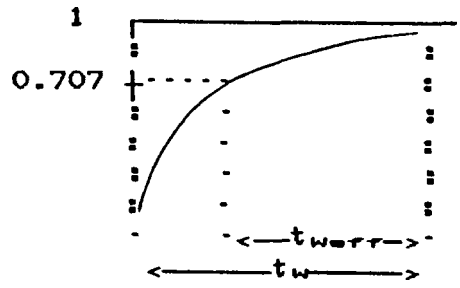

Fig. 3.9

Allowing a maximum error in amplitude of 3 dB, this constitutes a 60 % and 15 % error in bit width for 50 ns/bit and 200 ns/bit codes respectively. However, this does not imply the same percentage error occurs in the code length, as the actual number of low to high and high to low transitions within an N bit code is less than N/2. The error for the 50 ns width is obviously too large. Thus, raising the width value set as the lower limit to 100 ns, will limit the expected maximum error to about 30%.

For small array elements with static capacitances much less than the example quoted, this problem due to capacitive loading would not be significant. However, as the proposed system is also intended to be used for scan data acquisition using larger disc transducers with higher static capacitances, the bit width should not be less than that quoted earlier.

3.4.2 Code Size and Signal to Noise Ratio Enhancement

As indicated in eqn. 2.2, the utilisation of a long pseudo-random pulse train for transducer excitation

increases the transmitted and received energy by a factor proportional to the sequence length (Nt_w). Although the SNRE criteria cannot entirely determine the sequence length, it can however set a lower limit.

An SNRE of 10 dB per transmit/receive cycle is chosen to the minimum acceptable for the proposed system. This choice is based on the opinion that anything less would not justify the need to have the correlation system and a less complex averaging system would be preferable. A 10 dB SNRE implies that the system can tolerate noise margins of up to 5 times stronger than the input signals without losing its detection capability (assuming SNR_{MIN} = 2). By assuming an SNRE of 10, a bandwidth of 1 MHz and the transmission of a Golay code pair, i.e. n=2, a figure of 5 μs is obtained for the minimum overall sequence length (Nt_w). If the range of the bit width, t_w, is as given in the previous section, the minimum number of bits will be between 25 (for 200ns/bit) and 50 (for 100ns/bit). Any further increase will result in a correspondingly higher SNRE. The sequence length values closest to the indicated range and that are powers of 2 are 32 and 64 bits.

3.4.3 Code Duration and System Speed

To maximise the system operational speed so as to obtain real time or near real time performance, the code length must be minimised and its repetition rate maximised. The speed is more crucial for applications

which require data acquisition from moving targets. If the code duration is too long, the speed can only be increased at the cost of the length of scan data that can be acquired. It is also necessary to ensure that the code length is short enough not to be affected by the maximum expected target motion, as distortions and sidelobes may result. Hence the speed and SNR are opposing requirements.

(a) Effect of moving target

In this section the relationship between target motion and code duration and the effect on system performance will be investigated. It shall be assumed that the code repetition rate is synchronised to any target motion so that the system's performance is only affected by target motion during the transmission of a code burst. It is also assumed that the motion maintains a constant velocity during this period.

If the signal is transmitted on to a moving target the reflected signal is compressed or expanded depending on the direction of motion. The percentage shift can be evaluated as follows. Consider Fig. 3.10.

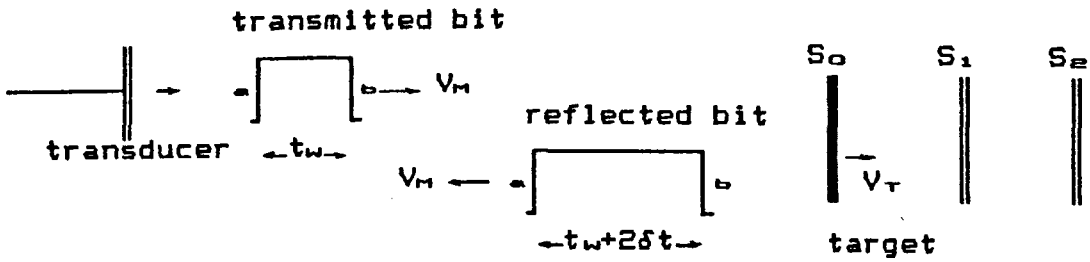

Fig. 3.10 Bit expansion due to a receding target

Where,

-V_M and V_T refer to the speed of sound in the medium and target velocity respectively.

-S_0 is the target position when the rising edge (a) reaches the target. This will be the reference position (S_0=0).

-δt is the difference between the time when (b) reaches the target if it had been stationary (at S_0), and the time it now actually reaches it (at S_2).

Then, $S_1 = V_T . t_W$ (target position when (b) reaches S_0)

$S_2 = V_M . \delta t$ (target position when (b) reaches target)

and $S_2 - S_1 = V_T . \delta t$ (target displacement in the time that (b) travels from S_0 to S_2)

Combining these gives:

$$\frac{\delta t}{t_W} = \frac{V_T}{V_M - V_T} \qquad .....3.24$$

The total % error will actually be $2\delta t/t_W$ x 100% since (a) will also be moving during δt.

Therefore, the % error in bit width and hence overall code duration as a result of target motion only depends on the speed of sound in the medium (V_M) and the target speed (V_T). It is not a function of the original code duration. However, as the correlation process involves multiplying and summing an entire set of samples, the same % error in duration results in differing error levels in the final output for different number of bits N. In general, the higher N is, the higher the resulting

sidelobe from code duration error. As in the case of self noise, these sidelobes limit the system's dynamic range and resolution. This is illustrated in Figs. 3.11(a) and 3.11(b) which show the degradation on the autocorrelated sums of 32 and 64 bit Golay codes due to a target motion of 0.75m/s in water. According to eqn. 3.24, such target velocity results in a 1 % change in code duration (for any bit width). Then, if for example, a 5% sidelobe level is acceptable, it may be noticed from the figures that the resolution from the 64 bit code has degraded by a factor of 20 , while the 32 bit one has only changed by a factor of 4. This measure is based on the ratio of the difference in pulse width before and after distortion ($2t_w$ and t') to the pulse width before distortion ($2.t_w$) [37]. The width after distortion (t') is the width extending up to the tolerable sidelobe levels (5 % in this example).

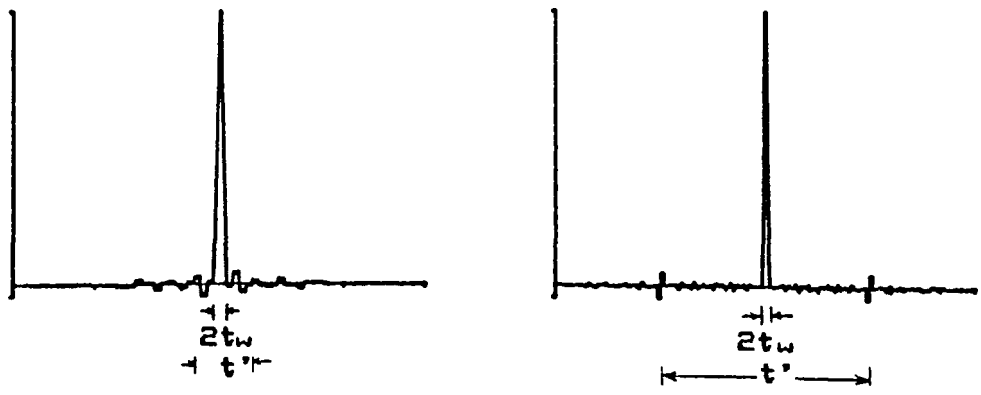

(a) 32 bit (b) 64 bit

Fig. 3.11 Autocorrelated sum of 32 and 64 bit Golay codes showing resolution degradation due to a target motion of 0.75m/s in water.

The acceptable sidelobe levels really depend on the application and the kind of targets expected. For example, much higher target speeds and hence, sidelobes, can be tolerated if the attenuation in the medium is low and strong signals can be received from the targets under observation. If for instance, signal amplitudes are strong enough for the system to tolerate sidelobe levels up to 10% of the peak, the system will not experience any degradation of resolution by the velocity quoted above.

3.5 QUANTISATION

One drawback in the digital approach is that the digitisation process introduces quantisation noise. As incoming signals are approximated to their nearest allowable level, the round-off errors contribute to an artificial noise which is a function of the number and distribution of these allowed levels. This section looks at SNR in a quantised signal and considerations for the selection of A/D resolution.

3.5.1 Quantisation and SNR

The artificial noise introduced due to quantisation puts a limit on the maximum obtainable SNR. The mean SNR in a quantised signal is a function of its probability density function (p.d.f.). The general method for computing the SNR of a quantised signal is outlined below and a particular expression for the SNR of a quantised

ultrasonic wavelet is developed.

The main assumptions made in the following derivations are,

1. The signal occupies the full range of the coder.
2. The quantisation is uniform; i.e. the increment between allowable levels is constant.
3. For the particular case of an ultrasonic wavelet, approximated by a damped cosine, the interval from $\frac{-5\pi}{2}$ to $\frac{+5\pi}{2}$ is sufficient to estimate the power; terms beyond being considered negligible.

For a time signal, v(t) or v(θ) as that shown in Fig. 3.12, the standard p.d.f. calculation involves first solving for θ in terms of v, finding its first derivative and multiplying it with the probability distribution of θ. Having found the p.d.f., integrating the product of the p.d.f. and the square amplitudes of the signal over the full amplitude range of v yields the mean square power (for example see [5]). These are shown in eqns. 3.25 and 3.26.

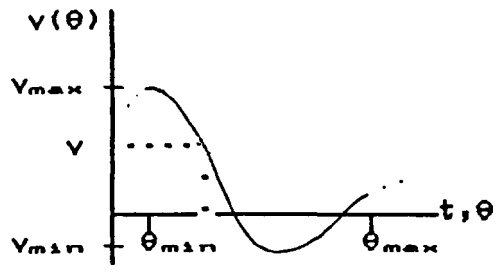

Fig. 3.12

In general the signal p.d.f. can be computed by [39],

$$p(v)=P(\theta).\frac{d[\theta(v)]}{dv} \qquad \ldots.3.25$$

Where, $P(\theta)$ is the probability distribution function of θ in the interval under consideration (θ_{min} to θ_{max}).

The mean square signal power is then given by,

$$\overline{S^2} = \int_{v_{min}}^{v_{max}} v^2 p(v)\, dv \qquad \ldots.3.26$$

On the other hand, the quantisation noise power calculation involves, first computing the error for each quantisation interval and summing the errors over the full amplitude range. Fig. 3.13 and eqns. 3.27 and 3.28 outline the process.

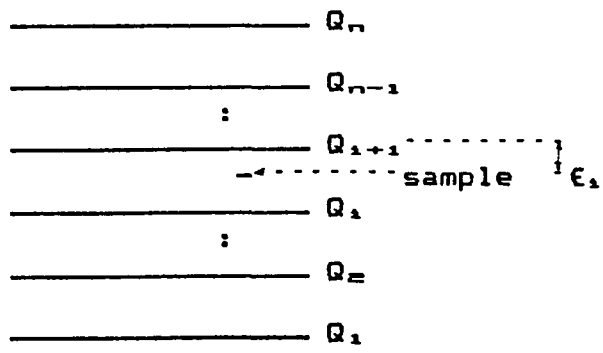

Fig. 3.13 Quantisation levels and round-off error

The error involved in quantisation , for each quantisation interval is given by,

$$\overline{\epsilon_i^2} = \frac{1}{Q_i}\int_{-Q_i/2}^{Q_i/2} \epsilon_i^2\, d\epsilon$$

$$= \frac{Q_i^2}{12} \qquad \ldots.3.27$$

Where, Qi is the increment between the i_{th} and $i+1_{th}$ quantisation intervals and ϵ_i is the error between the true sample value and the rounded-off value (shown in Fig.

3.13).

To calculate the total mean quantisation noise power, the individual errors given by eqn.3.27 must be summed over the whole amplitude range. Hence,

$$\bar{\sigma}_q^2 = \Sigma\ \bar{\epsilon}_i^2\ p(v_i) \qquad \ldots.3.28$$

Where, $p(v_i)$ is the probability for the signal to possess an amplitude of v_i ($v_{min} \leq v_i \leq v_{max}$). Based on the assumptions 1 and 2 given above;i.e. a uniform quantisation ($Q_i=Q$), and the signal occupying the full coder range (so that $\Sigma p(v_i)=1$), the mean quantisation noise power given by eqn.3.28 reduces to the following.

$$\bar{\sigma}_q^2 = \frac{Q^2}{12} \qquad \ldots.3.29$$

Therefore, the SNR will be the ratio of the quantities described by eqns.3.26 and 3.29.

In general, this procedure for calculating the signal power and the signal to quantisation noise ratio can only be implemented as long as there is a solution for p(v). For example, for a uniform triangular signal, subjected to uniform quantisation, p(v), $\bar{S}^2$ and the SNR may be computed as follows.

A triangular signal may be expressed by a function of the form given by,

$$y(t) = \frac{2K}{T}\ t,\ -\frac{T}{2} \leq t \leq +\frac{T}{2} \qquad \ldots.3.30$$

Where, T is the period and K is the peak amplitude of the signal.

Then, according to eqn. 3.25, the p.d.f. is given by,

$$p(y) = \frac{1}{T} \cdot \frac{T}{2K}$$

$$= \frac{1}{2K} \qquad \ldots.3.31$$

Similarly, the signal power is calculated using eqn.3.26. Thus,

$$\bar{S}^2 = \frac{1}{2K}\int_{-K}^{K} y^2 \, dy$$

$$= \frac{K^2}{3} \qquad \ldots.3.32$$

Alternatively, the peak value K can be expressed in terms of the quantisation increment Q, and the number of allowable levels n. Thus, as the signal occupies the full range, the peak to peak value can be expressed by,

$$2K = (n-1)Q \qquad \ldots.3.33$$

On the appropriate substitution, the expression for the signal power then reduces to,

$$\bar{S}^2 \approx \frac{n^2Q^2}{12} \quad (n>>1) \qquad \ldots.3.34$$

Finally, equations 3.29 and 3.34 yield the following expression for the signal to noise power of a uniform signal.

$$SNR_q \approx n^2 \qquad \ldots.3.35$$

Or letting $n = 2^M$,where M is the number of digitisation bits, the SNR in dB may be expressed as,

$$SNR_q \approx 6M \text{ dB} \qquad \ldots.3.36$$

The same procedure can be applied to a uniformly quantised sinusoidal signal to obtain the signal to quantisation noise ratio given by eqn. 3.37.

$$SNR_{dB} \approx 1.5\ n^2 \qquad \ldots.3.37$$

In a typical ultrasonic system, the signals are more gaussian than uniform. They are generally of the form shown in Fig. 3.14 and could be mathematically approximated by,

$$f(t) = Ke^{-\alpha|t|}\cos 2\pi ft \qquad \ldots.3.38$$

Where, α is a suitable damping factor, K is an amplitude scaling factor and f is the centre frequency.

The function f may be re-expressed as a function of angle, θ, instead of time, t. Thus,

$$v = f(\theta) = Ke^{(-\alpha/2\pi f)|\theta|}\cos\theta \qquad \ldots.3.39$$

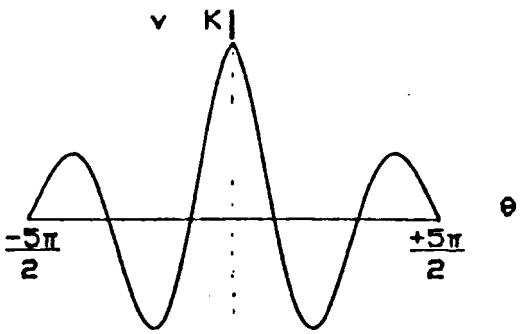

Fig. 3.14 Approximation of an ultrasonic wavelet

For the damped cosine function described above, there is no analytic solution for p(v). Hence, a different approach is required to estimate the signal power and SNR. For a signal approximated by a finite time (or angle) interval, the power could alternatively be calculated by integrating over the time (or angle) range instead of the

amplitude range. Hence,

$$\overline{S^2} = \frac{1}{\theta_{max}-\theta_{min}} \int_{-\theta_{min}}^{\theta_{max}} v(\theta)^2 \, d\theta \qquad \ldots.3.40$$

Or, in a sampled data system,

$$\overline{S^2} = \frac{1}{N} \Sigma \, v_i^2 \qquad \ldots.3.41$$

Where, N is the number of samples in the interval.

Now although, eqns. 3.40 and 3.41 may be used to compute the power magnitude, they are not convenient to be used as an empirical relation for the general case.

To derive a power expression for the gaussian signal described earlier, the following approach is used.

Firstly, close examination of eqns. 3.39 and 3.41 reveals that the power of $v(\theta)$ computed using these equations would be a function of the factor α/f. Then, for the selected interval, the power is calculated and plotted as a function of this factor. This is shown in dotted line in Fig. 3.15. It may be noted that as this curve appears to be of the form $y=a/(x+b)$, it should be possible to approximate it by such a function. Accordingly, the appropriate values of a and b are sought to get the best fit and the relatively simple SNR expression given by eqn.3.42 is arrived at.

$$\overline{S^2} = \frac{K^2\beta}{\alpha/f + 2\beta} \qquad \ldots.3.42$$

The factor, β, in general depends on the length

of time (or angle) interval considered. It is computed by minimising the error between the real and approximate power. For the chosen interval, $\frac{-5\pi}{2}$ to $\frac{+5\pi}{2}$, the value of β would be 0.3. The resulting approximate power curve with this value of β is shown in solid line in Fig. 3.15. A close agreement between the real and approximate power curves may be observed.

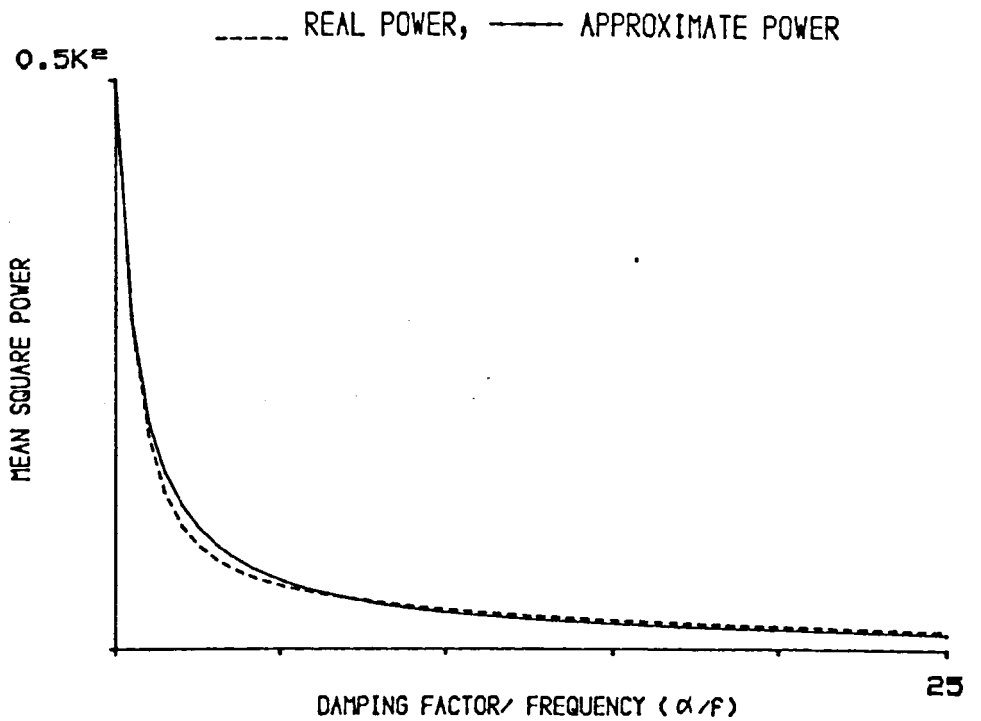

Fig. 3.15 Real and approximated power of an ultrasonic wavelet.

From eqn. 3.42 and the quantisation noise power derived earlier the expression for the SNR of a quantised ultrasonic wavelet is obtained. Thus,

$$SNR_Q = \frac{12K^2\beta}{(\alpha/f + 2\beta)Q^2} \qquad ....3.43$$

Additionally, it may be shown that the signal has a

peak to peak value given by,

$$nQ = K(1 + e^{-\alpha/ef}) \qquad \ldots.3.44$$

Combining eqns. 3.43 and 3.44 yields the following.

$$SNR_Q = \frac{12\beta n^2}{(\alpha/f + 2\beta)(1 + e^{-\alpha/ef})^2} \qquad \ldots.3.45$$

It may be observed from this result that for the undamped case (α=0), eqn.3.45 reduces to the SNR for an undamped sinusoid given by eqn.3.37.

Finally, it is evident that the SNR performance on a mean square basis is proportional to the square of the number of quantisation levels.

3.5.2 Selection of A/D Resolution

The main factors considered in the selection of quantisation accuracy are,

(a) Quantisation noise

As stated above, the maximum available SNR is proportional to the square of the number of levels. Therefore as far as this criteria is concerned , the number of digitisation bits should be maximised. Figures 3.16a and 3.16b illustrate the effects of 4 and 6 bit quantisation of typical ultrasonic input data on the correlator output. The data has a 1 MHz centre frequency and is sampled at a 12 MHz rate. Figure 3.16c illustrates the ideal output not subjected to sampling and quantisation effects. 4 and 6 bit quantisation limit the system SNR to the order of 24 dB and 36 dB respectively.

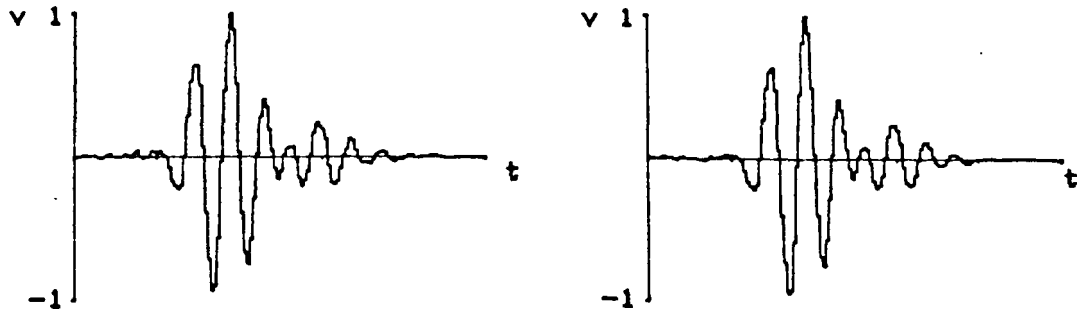

(a) 4 bit quantisation (b) 6 bit quantisation

Fig. 3.16 Correlator output for a 1 MHz ultrasonic input data. A 12 MHz sampling rate is assumed.

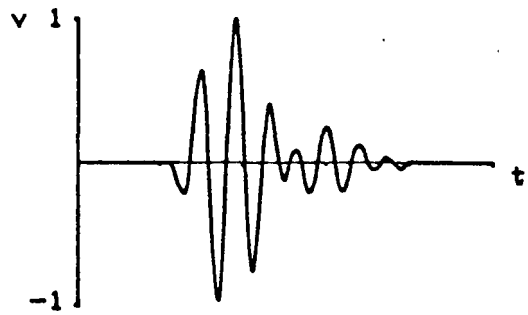

Fig. 3.16c Correlator output for a 1 MHz ultrasonic input data. No quantisation of data.

Finally, it is worthwhile to note that the number of digitisation bits is more crucial where low amplitude signals are encountered. In such cases a crude quantisation will amplify system noise to comparable levels as the signal or to portions of it. It will also result in the loss of accurate phase information. This in turn could, for example, result in poor images in a system used for such purpose.

(b) Cost and hardware complexity

The cost of A/D converters is proportional to their resolution. Additionally, the available digital correlators which can meet the high speed requirements of the system (i.e. capable of multiple sample correlation with sampling rates greater than 10 MHz) can only handle single bit data. Thus, as many correlators as the number of digitisation bits are required, also adding to the cost. The number of memory devices and other TTL components required also depends on the same factor.

The proposed data acquisition unit should be one that is fast, provides an acceptable SNR and is not complex or costly. The table below compares the SNR, complexity and main costs in utilising 4,6 and 8 bit digitisation in the proposed system.

Dig. bits	SNR(dB)	Main cost(£)	Complexity*[1]
		A/D : Corr.	max.parallel proc.
4	24	100 : 600	28 bits
6	36	200 : 900	42 bits
8	48	900 : 1200	56 bits

Table 3.1

*[1] quoted here are possible intermediate outputs at the correlation stage, which would be the number of correlators multiplied by the number of bits/correlator(7 in this case)

Considering these three constraints, a 6 bit resolution would obviously be a reasonable compromise and is therefore selected for the present system.

3.6. CONCLUSION

The main theoretical considerations preceding the digital correlation hardware development have been highlighted. A discrete time representation of the system and the related input/output relationships were described. The rationale behind the selection of the various system parameters have been discussed and actual parameter values were arrived at for some cases.

For the excitation part, the use of directly sequenced Golay codes has been proposed; their inherent properties and the technique for generating them have been detailed. It has been shown that they possess properties that allow self noise cancellation, that allow cancellation of non-common mode but correlated noise and that may allow the detection of moving targets only if required. Although the self noise cancellation property has been known for a while, the exploitation of Golay code properties for the latter two applications is a new idea. The moving target detection, although not pursued further here, is an area that is strongly recommended for further investigation. The other noise cancellation properties have been taken into consideration in the hardware design.

The selection of the code size has also been discussed. Based on the consideration of system excitation, speed and SNR a code range of 32 to 64 bits, with a bit width range of 100ns to 200ns has been selected.

An analysis of the system performance in the situation where moving targets are encountered showed that the resulting output distortion, although independent of the bit width, is influenced by the overall number of bits in a code.

It has also been concluded that the target speed the system can cope with is a function of the tolerable signal to sidelobe ratio, which in turn defines the tolerable resolution degradation. For acceptable sidelobe levels of 10%, the target velocity limit is around 0.75m/s in water.

Finally, effects of quantisation were reviewed. An approximate expression for the signal to quantisation noise ratio of a typical ultrasonic wavelet was derived in order to establish one selection parameter for the number of digitisation bits. Based on this and a consideration of the expected cost and hardware complexity, a 6 bit resolution was selected.

The hardware developed based on the concepts discussed here is described in the next chapter.

CHAPTER 4

CHAPTER 4

ELECTRONIC HARDWARE DEVELOPMENT AND EXPERIMENTAL EVALUATION

4.1 INTRODUCTION

In this chapter, the hardware system is described and its performance assessed. The system consists of five major modules, four of which have particular functions while one coordinates the rest. Due to the high speed requirements, all processing is performed in hardware, mostly with discrete Advanced Schottky TTL logic components. For the same reason, no microprocessor is included at the moment and no software controlled operations take place on the data acquisition side of the process. In the first section of this chapter, the underlying considerations in the design and construction of each module are briefly discussed followed by an outline and description of their operation. As standard logic design, minimisation and debugging techniques are adopted, it is considered unnecessary to provide circuit design details and only general descriptions are given. In the second section, a selection of results are presented to demonstrate the system's performance. The signal characteristics at different stages of the hardware is traced. Through experimental measurements carried out for three different transducers, it is shown that the correlation system indeed exhibits a marked signal to noise ratio enhancement, with signals being retrieved from

inputs having signal to noise ratios well below 0 dB. The experimentally measured responses are also compared with simulated ones, showing very good agreement.

4.2 SYSTEM DEVELOPMENT AND DESCRIPTION

4.2.1 General Outline

A basic digital correlation based data acquisition system should consist of the following main sections.

(a) A pseudo-random code source for generating the excitation and reference codes.

(b) A transmit/receive section which, on the transmission side, should include transmitting amplifiers or buffers and a multiplexing facility for multi-channel operation. On the reception side, it would include an analogue demultiplexer, an amplification section and a digitiser.

(c) A processing section which would perform the required functions of correlation, summation and averaging.

(d) An output interface which may include a digital to analogue converter for A-scan viewing and a data communication interface for passing the data to a host system for further processing and storage.

(e) A control unit for timing and synchronising the entire operation.

Based on these, the system outlined in Fig. 4.11 (page 93) has been designed. The reasons for requiring the various sections of the system and their functional

behaviour are described below, followed by a description of the overall operation.

4.2.2 Description of Main Sections

The main abbreviations and symbols used in the outline diagrams and descriptions are as follows.

(i) Abbreviations of sub-sections

TCU - timing and control unit.

DCU - delay control unit.

SYS CLR- system reset control.

OIU - output interface unit.

Other sections are symbolised in unabbreviated format.

(ii) Symbols of signals and functions

$\Phi_0, \bar{\Phi}_0$ - basic clock and its complement (12 MHz at present)

$\Phi_1 - \Phi_{16}$ - address, timing and control prior to and including the correlation stage, generated by the TCU.

$\Phi_1' - \Phi_{16}'$ - address, timing and control after the correlation stage, generated by the TCU.

$M_1 - M_{16}$ - multiplexer control, generated by the TCU.

Q_1 - delay control , generated by the DCU.

CLR_1, CLR_2- system reset (clear) signal, originating from the SYS CLR unit.

$A_1 - A_6$ - digitiser outputs.

$C_{01} - C_{016}$ - correlator outputs.

$CC_1 - CC_{16}$ - final summed and averaged output.

DO_1-DO_{16} - data transferred to a host system via DMA.

DC_1 - data transfer handshake signal from the OIU.

REQ - data transfer request to host system, from OIU.

Ack,IOR - handshake signals from host system during DMA data transfer.

(a) CONTROL SECTION

(1) Timing Control(TCU)

Such a unit is required to co-ordinate the operation of the entire system. It generates all the necessary timing and synchronising signals, clocks and addresses for the entire system. The configuration of the TCU in the present system is outlined in Fig. 4.1.

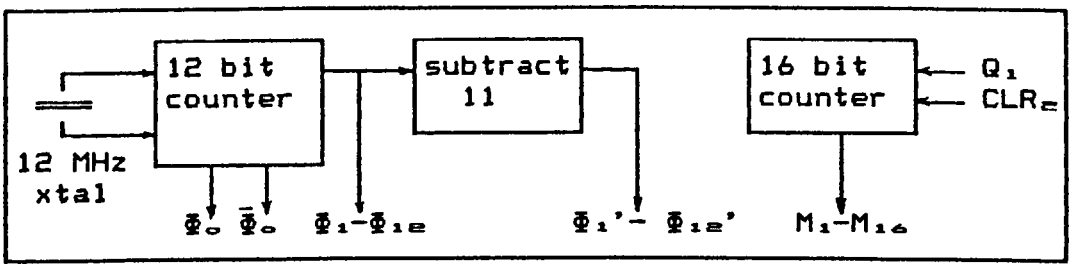

Fig. 4.1 Timing and control

As shown in Fig. 4.1, a 4096 level counter generates 12 bit words which are used for all timing before and at the correlator stage. As the correlation introduces a delay of 11 clock periods, addressing and other timing beyond that stage needs to be adjusted to compensate for it. Thus, the original 12 bit words used for timing (Φ_1-Φ_{12}) are shifted by a subtraction stage. The subtraction operation simply involves adding the two's complement of the delay (11 in this case) to the original timing words. The TCU also includes an additional 16 bit

counter for averaging and multiplexer control. It operates continuously unless halted temporarily by the SYS CLR unit described below.

(2) System Reset(SYS CLR)

Such a unit is required to detect the end or start of particular events, and accordingly reset or restart the entire operation. Possible events during which the system execution should be suspended are,

i. During the loading of excitation codes prior to transmission.

ii. During the waiting period prior to reception.

iii. At the completion of processing a single scan.

iv. At the completion of processing multiple scans or channels.

An OR function based decode logic carries out this operation in the system (Fig. 4.2)

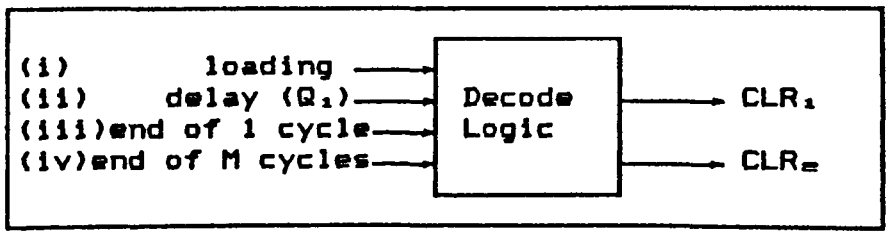

Fig. 4.2 System reset

The signals on lines (iii) and (iv) are feedback reset signals for cyclic repetition of single or multiple cycles. When either of the lines (ii) or (iii) is active all but the multiplexing counter are reset (CLR_1 activated), while the activation of lines (i) or (iv) resets the entire system (CLR_m activated).

(3) Delay Control(DCU)

Processing a very long scan of data would require a correspondingly large system memory. The system operational speed would also be slowed down proportionally. A much better alternative is to process a finite length of scan but have an option of moving this scan to any required cross section in space. The delay control unit serves this purpose by controlling the start of data acquisition. The unit halts the system operation just after transmission and restarts it after a pre-programmed time interval. Thus, scans of interest may be shifted to look at particular regions of interest. Additionally, such a unit has the potential of being used for reception beamforming in a multiplexed array system. This would involve adaptively varying the delay time before reception for each element, possibly using a microprocessor. The overall structure of the delay control section in the present system is shown in Fig. 4.3.

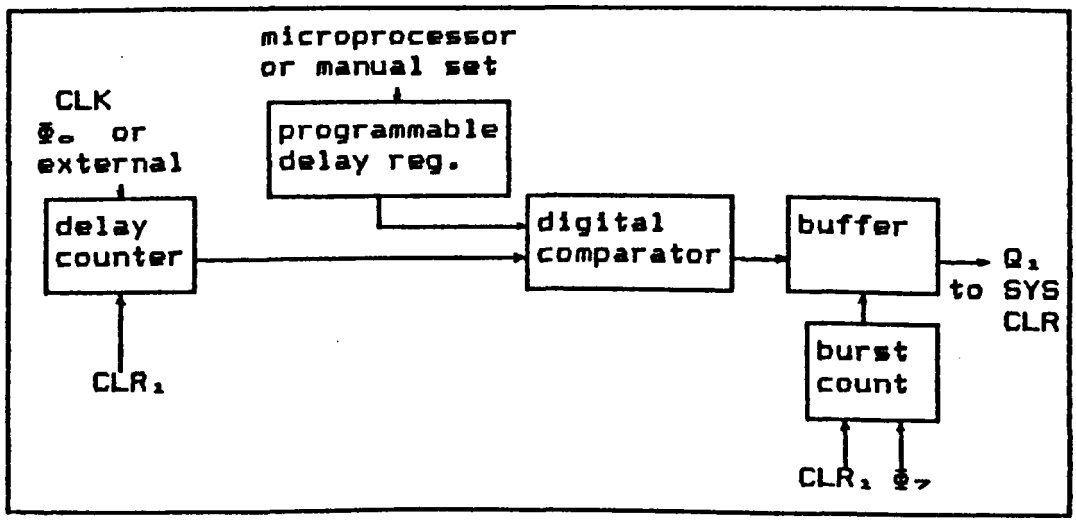

Fig. 4.3 Delay control

After the first burst is fired, this unit sends a halt signal to the SYS CLR, at the same time activating the internal delay counter. When the count value equals to that stored in the programmable delay register, a digital comparator is activated which removes the halt signal. A burst count section ensures that the halt signal is activated only after the first burst of every firing/processing cycle. The programmable delay register can be manually set to look at a particular section in space or continuously updated on every transmission by a microprocessor.

(b) CODE GENERATION

A unit is required to generate code sequences for transducer excitation and to provide a correlation reference. For finite length sequences, it is convenient to store them and read them out as required. Alternatively, though not applicable for Golay codes, codes such as m-sequences could be generated on-line using shift registers with appropriate feedback.

For permanent use the codes may be stored in an EPROM. But access times of EPROMs are too long to obtain code bit widths in the range selected in Chapter 3 (100-200ns). It is therefore necessary to use a fast access memory device during transmission. Thus, the code generation unit incorporates a loading section consisting of a standard EPROM and a generation section consisting of

a fast RAM. The actual code generation unit based on these concepts is shown in Fig. 4.4.

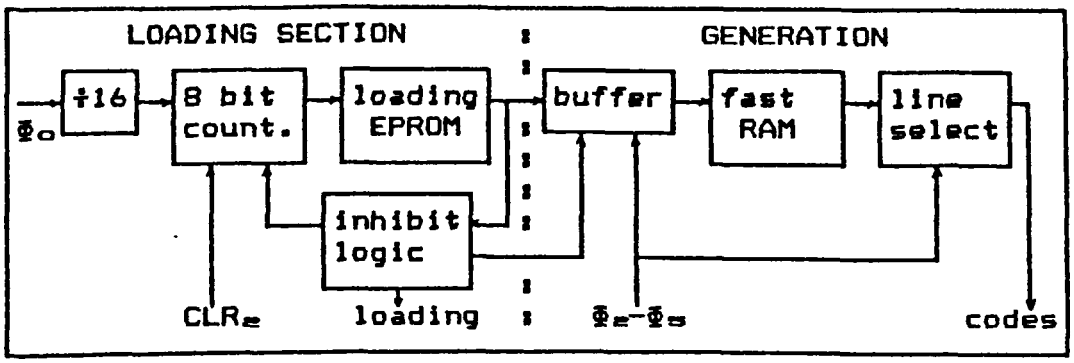

Fig. 4.4 Code generator

The operation is as follows:

On power up, the loading sub-unit resets the whole system via the SYS CLR ('loading' and CLR enabled), and down loads the codes stored in the EPROM on to a high speed RAM. After loading, the reset signal is removed ('loading' and CLR disabled) and the RAM addressing is passed to the TCU (via Φ_2-Φ_5). The output of this RAM is passed through a line select logic which selects the appropriate line of code and also ensures that the codes are latched only once per cycle. The codes are then passed to the selected transmitter buffers and the correlator reference channels.

(c) TRANSMIT/RECEIVE SECTION

On the transmitter side, as the system excitation is essentially digital, and low peak power operation is required, the utilisation of Advanced Schottky TTL line drivers for transducer excitation is proposed. Some possible problems may be identified, the first one being

capacitive loading and distortion as indicated in Chapter 3. However, as the output impedances of these drivers is only 25 Ω, there would be no problem in driving transducer devices with picofarad and low nanofarad capacitances. Additionally, the code duration is carefully selected to minimise the percentage distortion. A second problem may be that the TTL level output could prove to be too low for certain applications. Lastly, as these devices are designed for only 2 state operation with well defined limits, i.e. any level below 0.8V being interpreted as low while any level above 2V is high, a relatively high noise level is also apparent when considering their use for analogue operation. These devices are not designed for low noise analogue operation. For example, for the high and low level figures given here, noise levels of up to 400mV would not affect the digital operation while such noise margins are far too high for an analogue system.

On the reception side, it is necessary to maximise the SNR of the received signal and obtain sufficient gain before the data is passed to the digitisation and processing stages. Based on these considerations, the novel configuration shown in Figs. 4.5(a) and 4.5(b) has been utilised to maximise the transmitted power without requiring higher voltages and to maximise the SNR at the reception stage.

The transmitters are TTL buffers directly applied

across the transducer. The application of the excitation sequence and its inverse to both electrodes maximises the voltage difference seen by the transducer during rising and falling edges. The buffers are forced into a high impedance state during reception.

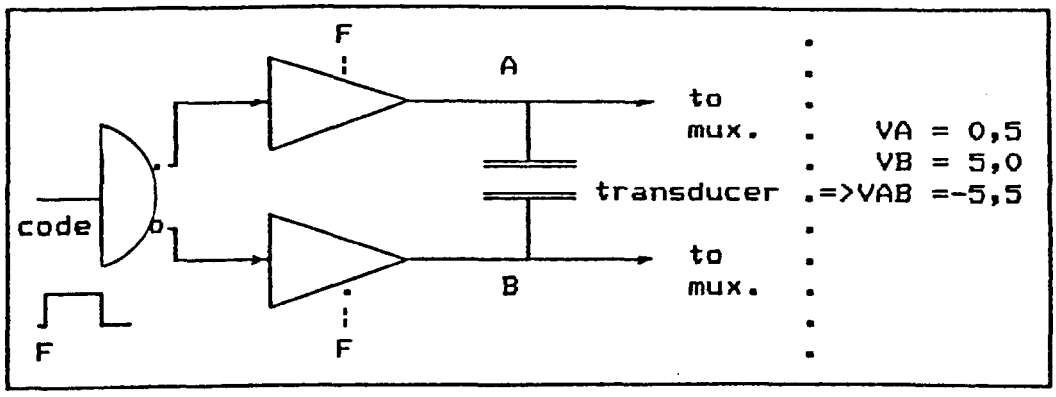

Fig. 4.5a Transmission

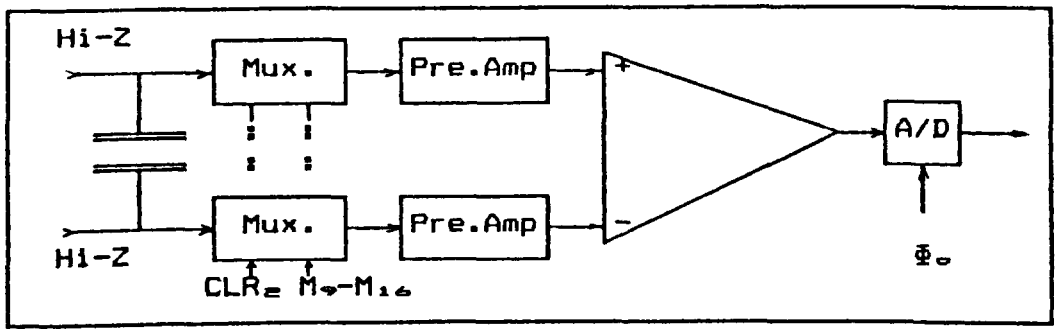

Fig. 4.5b Reception

The reception part consists of an analogue demultiplexer connected to each side of the transducer. The outputs of the demultiplexer are passed into buffer amplifiers with high input impedances followed by a high gain differential amplifier and a 6 bit analogue to digital converter. The differential detection and amplification rejects common mode system noise as explained in Chapter 3. Additionally, careful selection of

amplifiers with bandwidth just sufficient for the expected low MHz signal frequencies also contributes to the SNR improvement. In the present system, the combined amplification stage offers a voltage gain of up to 72 dB, with a common mode rejection ratio of the same order, for common mode voltages of up to a volt.

(d) PROCESSING

(1) Correlation and Weighted Summation

The core of the system is the correlation stage. Based on the arguments presented in Chapters 2 and 3, digital correlation has a number of advantages over analogue processing schemes. Hence, for the required on-line processing, dedicated devices with sufficiently high bandwidth to handle ultrasonic signals in the low MHz frequencies (i.e. capable of sampling rates of greater than 10 MHz) must be used. Additionally, for the same reason, they must be able to handle the entire reference code of 32-64 samples of single bit resolution, at the same time. The cross-correlation process thus involves multi-bit data (representing the analogue signals) and single bit code sequences. Therefore, to minimise hardware, multi-bit vs multi-bit or multi-bit vs single-bit correlators would be ideally suited. At the start of the project, the readily available and fastest device was the TDC 1023, a digital-in digital-out correlator (manufactured by TRW Ltd.). It offers sampling rates of up to 20 MHz while performing a 64 sample

cross-correlation. However, as it is capable of only single bit correlation, extra hardware is required to complete the operation. Firstly, as many correlators as the number of digitisation bits are required to complete the multi-bit operation, and secondly, an extra weighting and summing stage is required to form the combined score. With the development of high speed multi-bit and multi-sample correlators, it may in due course be possible to integrate the whole section described here into one chip.

The layout of the full section constructed for the present system and an expanded outline of the weighted summation configuration are shown in Figs. 4.6 and 4.7 respectively.

The first part consists of a bank of 6 digital correlators, one for each quantisation bit. These have been configured to work in XNOR logic, so that all bit agreements during the cross-correlation have a positive contribution to the overall sum while all disagreements have a negative contribution. The zeros in the binary codes must be considered to actually represent -1 so that 0 and 0 give 1 (-1 x -1 = 1). This is necessary to derive the self noise cancellation effect described earlier. However, for other applications the devices can be configured in AND logic, where agreements of 'low' bits is the same as a disagreement (1 and 0 is 0, 0 and 0 is also 0).

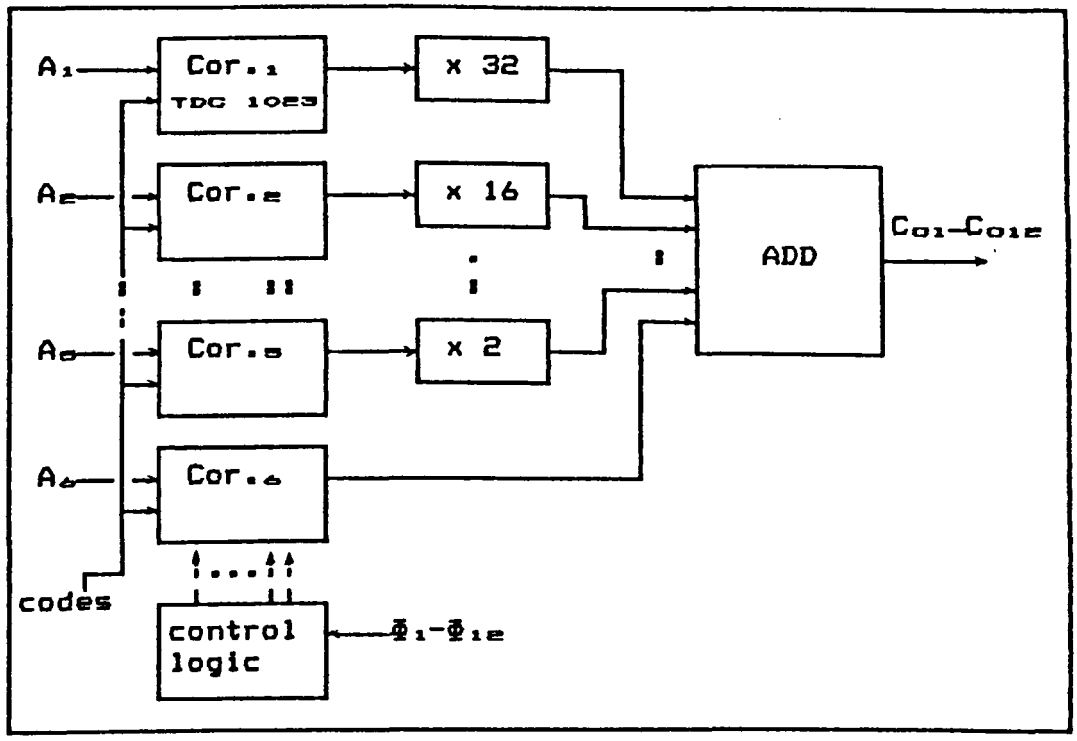

Fig. 4.6 Layout of correlation section

The 6 bit inputs arriving from the A/D converter are passed into individual correlators where they are continuously correlated with a double width 32 bit code which has been pre-loaded into the reference channel during transmission. The correlated outputs are then leftward shifted as they go into a three stage pipeline summer as shown in Fig. 4.7. The amount of shifting corresponds to the bit significance a particular correlator is handling. Loading and shifting of data is co-ordinated via a logic controlled by the TCU (Φ_1-Φ_{12}). Where speed is not important, it is also possible to use a single correlator with parallel/serial and serial/parallel interfaces.(A prototype system based on a single correlator had actually been constructed during an earlier

phase of the project in order to assess the device performance and develop design strategy for the new system.)

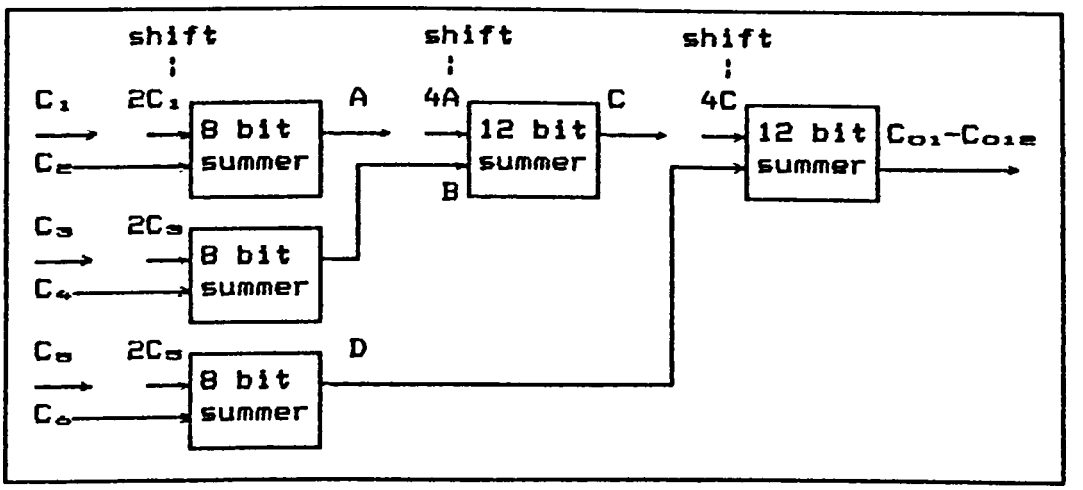

Fig. 4.7 Weighted summation

(2) Averaging and Summation

The processing is not complete at the correlation stage. Firstly, for self noise cancellation, the correlation integration must be carried out over two complementary codes. Secondly, it may be required to average the readings for better SNR. Two memory banks operating in alternate read/write modes were incorporated to achieve this purpose. One memory block reads out the previous sum for summation with the current correlation score while the other one writes the current sum. So, in effect all line scans are superimposed, thus averaging the results and cancelling out self noise as long as the number of superpositions is even.

Based on the idea of alternate read/write and sum, the unit shown in Fig. 4.8b has been constructed. Fig 4.8a

gives a general outline and is intended to assist in understanding Fig. 4.8b and its description. Fig. 4.8b shows major details.

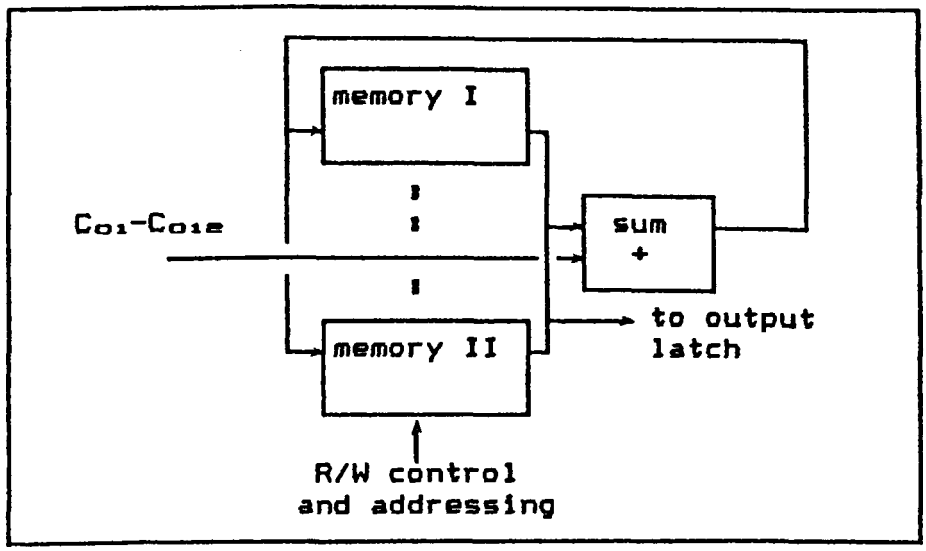

Fig. 4.8a General outline for averaging and summation unit

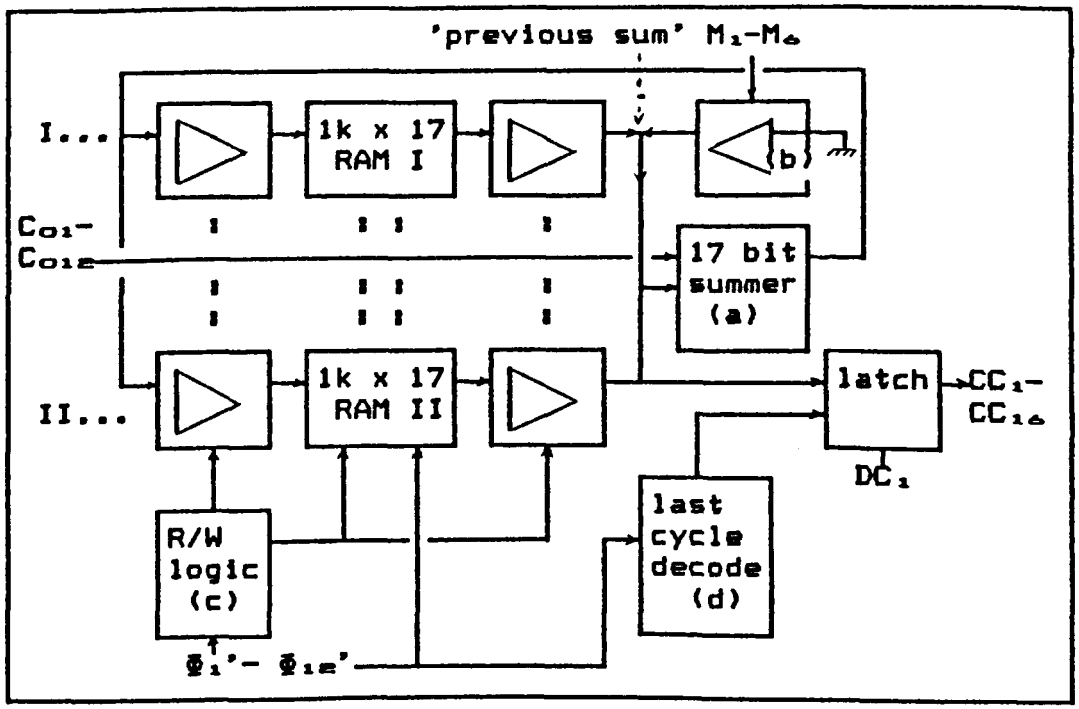

Fig. 4.8b Averaging and Summation

The correlated outputs (C_{o1}-C_{o12}) directly go into a 17 bit summer (a) to be added with the 'previous score' being read out by either memory I or II. The summed output is fed back as input to both memory blocks. The read/write logic (c) determines which memory block would be writing and which would be reading during a particular cycle. At the end of the required number of averagings, the 'last cycle decode' logic (d), activates an output latch and the result is read out (as CC_1-CC_{16}). As the first set of processed data arrives at the summer, the data on the 'previous sum' line would be erroneous as it is data from a from a previously processed channel. Thus, at the beginning, the first cycle is identified and the 'previous sum' line is forcibly pulled down by unit (b).

(e) OUTPUT INTERFACE

The sections described so far serve the purpose of obtaining a SNR enhanced series of digitised A-scan data. Apart from the relatively much higher SNR, the information contained in the processed output data is the same as that contained in any conventional pulse-echo system. Hence, any further application requires additional processing. If, as is the case here, the data is to be used for imaging, then the scan data from various elements must be collected and processed by the appropriate beamforming and image formulation algorithms. It may also be required to extract frequency information, by way of different filtering methods. Or, in the simplest case, the system

may be used for applications like thickness testing where only a direct A-scan display would suffice. Therefore, an interface unit is required to link the data acquisition system to a host computer or display system. A direct memory access technique is preferred to obtain high data transfer rates. The output interface unit designed here (Fig. 4.9) is intended to link the system with an IBM PC-AT. Also included is a simple passive digital to analogue converter for direct display of the scan data. To maximise the transfer rate, and at the same time avoid the need to use a large system memory, the scan data for each element is transferred while data for a subsequent element is being acquired and processed. The outline of the output interface unit is shown in Fig. 4.9.

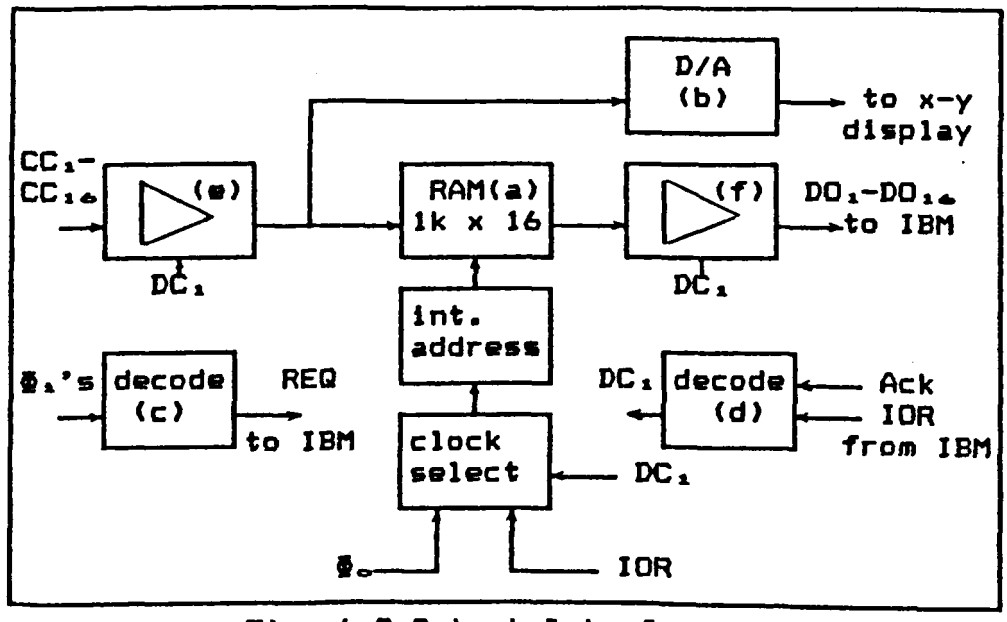

Fig. 4.9 Output Interface

The operation may be described as follows. At the end of the processing of one channel, the processed

outputs (CC_1-CC_{14}) are passed to a buffer RAM (a) for temporary storage. They are also passed to a passive digital to analogue converter (b) for direct display. Soon after the data is written into the RAM, a decode logic (c) sends a data transfer request signal to the IBM (REQ active), which in turn responds by sending back an acknowledge (Ack) and input/output read (IOR) signals. These are decoded by unit (d) to generate an internal data transfer control signal (DC_1). When DC_1 is inactive, it means that no transfer is taking place but new data is being written to the RAM. During this time, the RAM addressing is controlled by the system (via Φ_D). On the other hand, when DC_1 is active, the input buffers (e) are disabled, the output buffers (f) are enabled and the RAM goes into a read mode with its addressing controlled by the IBM direct memory access controller (via IOR). The data in the buffer RAM is then directly passed on to the IBM memory (as DO_1-DO_{14}). The set up program for the IBM DMA controller may be found in APPENDIX E.

(f) <u>OVERALL OPERATION</u>

The sections described so far are combined to form the system shown in Fig. 4.11.

The overall operation may be summarised as follows.

On power up, the code loading unit takes control and two 32 bit Golay codes are down loaded on to a high speed RAM. When the loading is over, control is passed to the timing and control unit which opens the appropriate

channel and sends addresses and command signals back to the code generation unit. One 32 bit code is then latched out and directly applied to the transducer at the selected channel via TTL buffers. At the same time the code is also loaded into the reference registers of the correlators.

After the first burst is transmitted, the entire system is halted by the delay control unit for a time that is equivalent to a selected return echo sequence. This sequence or 'scan packet' is 1024 samples long and may be offset by the delay controller which initiates the starting point of the data acquisition. The A-scan representation is outlined in Fig. 4.10.

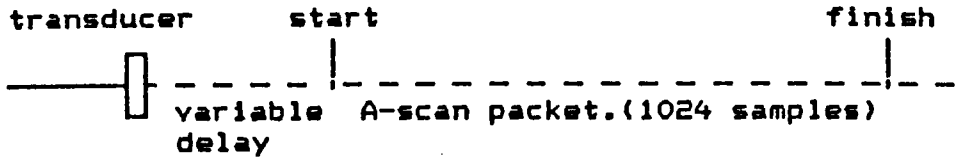

Fig. 4.10

After the required delay, the reception and processing begins. Incoming signals on the same transducer are passed through an analogue demultiplexer, a low noise amplifier and a 6 bit analogue to digital converter. The 6 bit data samples are fed into a bank of digital correlators where they are continuously correlated with the pre-loaded replica of the code. The correlated outputs are then weighted according to their bit significance, summed and stored in the in the output memory block. This is succeeded by a repetition of the

entire process for the complementary 32 bit code, its result being superimposed on the first one. The process described up to here constitutes one complete processing cycle, after which there are two optional procedures.

1. If the SNRE achieved in one cycle is assumed to be sufficient, the data is latched out to the output interface unit or directly displayed. If an array is being used, the system then proceeds to the next channel.

2. If more SNRE is required, the entire process is repeated on the same channel(transducer) up to a maximum of sixteen times, each successive result being superimposed on the previous one. The final result is then latched out after which the system proceeds to the next channel.

During the processing of the next channel, the result of the earlier one is passed on to an IBM-PC by the output interface unit using direct memory access.

Some major specifications of the hardware system are detailed in APPENDIX A.

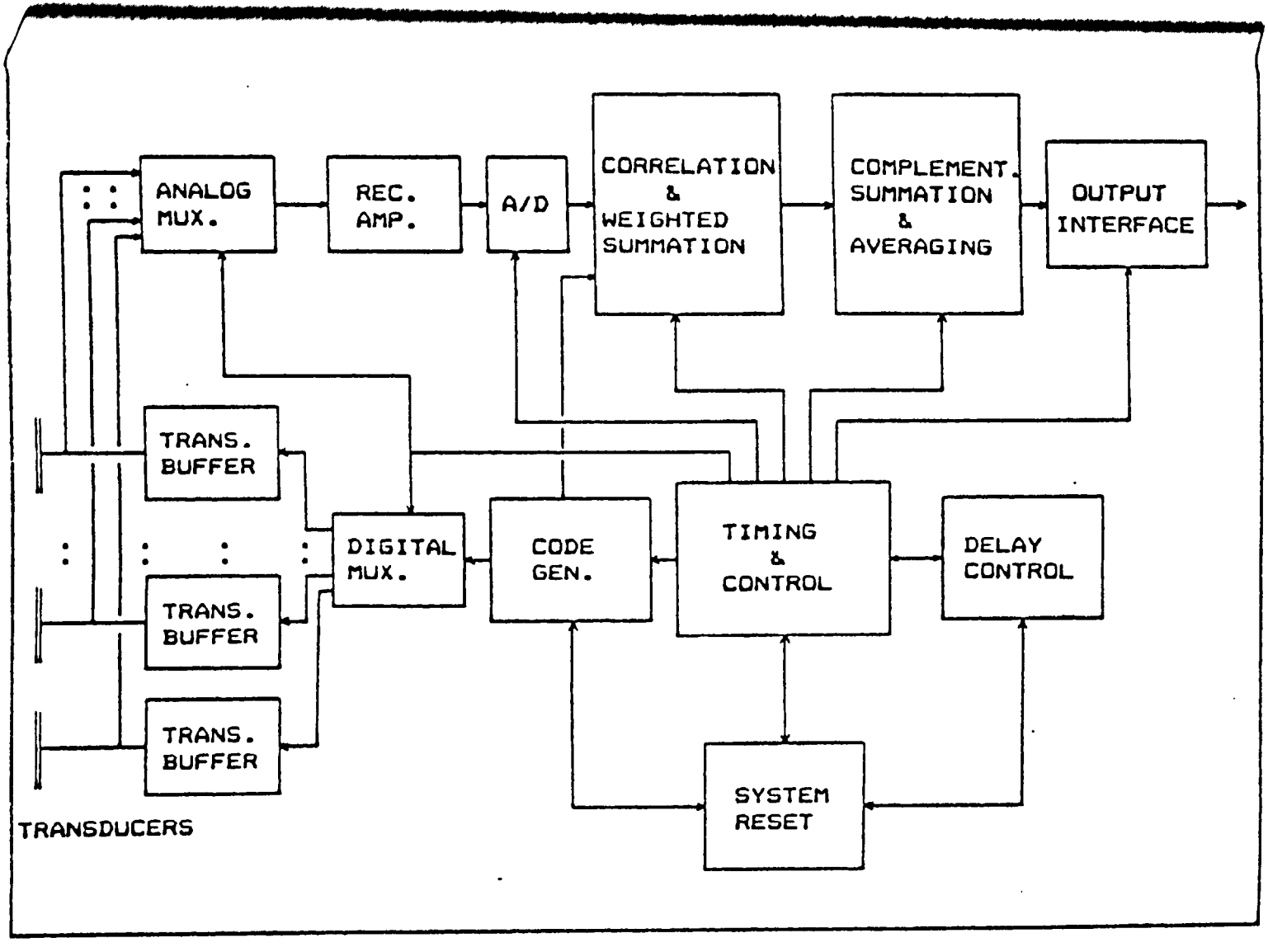

Fig. 4.11 Block diagram of the digital correlation system.

4.3 SYSTEM PERFORMANCE

In the first part of this section, the performance of the various hardware sub-sections described earlier is traced. Oscilloscope pictures of the signals at the main stages of the hardware are shown to illustrate the operations taking place. The second part demonstrates a few typical examples of the system performance under low SNR situations. A comparison is made with conventional pulse-echo operation at a higher peak excitation and similar input SNR as the system. The system is shown to be virtually immune to input noise levels that in the conventional case would result in signal to noise ratios that are well below 0 dB.

Additionally, the experimental results are compared with simulated results obtained using a digital correlation simulation package. The simulations are shown to predict accurately the measured pulse-echo responses. (A flowchart of the simulation package may be found in APPENDIX B.)

All pulse echo measurements are conducted in a water tank using a planar glass reflector positioned in the far field as target. The transducers used in the experiments are a 30mm diameter disc transducer with a centre frequency of 1 MHz (referred to as Transducer #1) and small array elements with centre frequencies of 1 MHz and 1.7 MHz (referred to as Transducers #2 and #3

respectively). The electromechanical parameters of these probes are detailed in APPENDIX C. In all cases the system sampling and processing rate used is 12 MHz. Additionally, the full 16 cycle averaging is used.

4.3.1 Operations of Sections

This section illustrates the transmission, reception and processing characteristics of the system using transducer #1 as transmitter and receiver.

In the first set of photographs, (Fig.4.12a and 4.12b) one of the 32 bit excitation code sequences (top trace) and its inverse (bottom trace) are shown as seen at the output of the line drivers used for transmission. In Fig. 4.12a, the TTL line drivers are unloaded so that no noticeable rise time effects appear in the sequence. Fig.4.12b proceeds to show the same traces, but after the drivers are loaded with transducer #1. As this transducer possess a 1.2nF static capacitance, a loading and distortion effect is apparent.

The second set of photographs (Fig.4.13a to Fig.4.13c) illustrate the three stages in the reception section. Fig. 4.13a shows traces of the receiver input and the output of the first pre-amplifier stage. A section of the received scan corresponding to a weak reception was selected as shown on the top trace. A fair amount of amplification and noise reduction is achieved in the first stage. In Fig. 4.13b, the outputs of the pre-amplifier and

differential amplifier stages are compared. The much better SNR of the differential amplifier output (bottom trace) suggests that most of the noise in the receiver input is common mode. Finally, Fig. 4.13c shows the output of the amplification section and that of the digitiser (bottom trace). The digitiser output waveform is obtained by passing the 6 bit data samples through a passive digital to analogue converter (DAC) (based on an R-2R resistive ladder). The received signal is observed to be reproduced fairly well. The very slight non linearity in the digitiser output is a result of resistance value errors in the DAC.

The output of the processing unit is shown in Fig. 4.14. As expected, the signal at this stage exhibits the sidelobes that arise when a single finite code length is used in the correlation process. The summation process of multiple cycles in the averaging section is outlined in Fig. 4.15. The process is observed using a 16 bit DAC. The increments show the successive superposition of the line scans. Each line scan consists of 1024 samples, sampled at a 12 MHz rate. The final averaged sum (top of the steps) is read out at a 750 KHz rate and hence appears longer than the preceding scans.

The final output of the system for transducer #1 is shown in Fig. 4.16. As this is averaged over the complementary code pair, it may be observed that the self noise that appeared in Fig. 4.14 has been considerably

reduced, thus verifying the sidelobe cancellation property of the system.

In the output interface unit, each sample which is written into the buffer memory is immediately read out for verification. This write/read operation is shown in Fig. 4.17 in conjunction with a trace obtained by connecting a DAC at the memory data input/output terminals. Finally, a plot of the output data transferred to an IBM-PC is shown in Fig. 4.18. A comparison of this figure with the oscilloscope picture of the output shown in Fig. 4.16 verifies the proper operation of the DMA transfer.

In section 3.3.3 (a) of Chapter 3, a technique for reducing non-common mode but correlated noise was suggested. The effect of such noise on the system output is shown in Fig. 4.19a while the improvement achieved by using the cancellation technique is shown in Fig. 4.19b. The photos concentrate on the initial part of the A-scan, which contains main bang and multiplexer switching effects in addition to coherent clock noise. It may be observed that the cancellation method has resulted in the significant reduction of these effects.

The last three photos (Fig. 4.20a to Fig. 4.20c) were results obtained using an earlier single correlator module, constructed to assess the performance of the digital correlator devices (TDC 1023). They show the autocorrelation and summation in hardware of Golay codes. The opposing sidelobes and the cancellation on summation

are clearly evident. With these results, among others, the applicability of the dedicated devices for the planned system was established.

4.3.2 SNR Performance

In this section, firstly, the SNR performance of the system is compared with that of a conventional pulse-echo system by deliberately creating a low SNR situation. Secondly, it is verified that the system is operational for use with small array elements with parameters and dimensions typical to those used for imaging applications. Simulated results are included to back experimentally measured responses.

For the comparison with a conventional pulse-echo operation, the disc transducer used earlier (transducer #1) is selected, as the relatively wide surface area makes it possible to achieve a suitable reflection signal. The simulated transmit/receive impulse response of this transducer and the expected correlation system output are shown in Figs. 4.21 and 4.22.

The response in conventional pulse-echo operation (Fig.4.23) was measured using a step excitation of 60 volts from a standard pulser unit to drive the probe. To investigate the performance under low SNR conditions, a 0.1Vrms white noise from a random noise generator was introduced into the input stage of the receiving amplifier. Such level of noise is found to result in an

output SNR of just under unity, as shown in Fig. 4.24. The transducer was then connected to the correlation system and the same level of noise was introduced at one of the receiver input terminals. The resultant output of the system (Fig. 4.25) shows very little difference from the external noise free output shown in Fig. 4.16 of the previous section. Thus, the high SNR supeiority of the system is verified. It is also important to note that the correlation system operated at one twelfth of the peak excitation used in the conventional system (i.e. 5 volts vs 60 volts).

The system pulse-echo measurements were repeated for two small array elements (transducers #2 and #3) to investigate if the SNR performance is valid under practical operating conditions with very weak receiver signals. The expected ideal outputs for the two elements are shown in the simulated plots of Figs. 4.26 and 4.27.

The influence of extraneous noise in the present system may be observed in Fig. 4.28 which depicts the transmit/receive echo burst of element #3 prior to processing. The measured responses after processing are shown in Figs. 4.29 and 4.30 for transducers #2 and #3 respectively. Again, the system exhibits an excellent SNR performance. Additionally, as in the case of the disc transducer, very good agreement between the simulated and experimentally measured output responses may be observed.

4.4 CONCLUSION

This chapter has given the general outlines and functional description of the various hardware modules of the digital correlation system. A sample input to output trace was shown to assist in understanding the operations taking place. Through sample experimental results, it has been shown that the system is operational over a wide variety of probe configurations and input signal to noise ratios. Additionally, for a low input SNR situation, the correlation system has been shown to be far superior than a conventional pulse-echo system. In general, the results conclusively validate the sound theoretical basis of the system detailed in Chapters 2 and 3. Most importantly, it has been established that ultrasonic data acquisition at less than 5 volt transducer excitation is possible, without having to sacrifice SNR. It is believed that such power reduction will widen the application areas of ultrasonic testing.

At present, the system is built on 6 standard eurocards. Future improvements are likely with the development of higher capacity TTL devices. The development of multi-bit vs multi-bit correlators, wider capacity fast memory devices and summers could considerably cut down the amount of hardware. It may also, in due course, be possible to integrate the entire system into a single special purpose processor.

The system's performance with regards to resolution is investigated in the next chapter.

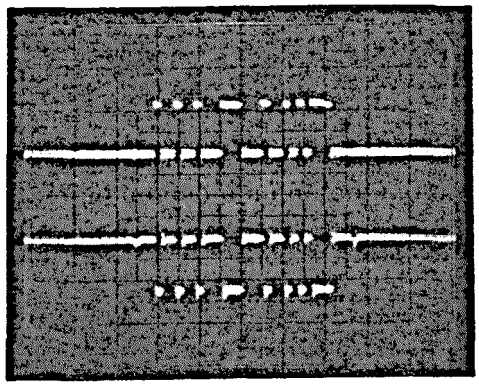

(a) unloaded

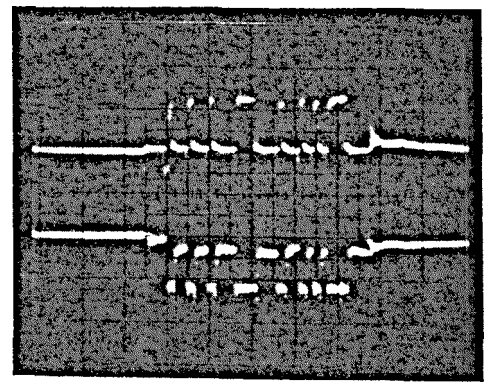

(b) loaded

Fig. 4.12 An excitation code sequence and its inverse as seen at the outputs of a TTL line driver. (x=.1μs/div, y=4v/div)

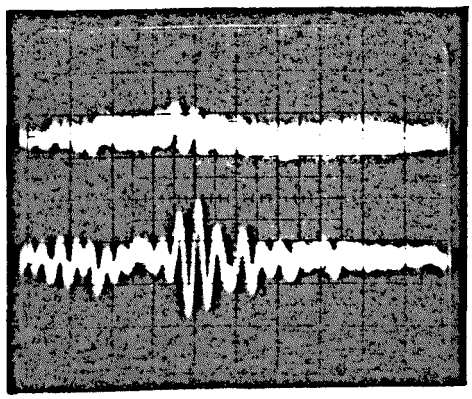

Fig. 4.13a
Receiver input and pre-amp output. (x=2μs/div, y_1=.02v/div, y_2=.04v/div)

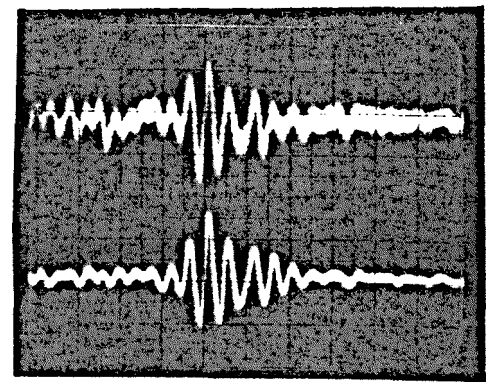

Fig. 4.13b
Pre-amp and differential amp. outputs. (x=2μs/div, y_1=.04v/div, y_2=.4v/div)

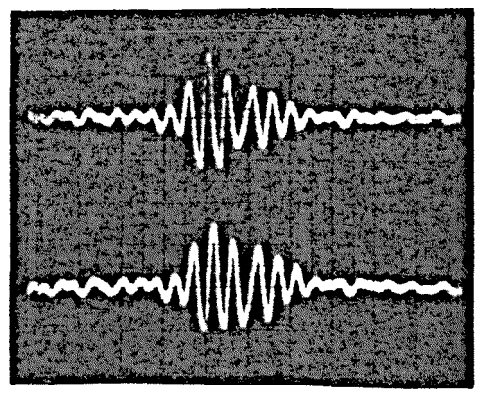

Fig. 4.13c
Differential amplifier output and digitised and reconstructed waveform.
(x=2μs/div, y_1=.4v/div, y_2=.4v/div)

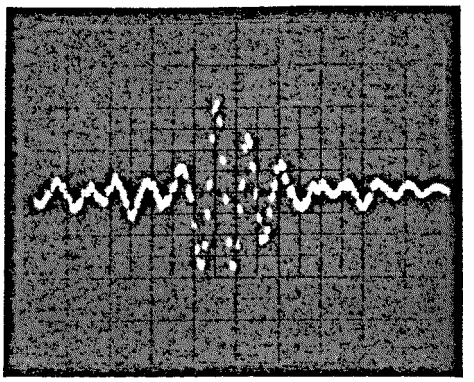

Fig. 4.14
Output of processing unit for one code.(750 KHz display, x=20μs/div, y=.1v/div)

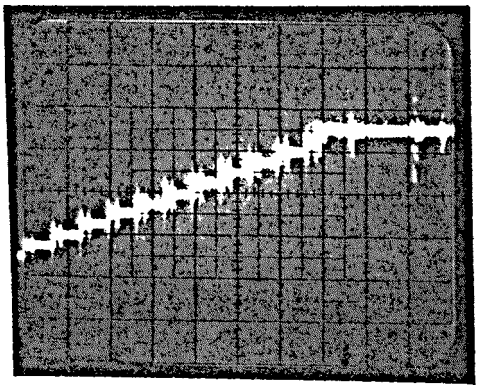

Fig. 4.15
Successive line scan additions in averaging section.(x=.04μs/div y=.2v/div)

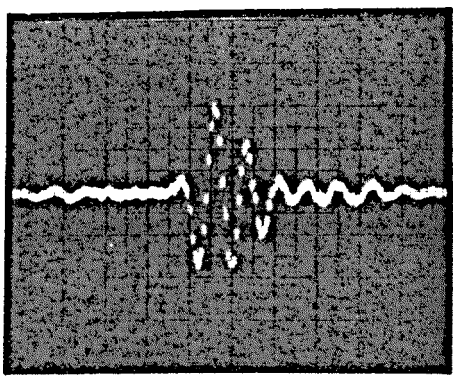

Fig. 4.16
Final averaged output. (750 KHz display, x=20μs/div, y=.1v/div)

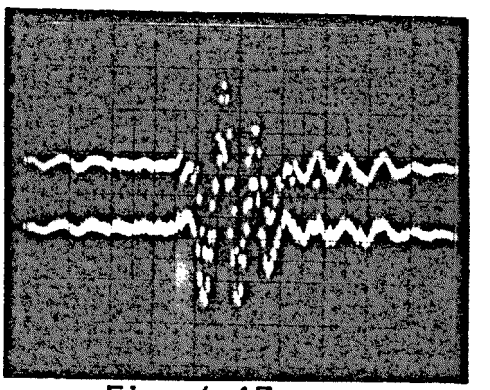

Fig. 4.17
Memory write/read operation in output interface unit. (750 KHz display, x=20μs/div, y=.1v/div)

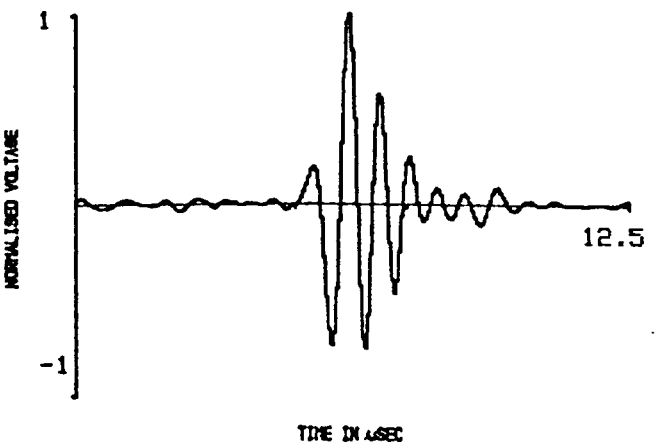

Fig. 4.18 DMA transferred data, transducer 1.

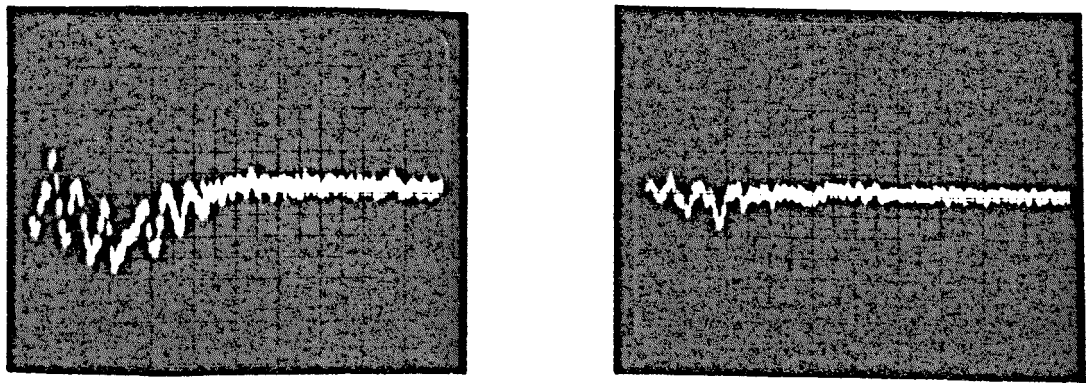

(a) before (b) after

Fig. 4.19 Initial part of A-scan before and after applying non-common mode noise cancellation technique.(x=20μs/div, y=.1v/div)

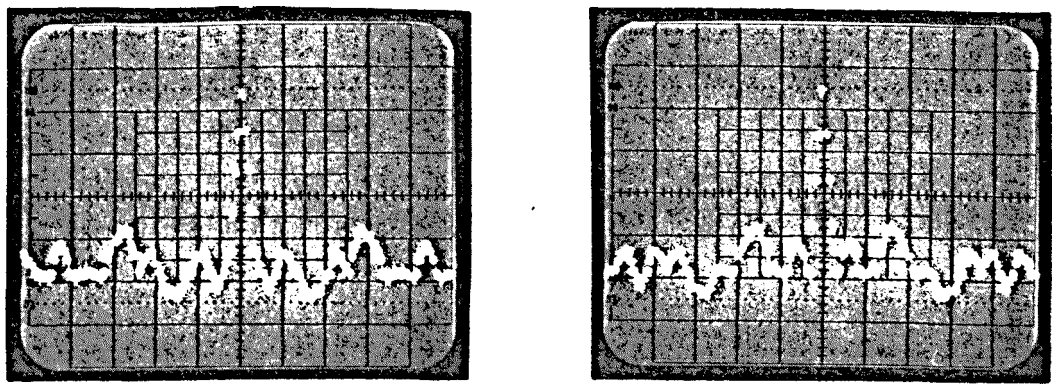

(a) code 1 (b) code 2

Fig. 4.20 Autocorrelations of 16 bit Golay codes. (x=.5μs/div, y=1v/div)

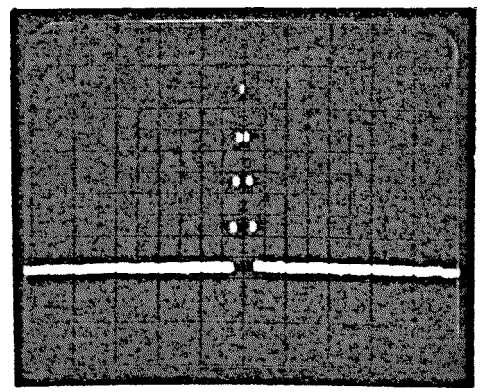

Fig. 4.20c The sum of autocorrelated Golay codes. (x=.5μs/div, y=1v/div)

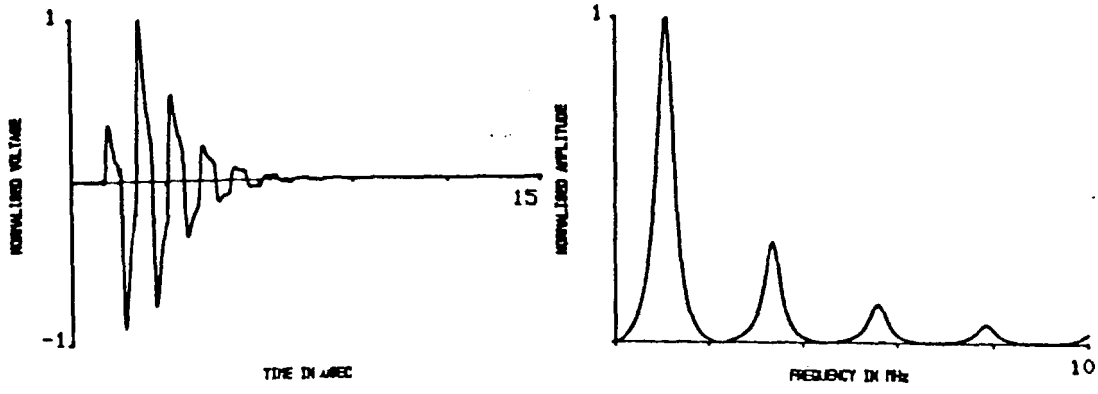

(a) time domain (b) amplitude spectrum

Fig. 4.21 Simulated transmit/receive impulse response of transducer 1.

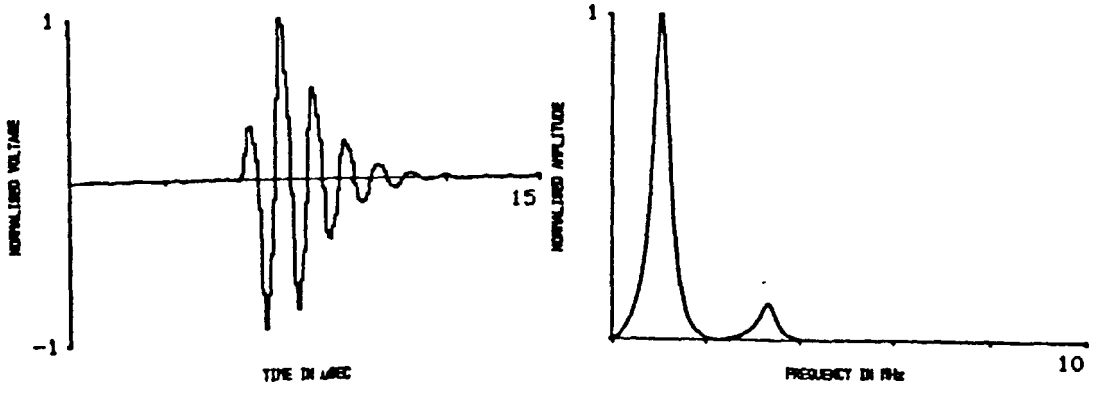

(a) time domain (b) amplitude spectrum

Fig. 4.22 Simulated correlation system output for transducer 1.

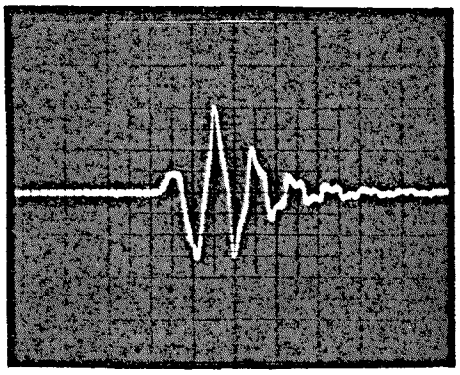

Fig. 4.23 Output of conventional pulse-echo system for transducer 1. SNR > 50 dB. (x=2μs/div, y=.4v/div)

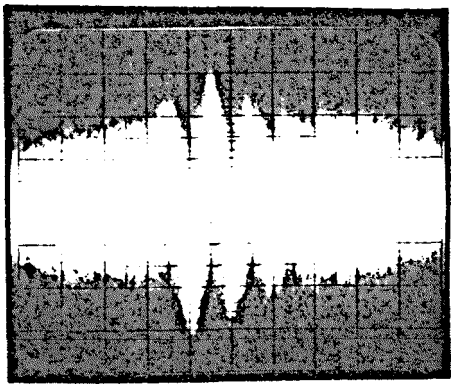

Fig. 4.24 Output of conventional pulse-echo system for transducer 1 with low input SNR. SNR < 0 dB.(x=2μs/div, y=.4v/div)

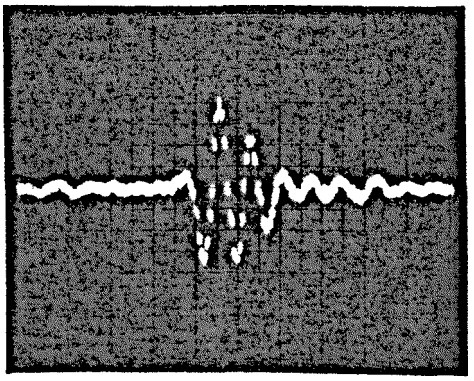

Fig. 4.25 Output of correlation system for the same input SNR as Fig. 4.24.(750 KHz display) (x=20μs/div, y=.1v/div)

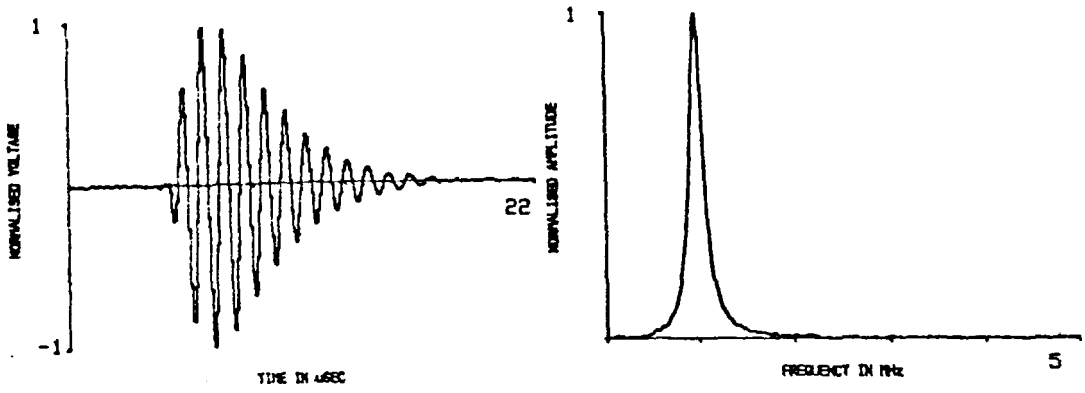

(a) time domain (b) amplitude spectrum

Fig. 4.26 Simulated correlation system output for transducer 2 (1 MHz array element).

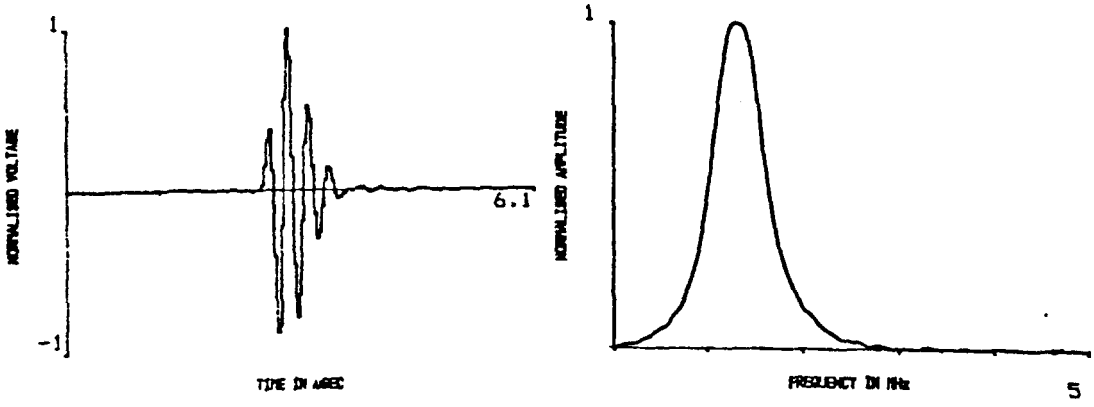

(a) time domain (b) amplitude spectrum

Fig. 4.27 Simulated correlation system output for transducer 3 (1.7 MHz array element).

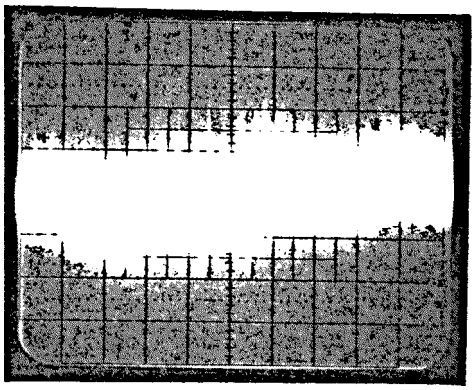

Fig. 4.28 Receiver signal for transducer 3.
(x=2μs/div, y=.01v/div)

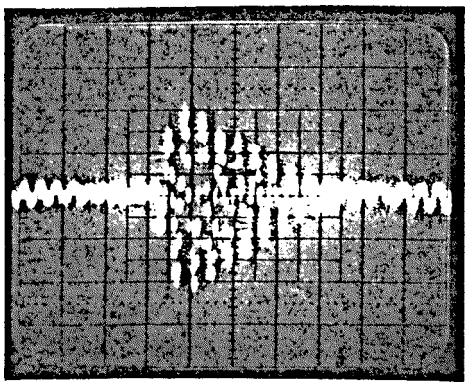

Fig. 4.29
Correlator output for
transducer 2.
(750 KHz display)
(x=40μs/div, y=.1v/div)

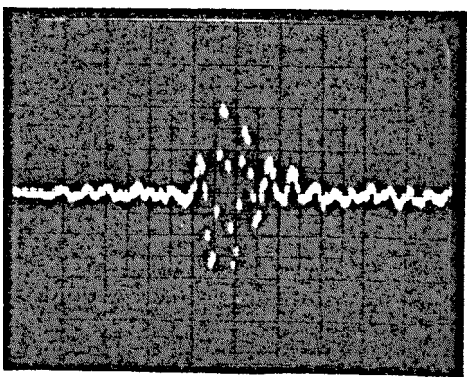

Fig. 4.30
Correlator output for
transducer 3.
(750 KHz display)
(x=20μs/div, y=.1v/div)

CHAPTER 5

CHAPTER 5

ALTERNATIVE IMPLEMENTATION

5.1 INTRODUCTION

The earlier implementation of the correlation scheme involved directly applying the driving code sequences to the transducer and cross-correlating the received signals with a delayed replica of the codes. It has been shown that due to the properties of the codes, the resolving capability of the system is, as in any conventional pulse-echo system, limited by the duration of the transducer impulse response. The applied code sequence, which generally has a wider bandwidth than the transducer, is bandlimited by the transducer impulse response function. For example, consider a 2 MHz probe with, say, a three cycle pulse. If a wide band excitation function is applied to this probe, the pulse derived will have a duration(T) of 1.5μs (3 x 1/f). Considering a sound propagation velocity(v) of 1.5mm/μs, the best resolution in water using this probe for pulse-echo measurement would be in the order of 1.12 mm (v x T/2).

In order to improve the resolution capability in a conventional system, deconvolution methods have been extensively investigated [36]. Algorithms have been developed for resolving multiple layers with spacings in the order of a wavelength in the propagation medium. One aspect of such investigation has involved the development of post-filtering techniques based on the transducer's

modelled or measured characteristics. As an alternative, a pre-filtering approach has also been proposed, where the filtering is performed at the transmission stage instead of performing it on reception [34,36]. This involves modifying the excitation function to derive a desired transmit/receive response from the probe. Hence, pulses with shorter duration may be derived from a given probe, improving the system resolution. An additional obvious advantage of pre-filtering as opposed to post-processing is that real time data acquisition and display would be possible.

This chapter considers the feasibility of combining pre-filtering with the correlation scheme. If the transducer is excited by an appropriate pre-calculated waveform in order to relatively enhance certain spectral components and suppress others so as to derive the required code sequence, the cross-correlation process on the reception side will result in a triangular pulse characteristic of the pseudo-random codes. Hence, such an approach has the potential of combining both signal to noise ratio and resolution enhancement.

The possibility of deriving pseudo-random code sequences from a transducer has been demonstrated by SUNG [19]. However, the approach used utilises a multiple layer stacked probe assembly, such that the output is derived as a result of the mechanical structure and not as a result of the nature of the excitation. The approach is therefore

inflexible and suitable only for the particular design sequence. The pre-filtering approach proposed in this context would theoretically work with any sufficiently wide band probe and moreover can be extended readily to comprise a range of code sequences.

In the following section, the spectral division technique used for generating the inverse filters is briefly reviewed. Simulated and experimental results for generating 8 bit Golay code sequences in water are then presented. This is followed by further software processing of the generated waveforms including cross-correlation, summing and high pass filtering.

As this approach is basically intended to improve on resolution limits arising from the transducer bandwidth, it is also useful to look at the correlation system performance in the situation where the transducer is not the bandwidth limiting factor; that is, when it possesses a wider bandwidth than the excitation code sequences. Therefore, in the final section, simulated and experimental pulse-echo responses obtained from a 10 MHz PVDF probe with a -3dB bandwidth of 6MHz are presented.

5.2. THE SPECTRAL DIVISION METHOD

The technique used for generating the driving filter function is known as spectral division [34,36]. The output of a linear system is the convolution of its impulse response with the input function. This process may be reversed;i.e. the input may be calculated by deconvolving

the output with the system impulse response. Both the forward and reverse computations are simpler to implement in the frequency domain, where the convolution operation simply becomes a multiplication of the respective spectra and the deconvolution becomes a division. This is illustrated in Fig. 5.1.

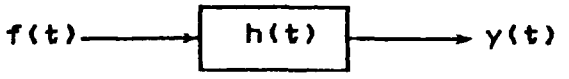

Fig. 5.1 Representation of a linear system

In time domain,

$$y(t) = f(t) * h(t) \qquad \ldots 5.1$$

$$f(t) = y(t) \underline{*} h(t) \qquad \ldots 5.2$$

Where, $\underline{*}$ is used to denote deconvolution.

Or in frequency domain,

$$Y(f) = F(f) \times H(f) \qquad \ldots 5.3$$

$$F(f) = \frac{Y(f)}{H(f)} \quad (H(f) \neq 0) \qquad \ldots 5.4$$

The spectral division method is simply an implementation of eqn. 5.4. For the particular application of generating desired waveforms from a probe, h(t) represents the combined impulse response of the transducer/amplifier system. Y(f) is the spectrum of the required output and F(f) is that of the input. F(f) is alternatively referred to as the inverse filter, as it is purposely used to selectively reject or enhance frequency components of H(f). Inherent in the spectral division approach is the assumption that the transducer response is spatially invariant. Should the transmit/receive impulse

response significantly vary with position, it would be necessary to re-calculate the inverse filter for each position of the transducer and reflector (or transmitter and receiver).

It may be observed from eqn. 5.4 that at zeros in H, corresponding to poles in F, there would be no solution for f(t). One commonly used approach for tackling this problem involves the use of a modified impulse response spectrum in which a certain threshold is applied on the original spectrum below which all values will be quantised to that level [34].

A modified spectrum $H_1(f)$ may be defined as follows:

$$|H_1(f)| = |H(f)| \quad (H(f) > c)$$
$$= C(f) \quad (H(f) \leq c) \qquad \ldots.5.5$$

Where, c is a suitable amplitude threshold and C(f) is the spectrum of the threshold function. These appear as shown in Figs. 5.2a to 5.2c.

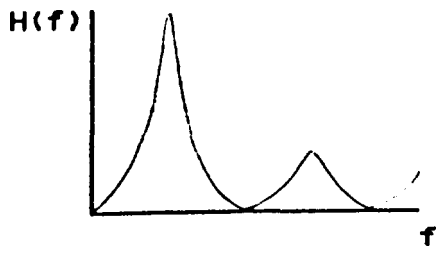

Fig. 5.2a Unmodified Spectrum

Fig. 5.2b Threshold function

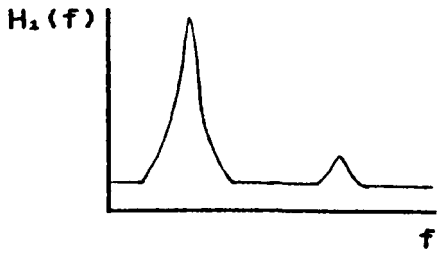

Fig. 5.2c Modified Spectrum

Thus, the spectrum used in the division will be the modified version ($H_1(f)$) of the actual impulse response spectrum ($H(f)$). It should be noted that it is only the amplitude and not the phase spectrum that is modified. The threshold, c, is selected on the basis of the level of external noise in the transducer bandwidth. To ensure stability in the inverse filtering process, it is necessary to consider not only the zeros but also the low amplitudes in the pass band of H which may be affected by external noise spectral components. The choice of the particular threshold value is made by a trial and error process in which it is attempted to select the minimum possible level that is just greater than the peak of the system noise spectrum. Based on such trial and error, for the particular probe used here (response shown in Fig. 5.3b), a threshold level of -40dB to -50dB from the peak of the transducer response, which assumes a peak signal to peak noise spectral component ratio of 100 to 320 was found to be sufficient. For the general case, it is also necessary to consider high frequencies where the spectral components introduced by the threshold become relatively large compared to those of the transducer response. Due to the wide bandwidth of the probe used here (Fig. 5.3b), a threshold level of -40dB to -50dB is also sufficiently low so as not to cause significant errors up to about 20 MHz (where the threshold will still be -20dB to -30dB down from the peak of the transducer response harmonics).

5.3 SIMULATED AND EXPERIMENTAL RESULTS

The selected test method for investigating the feasibility of incorporating a pre-filtering approach with a correlation system involved the generation of an 8 bit Golay code pair from a probe with a 1 MHz centre frequency. The electromechanical parameters of the probe are outlined in APPENDIX C (Transducer #4). A spectral division software routine which operates according to the principles outlined earlier was modified to include the generation of 8 bit codes, with a bit width corresponding to half a period of the transducer response. Thus, for the 1 MHz probe, the expected bit width would be 0.5 μs. Theoretically, this size of code would provide an SNRE in the order of 9 dB. The actual code sequences are,

$$G_1=(1,1,-1,1,1,-1,-1,-1) \qquad ....5.6a$$

$$G_2=(1,1,1,-1,1,-1,1,1) \qquad ....5.6b$$

On the other hand, the best resolution (after correlation) from such a size of code, would be 0.75mm in water or 3mm in steel. From the characteristics of the probe shown in Fig. 5.3a, it may be observed that this constitutes approximately a four fold improvement in resolution, as the probe response pulse length is in the region of 4-5μs. Hence, the transducer resolution capacity without any data processing is limited by the impulse response duration.

The modelled probe impulse response data (H) is used as an input to the spectral division software together with a specification of the parameters of the codes to be generated. For the present application, the use of modelled impulse response data has some important advantages over the use of measured data, although the latter is more usual. Firstly, it has been shown that in the generation of wide band profiles such as square waves, simulated data provides a relatively wider bandwidth for the inverse filter design process resulting in more accurate profile generation [35,36]. This is because the measured data is, in most instances, filtered by the measurement system. This filtering effect by the measurement system may be observed by comparing Fig. 5.3b and 5.3c which show the modelled and measured impulse response spectra of the transducer used in the present experiment. It is necessary to consider this factor here because pseudo-random binary codes are generally wide band. Additionally, the use of modelled data is faster and more flexible since modifying it in software for different positions of transmitter and receiver (or transmitter and reflector) as well as different transmit/receive circuitry is easier and faster than making repeated experimental measurements of the impulse response. Finally, provided that the transducer parameters are accurately known, the use of modelled data offers the

advantage of being free from the additional experimental errors that are likely to arise in the measurement process. These include errors such as those arising from extraneous system noise as well as inaccurate probe positioning. Attempts to initially use measured data for this experiment were in fact unsuccessful, most likely due to the bandlimitation discussed earlier.

Thus, inverse filters (F_1 and F_2) are calculated for generating the two sequences as expressed by eqns. 5.7a and 5.7b.

$$F_1(f) = \frac{G_1(f)}{H(f)+c} \qquad \ldots.5.7a$$

$$F_2(f) = \frac{G_2(f)}{H(f)+c} \qquad \ldots.5.7b$$

The first phase of the hardware implementation involves the downloading of the required driving waveforms on to an emitter coupled logic (ECL) based programmable waveform generator. The waveform generator is capable of providing a data repetition rate of up to 700 Hz and an output sampling rate of up to 50 MHz; both factors being user selectable. Its output is amplified by a suitable RF power amplifier (12 MHz bandwidth) for application to the transmitting probe. A wide band PVDF membrane hydrophone placed 20mm away is used for reception. The PVDF hydrophone used for this purpose is chosen as it possesses a relatively flat bandwidth from 0.05 MHz to over 20 MHz if used with a high input impedance amplifier and hence

would have no significant filtering or distortion effect on the transmitted pressure wave characteristics. The signals received by the membrane hydrophone are amplified, digitised, passed on to an IBM P.C. through a GPIB interface and further passed on to a VAX computer for additional processing. The entire experimental set up for waveform generation and data acquisition is outlined in Fig. 5.4.

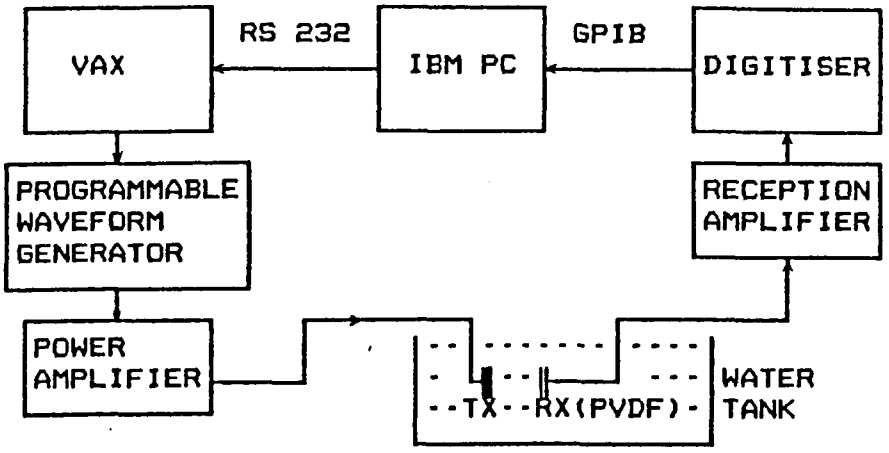

Fig. 5.4 Outline of set up for pre-filtering experiment

The simulated and experimental results obtained are presented in Figs. 5.5 to 5.9. To assist in comparison, simulated and measured responses are shown on the same diagrams with different line types.

The theoretically expected profiles are generated in software by convolving the calculated inverse filter function by the transducer impulse response. These are then verified experimentally using the apparatus described

above. The first set of figures (Fig. 5.5a and Fig. 5.5b), illustrate the ideal codes, the theoretically expected outputs and the experimentally measured profiles respectively. It may be observed that at least as far as the phase information is concerned, the measured outputs show reasonable performance. Low frequency radial modes currently not predicted in the modelling process as well as diffraction effects are two most likely reasons for causing both the amplitude and the limited phase errors. It should be noted that in the waveform generation of binary codes, accurate reproduction of phase is more crucial than amplitude. As the amplitude can only have two levels, it may easily be reconstructed on reception based on the phase information. The use of comparators on reception is one possibility for reconstructing the amplitude information. Furthermore, it should be stressed that ultimately, in such a system, the desired information exists in the cross-correlated (pulse compressed) result. Hence, the performance assessment should be based on the comparison of the processed results and not in the originally generated waveforms.

The processed data are illustrated in the second set of figures (Fig. 5.6 to Fig. 5.9). Figs. 5.6a and 5.6b illustrate the autocorrelation of the ideal codes and the cross-correlation of the experimentally generated and received codes with the ideal codes. For both codes, the results compare very well to the ideally expected outputs.

For the two sets of results shown in Fig. 5.6a and 5.6b, a measure for the relative degree of likeness between ideal and experimental data could be established in several ways. As the quantities shown are normalised, parameters like ratio of peak to peak sidelobe to peak signal level or the ratio of the mean square error to peak signal level may be used to compare the performance. For example, using the first method, that is, comparison of the peak to peak sidelobe to peak signal level shows that this ratio is ideally equal to 2.7 for both codes (measurement performed on Figs. 5.6a and 5.6b). The experimentally obtained results give a ratio of 2 for code 1 and 1.57 for code 2, indicating a slightly higher relative error in the processed result of code 2. This slight difference may be explained by the fact that complementary codes possess different spectral characteristics, such that their generation would result in the unproportional excitation of the different transducer vibrational modes. Hence, identical transmission efficiencies cannot be realised for both codes of a complementary pair.

As mentioned earlier, the output of a Golay code based system is the sum of the response for the complementary pair. Hence, the ideal autocorrelated sum and the sum of the experimentally obtained, cross-correlated results (the sum of Figs. 5.6a and 5.6b)

appear as shown in Fig. 5.7a and 5.7b in time and frequency domains. Except for the low frequency modulation, the experimentally derived pulse compares very well with the ideal autocorrelation. The sidelobes arising from errors in the generated waveforms are well below 20dB from the peak indicating a good performance.

A limited processing was attempted to improve the finally derived pulse. Fig. 5.8 is obtained by filtering the output with a high pass filter of 1 MHz cutoff frequency. It may be observed that although this process has reduced the main low frequency component appearing on the original trace and sharpened the main pulse, it has on the other hand enhanced higher frequency sidelobes. Alternatively, better improvement may be achieved by pre-processing the generated waveforms prior to cross-correlation.

Quantising the received waveforms to binary levels by the use of suitable thresholding is one approach. As only two signal levels are expected, assuming a fair phase reproduction, the optimum threshold to eliminate errors arising from amplitude variations is the 0 level. The result obtained using such threshold is shown in Fig. 5.9. It may be observed that a very good improvement on the low frequency sidelobe levels that appeared in the original cross-correlated result has been achieved.

The results obtained in the present exercise are fairly good and give a strong indication of the

feasibility of the method for practical applications. In a future system, it may be best to include error correcting bits with the transmitted code sequences as in other digital transmission to allow correction of the binary sequence derived after thresholding at the 0 level. Additionally, instead of attempting the direct generation of the codes, generation of a sequence modulated by a carrier with frequency components corresponding to the transducer pass band and succeeded by the appropriate demodulation on reception may be a better, more efficient alternative. Last but not least, the continued improvement of transducer modelling strategies will have a positive contribution.

5.4. RESOLUTION AND WIDER BAND TRANSDUCERS

The pre-filtering approach discussed above is basically intended as a method of resolution improvement in situations where the probe response constitutes the band limiting factor in the transmit/receive system. In the situation where the transducer exhibits a wider or comparable bandwidth with the excitation codes, the system resolution is more dependent on the excitation. Thus, for example, for the codes used in the present system (tw= 166.66 ns), the best resolution that may be achieved is 0.25 mm in water, regardless of the transducer bandwidth or centre frequency (calculated by the product v x tw,

assuming a sound velocity v of 1.5mm/μs). This is a resolution that can be achieved using a 3 MHz probe with a single cycle output. This section is intended to show how the correlation system behaves when it is used in conjunction with a wide bandwidth probe for pulse-echo measurement and to determine the resolution limit of the system. As such, although this is a continuation of the discussion on resolution, it is not a continuation of the pre-filtering aspect of it.

The effect of using a wide band sensor was investigated by using a 10mm disc PVDF probe with a 10 MHz centre frequency. As the period of a 10 MHz pulse is 100ns, a temporal resolution of that order would be expected from this probe.

The simulated pulse-echo response of this probe is shown in Figs. 5.10a and 5.10b in time and frequency domains respectively. It may be observed that although its resonance is at 10 MHz, the probe exhibits a wide bandwidth with high energy at frequency regions corresponding to the code pass band. Additionally, the time domain response exhibits a very short duration indicating that the probe is capable of the resolution quoted above.

The modelled pulse-echo response of the 10MHz probe was introduced into the correlation system simulation package to investigate the resolution behaviour. The expected receiver signal in transmitting and receiving one

32 bit Golay code with this probe is shown in Fig. 5.11, where although the code phase information seems to have been maintained, a limited high pass filtering effect by the transducer is apparent. The simulated output of the correlation system is illustrated in Fig. 5.12a. As may be observed in this figure, the result predicts a temporal resolution of about 800ns (the width considered is between points where the magnitude of the response is down by 20dB from the peak). The ideal triangular pulse expected from a pure autocorrelation of the sequence is shown in the same figure with dotted lines. That is the output that would be obtained if the codes are received totally unfiltered by the system. Thus, it appears that while the excitation filters the transducer response and brings down the resolution to 333ns (2tw), the relatively weak low frequency components of the probe in turn filter the excitation resulting in a pulse width of more than 800ns.

Experimental pulse-echo measurements indicated a further filtering effect. The pulse-echo response was measured in a water tank using a planar glass reflector as target. The data, which was acquired through the DMA facility is shown in Fig. 5.12. As may be observed in Fig. 5.12, the temporal resolution has degraded to 1.75μs. The additional cycles in the measured output are due to a further bandlimitation of the received signal within the amplifying stages. It is thus concluded that the present resolution limit of the system is 1.75μs (which is

equivalent to a pulse-echo spatial resolution of 1.3mm in water).

Finally, the resolving capability was experimentally checked. A stacked target of a 3mm thick glass plate followed by a 1mm thick water layer and a thick glass block was used in the experiment. All three layer interfaces were clearly resolved as shown in Fig. 5.13, although it is also evident that the limits of the resolving capability have been reached. Peak detection and thresholding can be used to improve the data further as shown in Fig. 5.14.

The results presented here establish the present resolution limit of the correlation system. Its resolution has been shown to be 20 % of the ideally expected performance for the particular sequences used. Ideally, in pulse-echo mode a resolution down to 1 mm in glass and 0.25mm in water may be achieved (assuming sound velocities of 6mm/μs and 1.5mm/μs respectively) for the particular code sequences. This limit has been attributed to a bandlimitation in the amplifying stages and an inevitable limited filtering by the lack of strong low frequency components in the transducer response.

5.6. CONCLUSION

The first section of this chapter has looked at an alternative implementation to improve on a correlation system's resolving capability for the case where the

transmit/receive probe is the main system bandlimiting factor. The suggested alternative implementation involves modification of the transmission side to allow pre-filtering the transmitted waveform. The method has been shown to be feasible by the generation of waveforms closely approximating an 8 bit Golay code pair from a 1 MHz probe. Results obtained by post processing the data showed that a pulse compression resulting in a resolution close to the ideal case can be achieved.

Further work in this line could involve an improved generation of 8 bit codes using better characterised probes and measuring set up as well as using improved waveform generation and RF amplification hardware. The generation of higher order codes would be an interesting attempt, provided that the lower order code generation is reasonably perfected. During the course of the present exercise, it has been observed that the need to excite occasionally weak transducer response spectral components necessitated the use of high power excitation. On the other hand, as stated earlier, one main advantage of the correlation approach is the possibility of using low energising levels. Hence, a study of energising levels in pre-filter performance may be beneficial in order to have a more complete picture of the applicability of this method to a low power correlation system.

As a contrast to the usual case in which the transducer response is the main resolution limiting

factor, the second section presented simulated and experimental results to demonstrate the resolution of the correlation system when the excitation function and reception hardware constitute the main bandlimiting factors instead of the probe. The results were used to determine the present resolution limit of the correlation system.

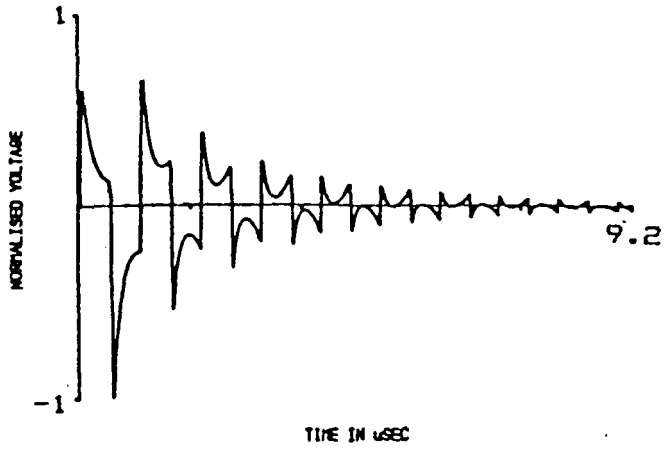

Fig. 5.3a Simulated characteristics of probe used in the pre-filtering experiments (time domain).

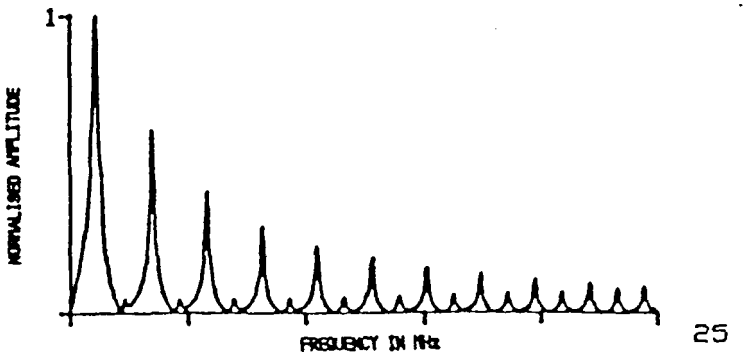

Fig. 5.3b Simulated characteristics of probe used in the pre-filtering experiments (frequency domain).

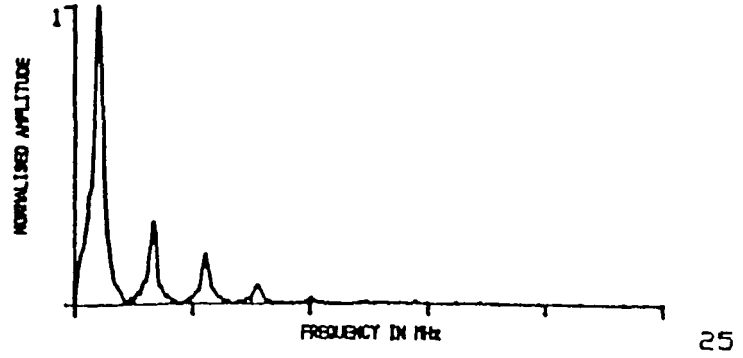

Fig. 5.3c Measured characteristics of probe used in the pre-filtering experiments (frequency domain), showing band-limitation by measurement system.

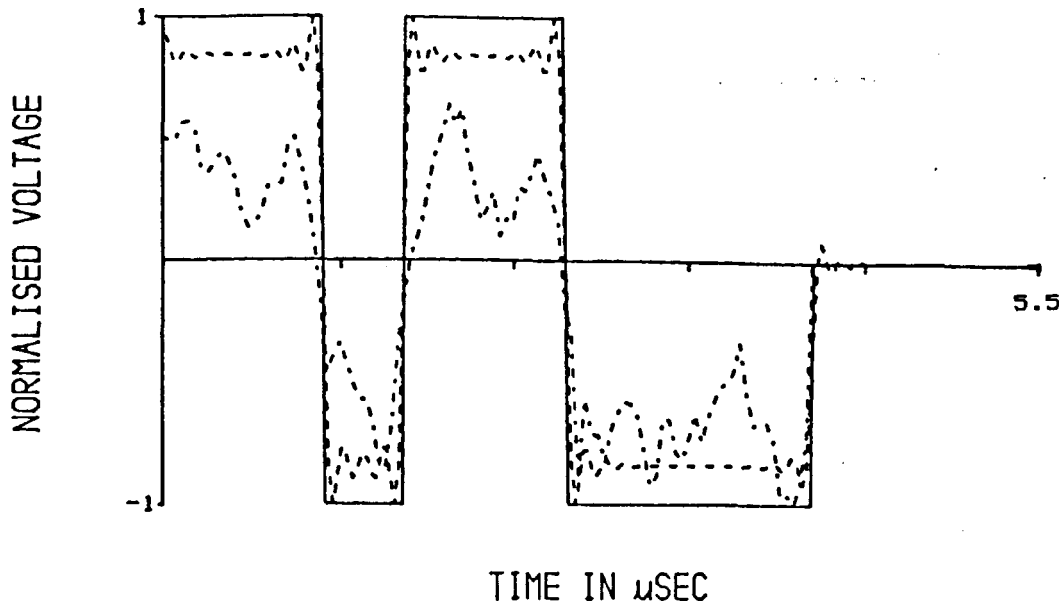

Fig. 5.5a Ideal(——), simulated(---) and measured(_·_·) transmission responses for code 1.

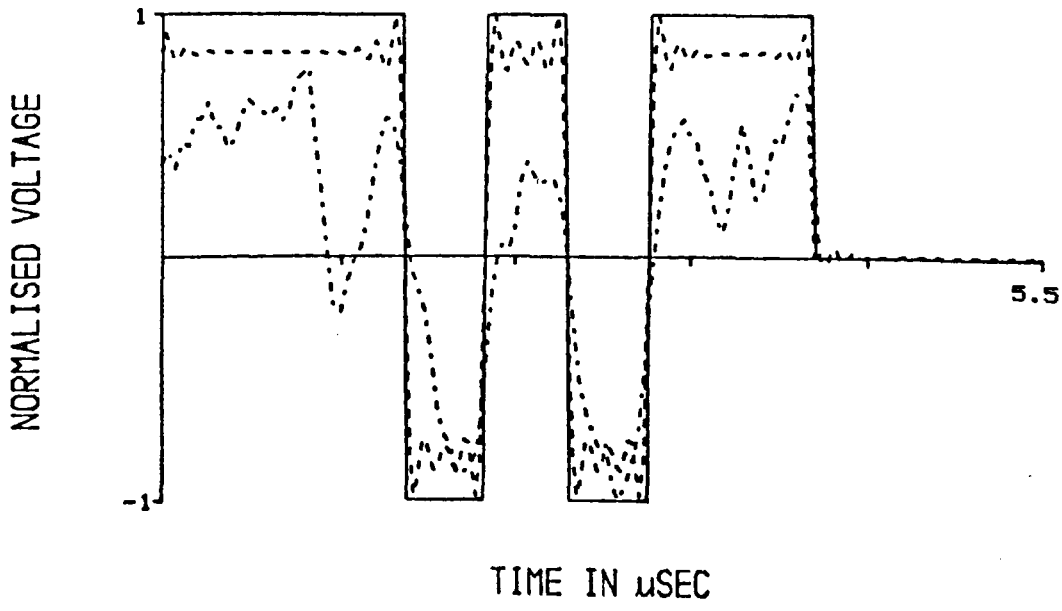

Fig. 5.5b Ideal(——), simulated(---) and measured(_·_·) transmission responses for code 2.

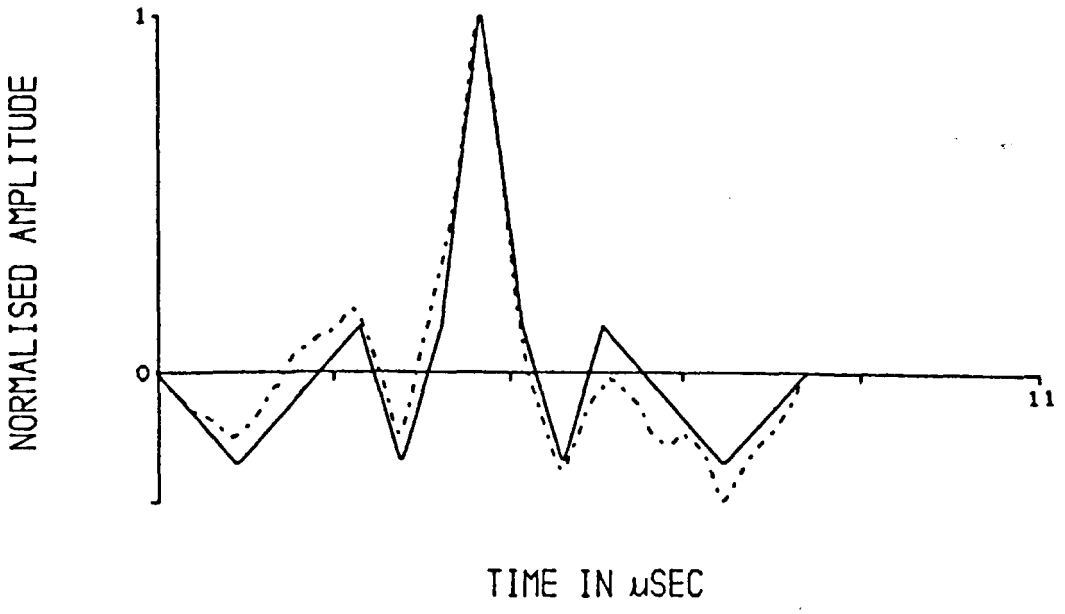

Fig. 5.6a Ideal autocorrelation of code 1 (——) and cross-correlation with measured response (—·—·).

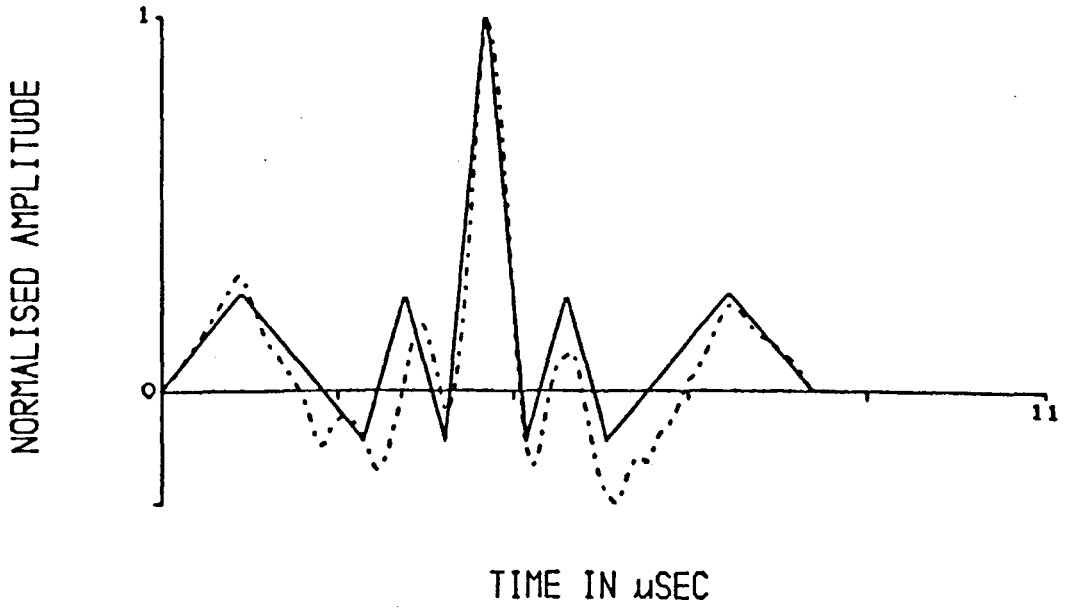

Fig. 5.6b Ideal autocorrelation of code 2 (——) and cross-correlation with measured response (—·—·).

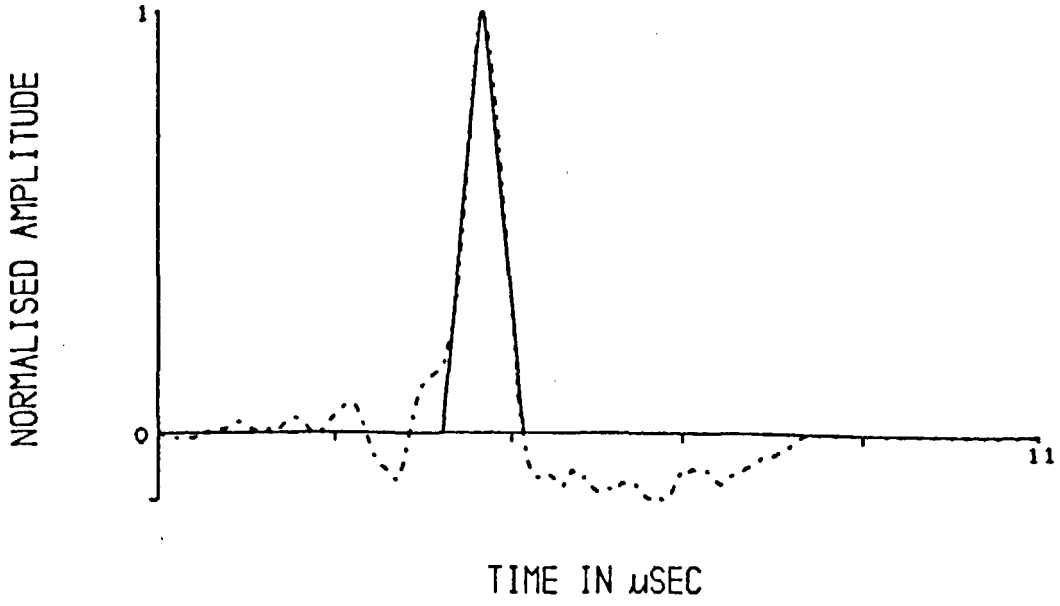

Fig. 5.7a Sum of the ideal autocorrelated codes (——) and sum of the cross-correlations with the measured responses (—·—·).(time domain)

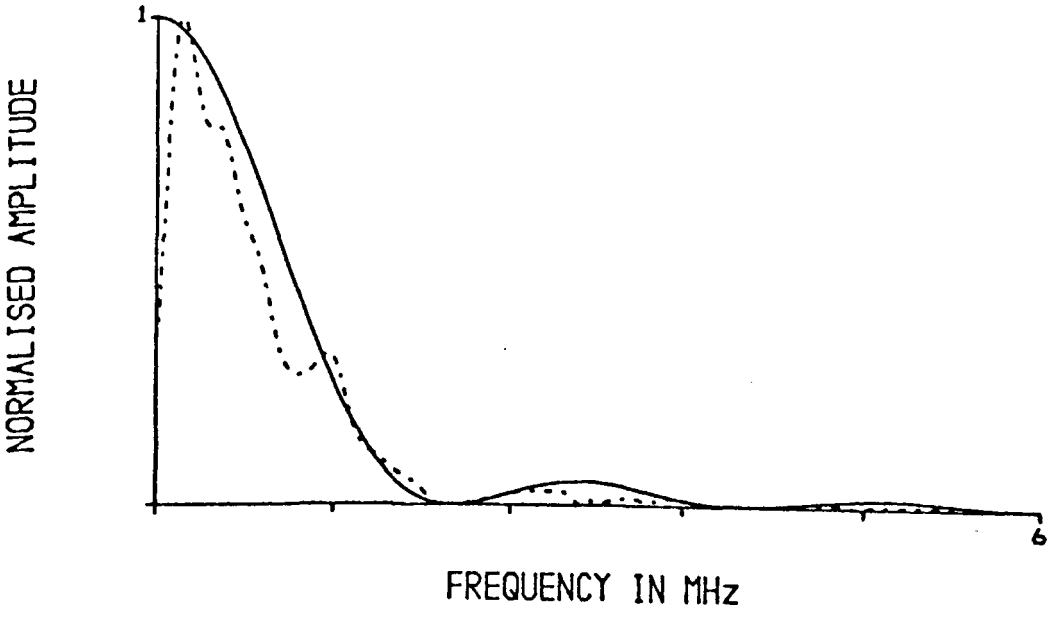

Fig. 5.7b Sum of the ideal autocorrelated codes (——) and sum of the cross-correlations with the measured responses (—·—·).(frequency domain)

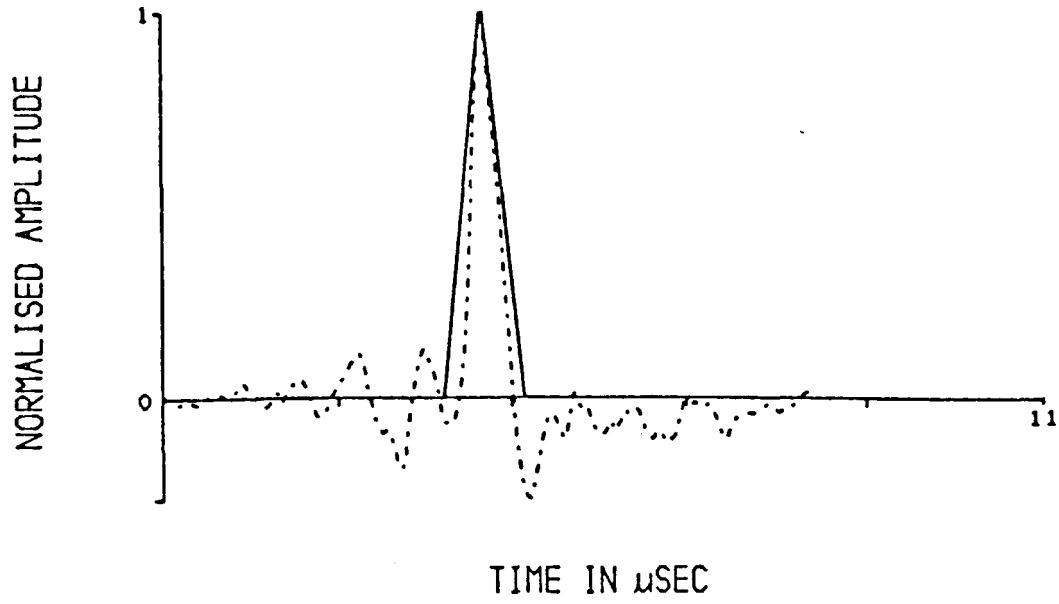

Fig. 5.8 Ideal processed output(——) and the result obtained from measured responses after high pass filtering at 1MHz(—·—·).

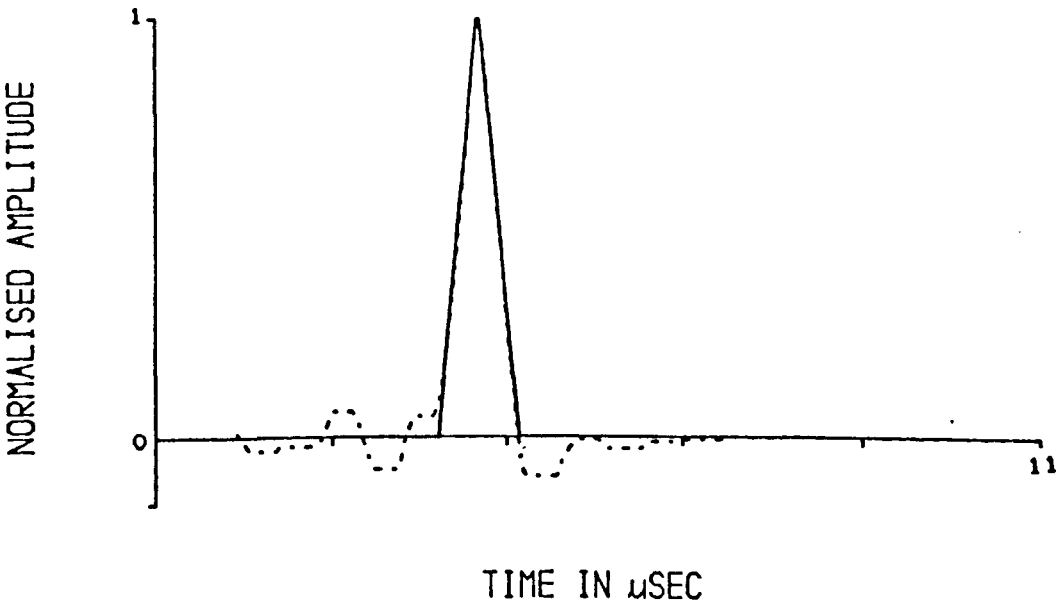

Fig. 5.9 Ideal processed output(——) and the result obtained after thresholding the measured responses prior to cross-correlation(—·—·).

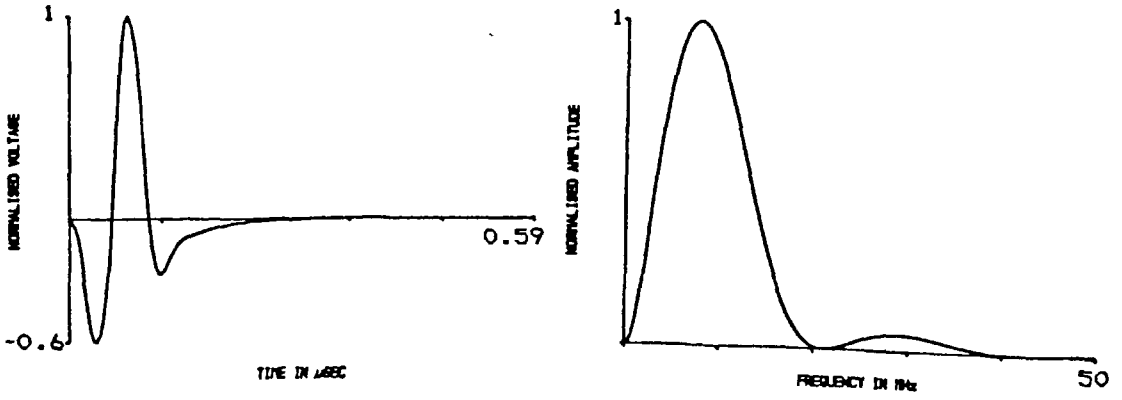

(a) time domain (b) frequency domain

Fig. 5.10 Transmit/receive characteristics of PVDF probe.

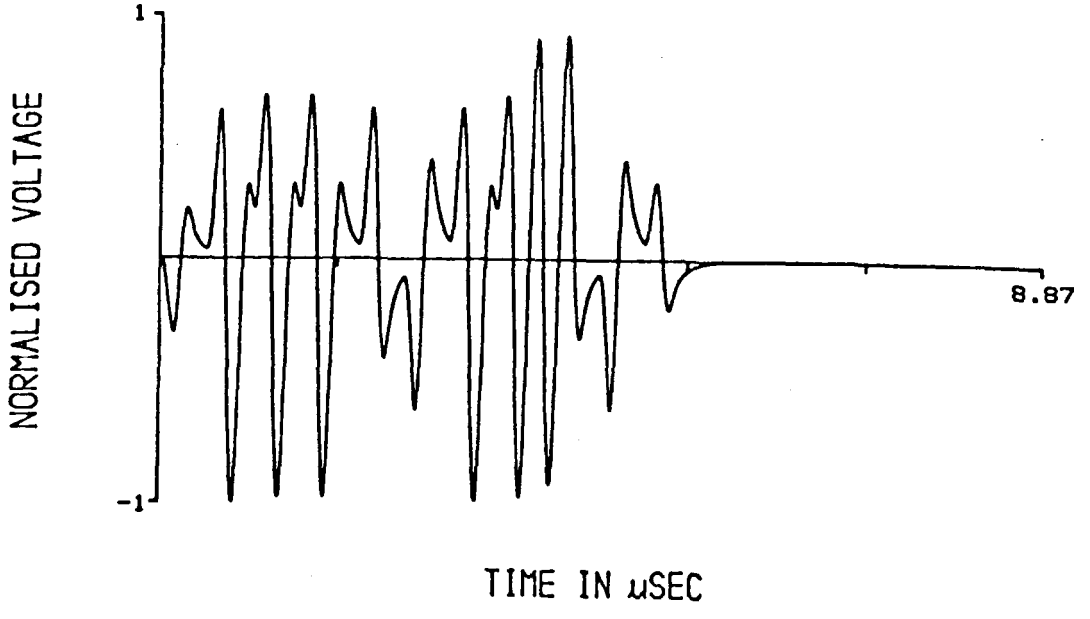

Fig. 5.11 Received signal after applying one 32 bit code to the PVDF probe.

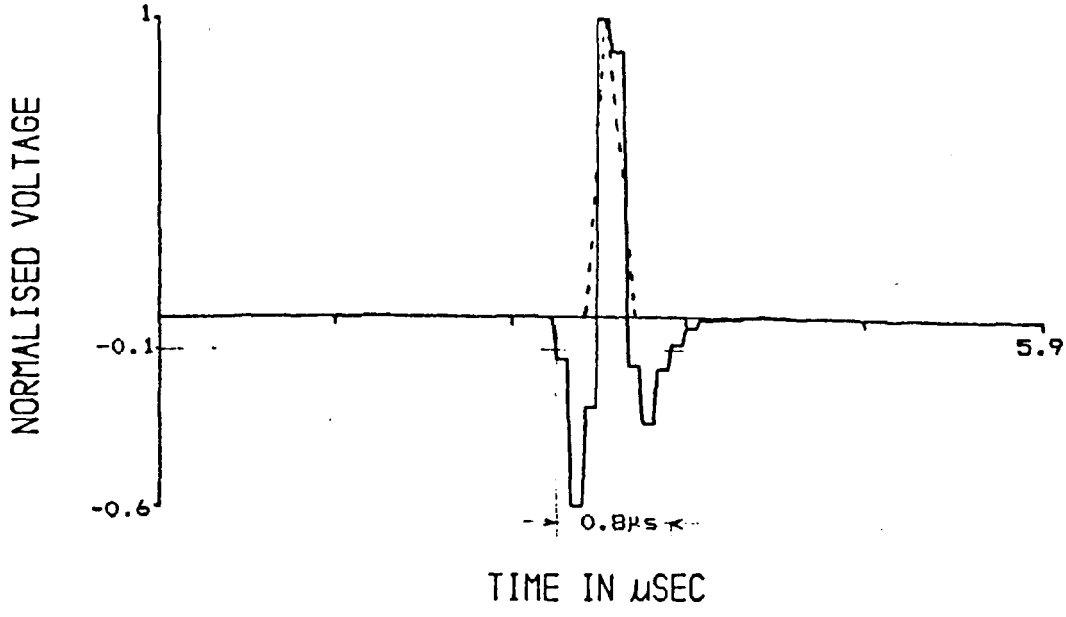

Fig. 5.12a Simulated correlator output using the PVDF probe.

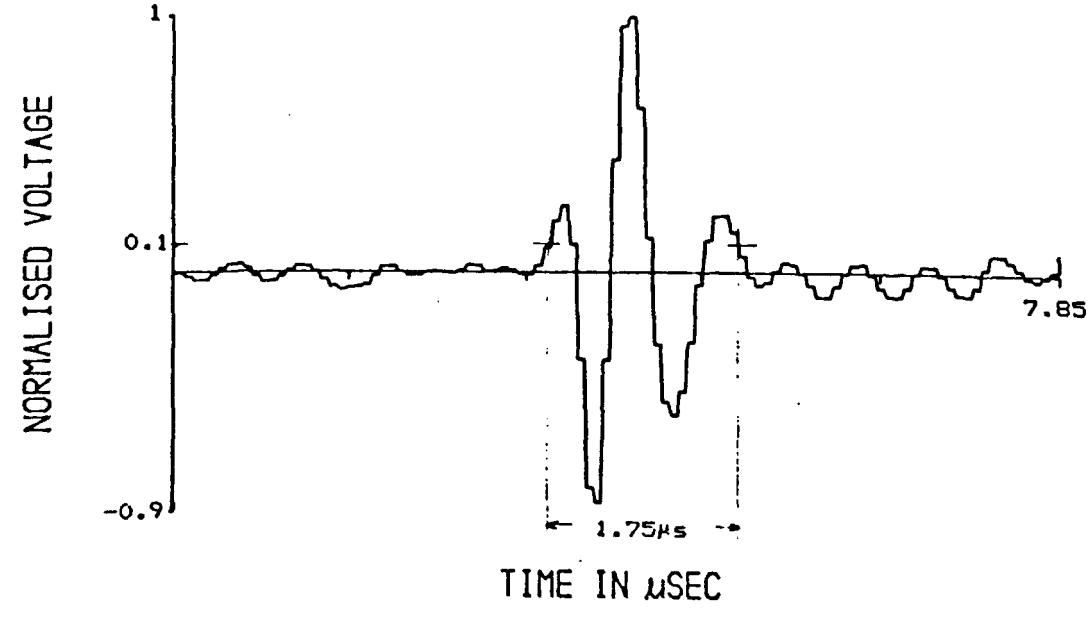

Fig. 5.12b Measured correlator output using the PVDF probe.

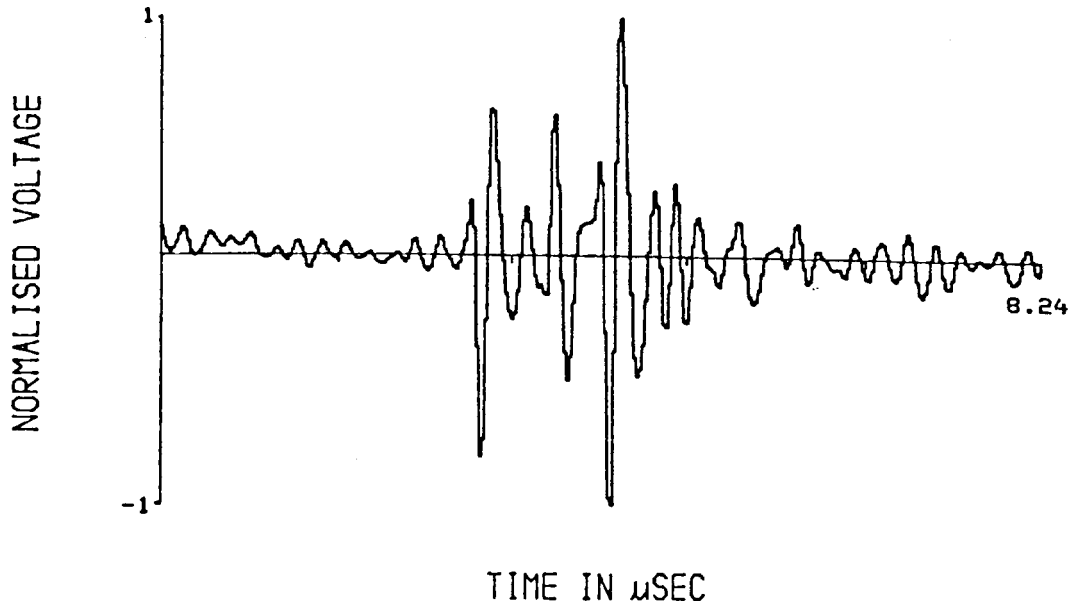

Fig. 5.13 Measured correlator output with PVDF firing into a 3 layer target (3mm glass,1mm water,5mm glass).

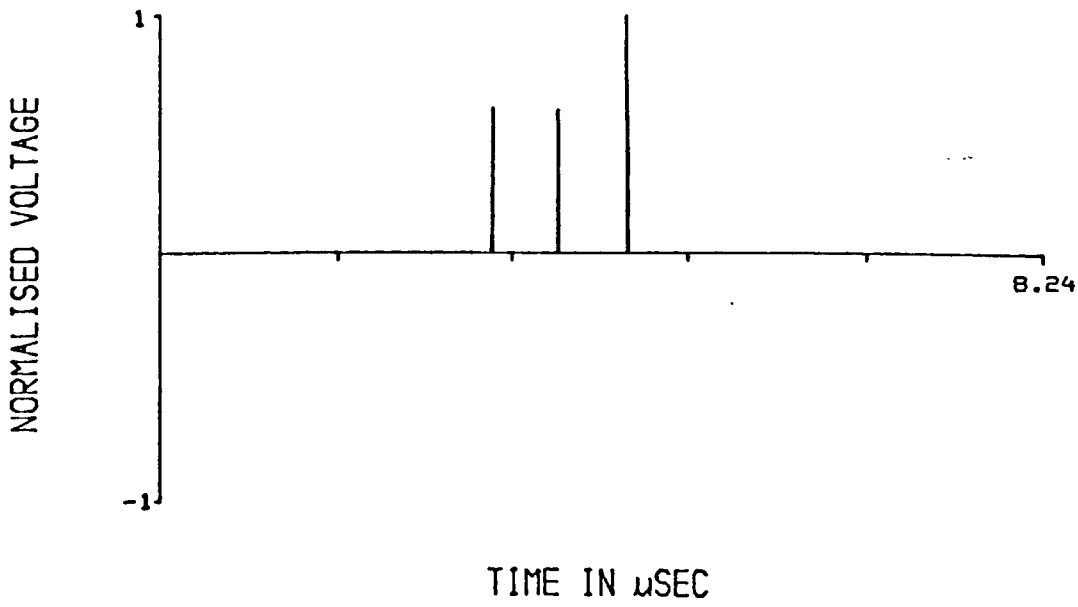

Fig 5.14 The three layers in Fig. 5.13 being identified after thresholding and peak detection is applied.

CHAPTER 6

CHAPTER 6

IMAGE FORMATION AND PROCESSING

6.1 INTRODUCTION

In the preceding chapters, the first phase of this project, which involved the development of a means of obtaining SNR enhanced scan data at low operating power levels and high operating speeds has been described. As the data acquisition hardware system has been designed to form the front end of a low power ultrasonic imaging unit, the development of an optimal imaging strategy is highly desirable. This forms the second phase of the work.

The image formation techniques considered were linear array scanning (also called B scan), transmission and reception focussing and reception only focussing. The selected technique may be apparent already from the hardware description given earlier. Mainly due to the need to minimise hardware complexity, and the cost associated with it, a Synthetic Aperture Focussing Technique (SAFT) has been selected. Basically, this involves sequential excitation of array elements and focussing the scan data on reception.

The first section of this chapter reviews the basic features of the SAFT. Two areas of investigation are then presented. Firstly, the dependence of the SAFT performance on the SNR of the scan data and the improvement achieved by using correlation based data acquisition are theoretically demonstrated. Secondly, the influence of

the shape and/or distribution of the object to be imaged on the SAFT performance is assessed. It is shown that using this approach for large object imaging (i.e. where the object dimensions greatly exceed the wavelength) has certain limitations and possible methods of improvement are suggested. In the second section, the performance of the system is demonstrated. A selection of applicable image processing techniques are reviewed and real images obtained using the system are presented. The data is collected from different sets of weakly reflecting targets in order to verify the performance of the system under low input SNR. Image improvements by limited image processing are also demonstrated. In general, the system is shown to perform very well.

6.2 THE SYNTHETIC APERTURE FOCUSSING TECHNIQUE (SAFT)

6.2.1 Method and Parameters of SAFT

(a) Technique and advantages

The SAFT is essentially a reception focussing method in which transducers placed at different positions are sequentially excited. The data from each is collected and stored, and the image formulated by summing the various scan data, taking into consideration the appropriate signal arrival time delays to each transducer. Fig. 6.1 illustrates the situation.

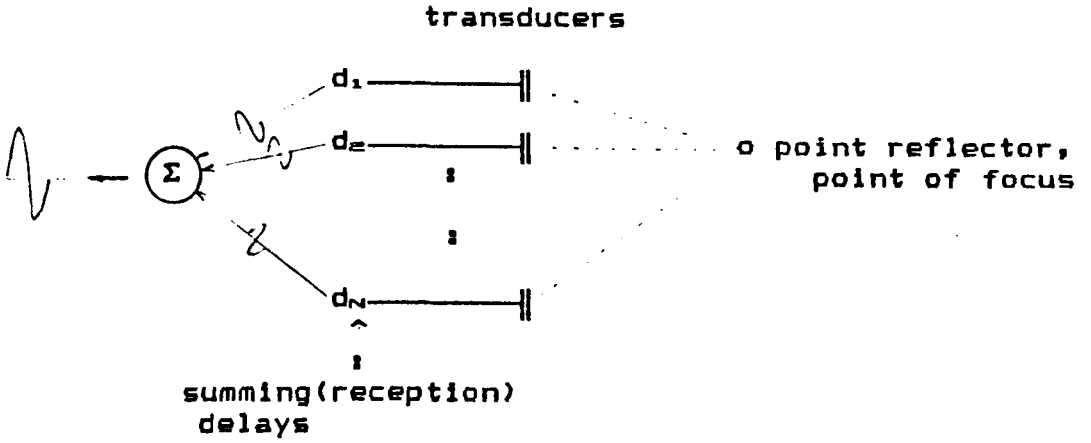

Fig. 6.1 SAFT outline

Data from the point reflector at o arrives back to each transducer (N transducers in all) at different time delays ($d_1, d_2, \ldots, d_N$). Then to focus at o, the data at the delays d_1 for transducer 1, d_2 for transducer 2, and so on up to d_N for transducer N are summed. Thus, if a unit pulse had been reflected back to each transducer, the image representing the point reflector at o will have an amplitude of N.

The main advantage of the SAFT approach is that only one front end amplifier and one digitiser are needed, regardless of the number of transducers used. This would amount to a considerable saving in cost and hardware bulkiness, especially where a large transducer array is to be used. A better, more thorough design of the front end hardware would therefore be possible.

Another advantage is that the transverse resolution

is twice as good as a system in which a parallel beam is transmitted and the system focusses on reception. This is because the time and phase difference to a given point from a transducer element is doubled, as the signal travels to the image point and back.[20]

Two disadvantages may also be stated. The first is that as the excitation of each transducer and subsequent reception are sequential the system data acquisition speed is considerably reduced. It will be slower by approximately a factor of 1/N compared to a system in which all transducers are simultaneously excited and all are prepared to receive at the same time. The second disadvantage is that the transmitted signal power and hence the received signal power is less by the same factor, compared to a system that is also focussed on transmission.

(b) The Point Spread Function (P.S.F.)

If during the data acquisition, the data is collected from a single point, its reconstructed image is the P.S.F. of the system. This parameter is often used to assess the performance of an imaging system. It is used to predict sidelobe levels and determine the effects of various system parameters such as pulse length, quantisation, scan SNR, delay noise, etc. The P.S.F. is essentially a two dimensional quantity. In a rectangular coordinate system, one can talk about the P.S.F in the

lateral direction (i.e. parallel to the array) and the P.S.F. in the range direction (i.e. perpendicular to the array). Although both are considered here, it should be noted that in most relevant references only the lateral case is considered for system assesment.

An approximate expression for the P.S.F. may be derived as follows.

Consider an N-element array, situated at x=0 and focussed at an arbitrary point p(x,y). A point reflector is situated at the point $o(x_o,y_o)$. These are shown in Fig. 6.2.

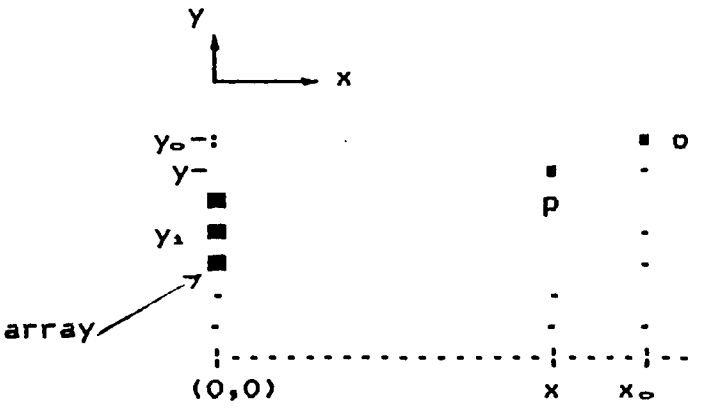

Fig. 6.2 Array, point of focus and point reflector positions for the derivation of P.S.F.

The emitted signal is assumed to be of the form F(t) exp(jwt). Then the summed signal for N elements will be of the form,

$$S(t)=\sum_{i=1}^{N} F(t+\tau_i)\ \exp[jw(t+\tau_i)] \qquad \ldots.6.1$$

Where, $\tau_i = (2/v)\ [x^2 + (y_i-y)^2]^{1/2}$ (round trip delay from element at $(0,y_i)$ to point of focus p; v is the

propagation velocity.)

If there is a point reflector at o, the signal round trip delay will be,

$$\tau o_i = (2/v)\ [x_o^2 + (y_o - y_i)^2]^{1/2}$$

Thus, the system focussed at p(x,y) will observe the signal reflected from o(x_o,y_o) as:

$$S(t) = \sum_{i=1}^{N} F(t+\tau_i-\tau o_i)\ \exp[jw(t+\tau_i-\tau o_i)] \qquad \ldots.6.2$$

Making the paraxial approximation [20] that $(y-y_i)^2 << x^2$ and $y_o^2 << x_o^2$, and substituting δx for $x-x_o$ and δy for $y-y_o$, eqn.6.2 will reduce to the following.

$$S(t) = \sum_{i=1}^{N} F\left[t - \frac{2}{v}\left[\delta x + \frac{\delta y . y_i}{x_o}\right]\right]\ \exp\ jw\left[t - \frac{2}{v}\left[\delta x + \frac{\delta y . y_i}{x_o}\right]\right] \qquad \ldots.6.3$$

The range resolution is then given by (setting y=yo),

$$S_R(t) = \sum_{i=1}^{N} F\left[t - \frac{2\delta x}{v}\right]\ \exp\ jw\left[t - \frac{2\delta x}{v}\right] \qquad \ldots. 6.4$$

This is independent of of the number of elements, spacing,etc.

The transverse definition ($x=x_o$) is given by,

$$S_L(t) = \sum_{i=1}^{N} F\left[t - \frac{2}{v}\left[\frac{\delta y . y_i}{x_o}\right]\right]\ \exp\ jw\left[t - \frac{2}{v}\left[\frac{\delta y . y_i}{x_o}\right]\right] \qquad \ldots. 6.5$$

If the signal F(t) is many cycles long $S_L(t)$ will be of the form given by eqn.6.6 [20].

$$S_L(t) = \left|\frac{\sin \pi\delta x/ds}{\sin \pi\delta x/dg}\right| \qquad \ldots. 6.6$$

Where, $ds = \lambda x_o/2NL$ ... 6.6a (lateral spot size

for N elements, L spacing and λ wavelength)

$$dg = \lambda x_o / 2L \qquad \ldots 6.6b \text{ (grating lobe spacing)}$$

As an illustration of eqn. 6.6, the lateral P.S.F. for a 32 element array focussed at a depth of 5cm is shown in Fig. 6.3. The element spacing is considered to be equal to one wavelength in the medium of propagation (λ = L). It may be observed that the main pulse has a width of 0.8 mm as theoretically expected (eqn. 6.6a). Similarly, grating lobes appear every 25 mm (eqn. 6.6b).

(c) Implementation procedure

The implementation of SAFT involves a combination of both hardware and software processing. The data acquisition front end involves hardware processing, while the focus and image formulation are often performed in software. The entire procedure may be considered to involve four data fields (data arrays). The first is the target (reflectors) field; the second is the scan data field; the third is the focus data field; the fourth is the image field.

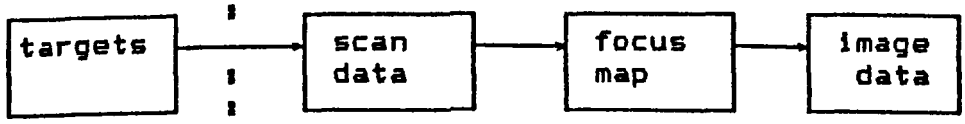

Fig. 6.4 SAFT data fields

These will be discussed in general terms and then illustrated with a specific example.

The target field is a rectangular plane in space parallel to the array axis and containing the items to be

imaged. For discussion purposes, it will be assumed to have dimensions of J x R units. It may have an offset J_o from the array. The scan array contains the data collected from N transducers; the length of each scan being just sufficient to capture data from the most distant point in the target field. The minimum length will be, $2(J+J_o)/v$ (in time), or $2(J+J_o)/v.ts$ (as number of samples). The propagation speed of ultrasound in the medium is denoted by v and ts is the data sampling period. If the data is digitised to m bits, the scan array requires a memory of $N.m.2(J+J_o)/v.ts$ bits.

The focus field is a data array consisting of the time delay information from each transducer to each point in the target field. As the data size cannot be indefinitely large, a limit has to be set to the acceptable picture resolution. If a resolution of Pr is acceptable in both dimensions of the J x R target plane, the focus map will consist of J/Pr x R/Pr data points. The focus field maps the scan data to the image field as the time delay information is used to address the scan data prior to summation. The summed data for each resolvable point then forms the image field.

For example, a 32 element array operating into water, using 20 MHz sampling, 8 bit digitisation and required to image a 10cm x 10cm plane with no offset and a pixel resolution of 1mm will require the following.

The number of samples in an individual scan is given by,

$$\frac{2 \times 100\text{mm}}{1.5\text{mm}/\mu\text{s} \times 0.05\ \mu\text{s}} = 2666$$

The scan array size is thus,

32(elements) x 2666(samples) x 8(bits) (≈ 86 K bytes).

The focus data size will be 100 x 100 x 8 bits (= 10K bytes). The image data field will also have the same size.

To conclude, the SAFT implementation procedure involves respectively; the decision of the target field size and resolution, scan data acquisition, formation of the focus (time delay) data and, based on that, formation of the image data. This is followed by the appropriate display.

(c) Assumptions and requirements for optimal performance

Optimal performance refers to being able to get an image of relative amplitude N for any object in the target plane (where N is the number of sensors). Thus, the SAFT method of imaging requires and inherently assumes that the following are true.

(i) Omnidirectional sensors - All sensors should receive the same signal amplitude and shape from a given reflector placed at any point in the target plane.

(ii) Omnidirectional scatterers - The targets are assumed to be composed of point reflectors which reflect back signals of equal amplitude to all sensors.

(iii) Homogeneous medium - The propagation medium must be

homogeneous as velocity differences may result in time delay errors (known as delay noise [23]) which in turn will have a defocussing effect in the image formation.

Although a perfectly omnidirectional sensor is not physically realisable, the element directivity can be maximised in the array/transducer design stage. Also, given a properly characterised array, compensatory weighting factors may be included in the focussing process. However, this is achieved at the expense of SNR, as the weighting operation would also enhance the noise present in the scans.

With regard to the scatterer characteristics, if mainly specular targets are encountered, it will be necessary to use a number of different techniques other than straight forward SAFT. A combination of SAFT and B-scans using different sensor positions and separate transmitting and receiving transducers are possible approaches. However, the present discussion will be limited to SAFT and the reader may refer to [25] for discussions on specular target imaging.

6.2.2 Correlation and SAFT

(a) Dependence of SAFT on scan SNR

The signal to noise ratio of the array scan data determines the low contrast resolution achievable by the SAFT approach. Low contrast refers to the situation where the value of an image parameter, such as a pixel

amplitude, is low relative to the average value [15]. As mentioned earlier, the transducer response determines the temporal (range) resolution while the transverse definition depends on the array dimensions, the depth of target and its lateral position with respect to the array centre. The SNR of the scan data affects the resolution in both dimensions. Consider the P.S.F. expressions given by eqns.6.4 and 6.5. If the signal data F(t) is replaced by F'(t), where F'(t) is the sum of the signal and a noise component $N_w(t)$, with regard to the range definition, the P.S.F. will appear as shown by eqn. 6.7. It should be noted that as the noise component in each element is assumed to be statistically independent, it is represented not only as a function of time (t) but also the element (i).

$$S_R'(t) = \sum_{i=1}^{N} F'\left(t-\frac{2\delta x}{v}\right) \exp\left[jw\left(t-\frac{2\delta x}{v}\right)\right]$$

$$= S_R(t) + \sum_{i=1}^{N} N_{wi}\left(t-\frac{2\delta x}{v}\right) \exp\left[jw\left(t-\frac{2\delta x}{v}\right)\right] \quad ..6.7$$

It may thus be concluded that the range resolution as well as the ability to image targets with low reflection either due to small size or attenuation, directly depend on the ratio of ΣF and ΣN_w. (Note that this is different from the scan SNR simply given by the ratio F/N_w.)

If N_w is a Gaussian white noise quantity, due to the inherent averaging in the focussing process, the image

signal to background noise ratio, manifested as image resolvability, will actually be higher by a factor of $\sqrt{N_e}$ [28] (where N_e is the number of elements). If the scan data is taken from K different positions (henceforth referred to as K compounding), the SNRE factor will then be $\sqrt{KN_e}$. Thus, the SAFT approach will result in a resolvable target image so long as the average SNR of the array pulse-echo data is greater than $1/\sqrt{KN_e}$. This may be illustrated conveniently by the following set of simulated results.

Figures 6.5a and 6.5b illustrate the dependence of the range resolution on the SNR of the scans. Fig. 6.5a illustrates the P.S.F. in the range direction for a 32 element array, with no spatial compounding and no added noise, while Fig. 6.5b illustrates the same situation but with noise of $\sigma_n \approx 0.04$ added (resulting in an SNR$\approx 1/\sqrt{32}$). The P.S.F. is computed for a depth of 5 cm from the array and the medium of operation is assumed to be water. The transducer response function used for these illustrations is the array element response given in Fig. 4.27, Chapter 4.

Similarly the lateral P.S.F. of eqn. 6.5 may be re-expressed as follows.

$$S_L'(t) = \sum_{i=1}^{N} F'\left(t - \frac{2y_i\delta y}{vx_c}\right) \exp\left[jw\left(t - \frac{2y_i\delta y}{vx_o}\right)\right]$$

$$= S_L(t) + \sum_{i=1}^{N} N_{wi}\left(t - \frac{2y_i\delta y}{vx_c}\right) \exp\left[jw\left(t - \frac{2y_i\delta y}{vx_o}\right)\right] \quad \ldots 6.8$$

The same averaging effect as for the range case will occur here and the tolerable input signal to noise ratio is of the same magnitude. A similar assesment of the performance is made in Figures 6.6a and 6.6b. The lateral P.S.F. without noise is shown in Fig. 6.6a while the one with an input SNR of -8 dB is shown in Fig. 6.6b.

Thus, for very low SNR situations, such as Figs. 6.5b and 6.6b, the incorporation at the front end of a high SNRE data acquisition unit is imperative.

(b) Improvement by the Correlation Technique

The correlation technique of data acquisition would provide the necessary front end SNRE. As an illustration of the improvement that can be achieved, a single cycle A-scan correlation processing prior to synthetic aperture focussing shall be considered. Using the parameters of the actual data acquisition unit described in Chapter 4, the P.S.F.s illustrated in Figures 6.5b and 6.6b will appear as shown in Figures 6.7a and 6.7b. A marked improvement may be observed. For a 32 element array using 1 to 16 cycle correlation followed by a synthetic aperture focus, the overall SNRE from input to output will be in the range 16 to 30 dB. This includes an SNRE of 8 to 22 dB in the data acquisition stage (see Chapter 4), and 8 dB ($\approx$J32) in the focussing process. The overall P.S.F. (in 2 dimensions) with correlation processing is shown in

Fig. 6.8.

6.2.3 Target Distribution and SAFT

(a) Object focussing

A point that has not been given sufficient attention in reception focussing is artefact focussing or target image defocussing effects arising from the shape and distribution of the objects to be imaged. In reception focussing, the image is formed by the intersection of scan arcs centred at the array elements and with radii proportional to the distances (or time of flight delays) between the elements and the point of focus. Thus, as shown earlier, scan arcs from N elements intersect to form an image point of amplitude N. The arcs in the background will have a unit amplitude. Using 2 dimensional FFT, it is possible to show that these errors have similar spectra as those of the target images. Hence, they cannot be reduced by filtering without distorting the useful image.

Consider the simplest case shown in Fig. 6.9a where two sensors focus on a point reflector. The resulting image will have an image to artefact ratio of 2. Now if a second reflector p is introduced into the field, focussing on both will result in additional focussed artefacts of the same amplitude as the actual object images. This situation can be observed in Fig.6.9b.

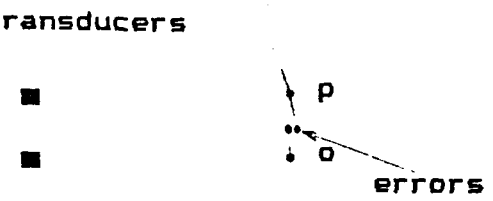

Fig.6.9a SAFT with 2 sensors 1 reflector.

Fig.6.9b SAFT with 2 sensors 2 reflectors.

It is concluded readily that reception focussing from a stationary linear array is effective only when the number of receiving sensors is greater than the number of reflectors in the target plane. The larger this ratio, the higher the resulting image to artefact ratio. The number of transducer elements may be increased to some limit. However, what is expected to happen if SAFT is applied to image a complete cross section of a large surface which may be considered to be composed of a large number of point reflectors?

For example, consider the simulated SAFT image of an arc consisting of 100 individual point sources, spaced a distance of half a wavelength apart. The image is formed by assuming that all points on the arc reflect equal amplitude signals to all elements of the sensor array. This is shown in Fig. 6.10.

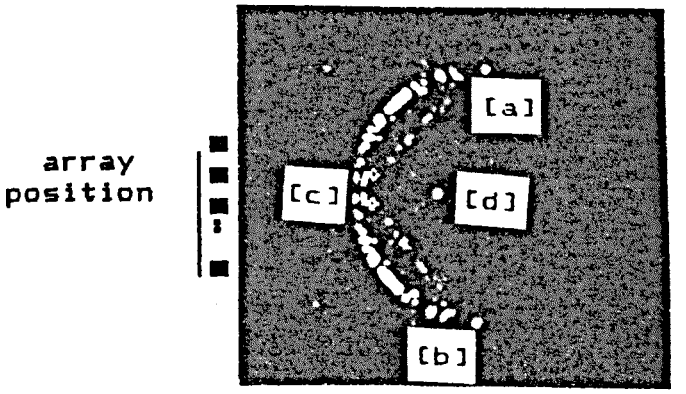

Fig. 6.10 Image of curved surface with centre of curvature away from array.

Defocussing effects may be observed at points (a), (b) and (c) where the sidelobe distribution interferes destructively with the focussed image. On the other hand, constructive sidelobe interference behind the target results in a false image at (d). If the expected target shape is known it may be possible to visually discriminate the actual image boundary from artefacts. But if the information obtained from the image data is to be used for further processing such as pattern identification, as intended here, an image with sufficient resolution for non-subjective assessment is required.

(b) Possible improvements

(i) Increasing the number of transducers

Each additional sensor results in a constructive addition to the real image while its contribution to artefacts varies from constructive interference to total

cancellation. Thus, maximising the number of transducers as far as design and hardware complexity permit is the first step.

(ii) Varying array shape and target access

As shown in Fig. 6.9, the sidelobes that constructively interfere to form the artefacts lie along arcs with centres of curvature at the array element locations. Thus, if a set of point reflectors are oriented in the same sense, the sidelobe interferences will occur very close to the object image and would not manifest as widely distributed artefacts. This is best demonstrated by an example. For example, if a curved surface to be imaged is oriented in the opposite direction to that shown in Fig. 6.10, i.e. with its centre towards the array, the resulting image would be as shown in Fig. 6.11.

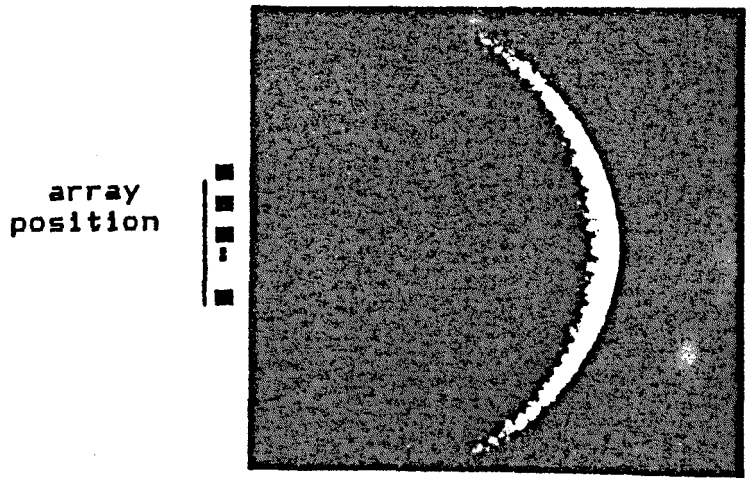

Fig. 6.11 Image of curved surface with centre of curvature towards array.

As can be seen, all the sidelobe interferences have

occurred on or very near to the object. The object is much better defined in this image and no isolated object caused artefacts are visible as in the previous example. This may suggest two possible strategies. The first is careful selection of an optimum array position. If the possible orientation of the specimen/defect to be imaged is known, and if there is sufficient degree of choice of access, the array must be placed along the inner sides of the expected curving/bending target surfaces (such as in Fig.6.11).

Another possibility is using specially made arrays, with shapes roughly following the expected target shape or distribution. Thus, for example, to image a curved surface, less artefact interference will occur if a similarly curved array is utilised. Fig.6.12 shows a possible array shape for imaging a curved surface. The focussing procedure will, of course, take the array shape and distribution of elements into consideration.

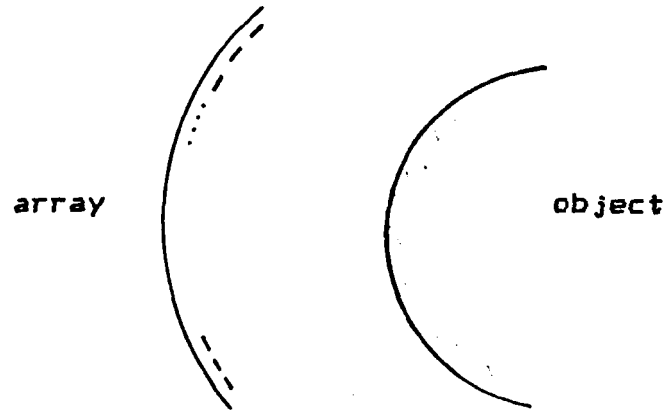

Fig.6.12 Array shape following target shape

(iii) Spatial compounding

This technique refers to the construction of an image utilising scan readings from different array locations. It may be achieved in two ways. The first involves coherent imaging of the same aperture. That is, the same points in space are imaged from different locations and added up. Alternatively, it could be performed incoherently where each array location is used to image a sub-aperture, and all the sub-apertures imaged from different locations are combined to form the entire image frame. The incoherent technique has been used for speckle reduction in medical imaging [24]. The compounding proposed in [24] is from a single array position but using alternate sets of elements for imaging sub-apertures of alternate rasters. A fair degree of speckle reduction has been demonstrated, although it was shown to be at the cost of lateral resolution.

For the problem here, the coherent technique is proposed. This choice is based on the assumption that coherent addition enhances the image but depending on the array locations, randomises the artefact distribution. Hence, for this method to be effective both the amplitude and phase of single scan image points must be used in the coherent addition. A re-derivation of the P.S.F. expression of eqn.6.3, but considering array positional changes verifies this fact.

Consider the same x-y coordinate system, original

array location, original point of focus p(x,z) and point reflector o(x_o,y_o) shown in Fig. 6.2. A simple rotation of this array by θ degrees around its centre is considered as shown in Fig. 6.13.

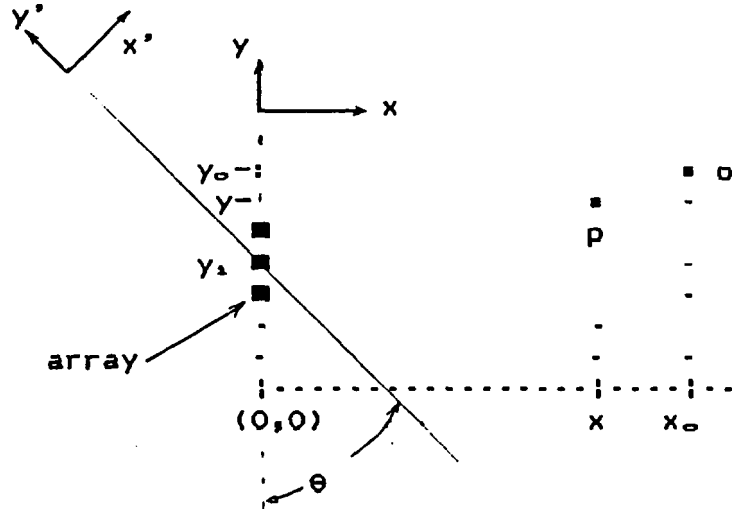

Fig. 6.13 Array, rotated array, point of focus and point reflector positions for the derivation of P.S.F. in spatial compounding.

The P.S.F. expression for this new position will be as follows.

$$S'(t)=\sum_{i=1}^{N} F\left[t-\frac{2}{v}\left[\delta x'+\frac{\delta y'.y_i'}{x_o'}\right]\right]\exp\ jw\left[t-\frac{2}{v}\left[\delta x'+\frac{\delta y'.y_i'}{x_o'}\right]\right] \quad .6.9$$

Where, the ' refers to the coordinates in the rotated axes.

Using simple geometry, it can be shown that

$x' = y \sin\theta + x \cos\theta$

$y' = y \cos\theta - x \sin\theta$

On making the appropriate substitutions, eqn. 6.9 reduces to the form,

$$S'(t)=\sum_{i=1}^{N} F\left[t-\frac{2}{v}[\delta x.f_1(x_i,y_i,\theta_k)+\delta y.f_2(x_i,y_i,\theta_k)]\right]\exp jw(\ldots) \quad \ldots 6.10$$

Where,

$$f_1(x,y,\theta)=\cos\theta\left[1+\frac{x\tan\theta - y}{x_o\cot\theta + y_o}\right]$$

$$f_2(x,y,\theta)=\sin\theta\left[1+\frac{y\cot\theta - x}{y_o\tan\theta + x_o}\right]$$

If this is then performed for K number of rotations and all the results are summed over a fixed aperture, the resulting P.S.F. will be in the form,

$$S^k(t)=\sum_{j=1}^{K}\sum_{i=1}^{N} F\left[t-\frac{2}{v}[\delta x.f_1(x_i,y_i,\theta_j)+\delta y.f_2(x_i,y_i,\theta_j)]\right]\exp jw(\ldots) \quad \ldots 6.11$$

Then, if the point of focus corresponds to where the object is located ($x=x_o$ and $y=y_o$), the output will be in the form,

$$S^k(t) = K.N.F(t)\exp jwt \quad \ldots 6.12$$

Thus, the actual reflector images are enhanced by a factor of K. However, the influence of a reflector on a neighbouring focal point is not automatically multiplied by the same factor. One may conclude this by a study of the delay term in eqn. 6.11. The delay term is not just a function of the array dimensions but also of its position (θ_j). Thus, summing focussed objects from different positions proportionally enhances the actual focussed image but not its influence on points around it. As it is

the constructive interference of such influences which is responsible for artefact generation, it may be concluded that spatial compounding reduces this effect. Although only rotation has been considered here, any set of transformations may be used. For example, a combination of translation and rotation would be the best for imaging a larged curved surface (Fig. 6.14).

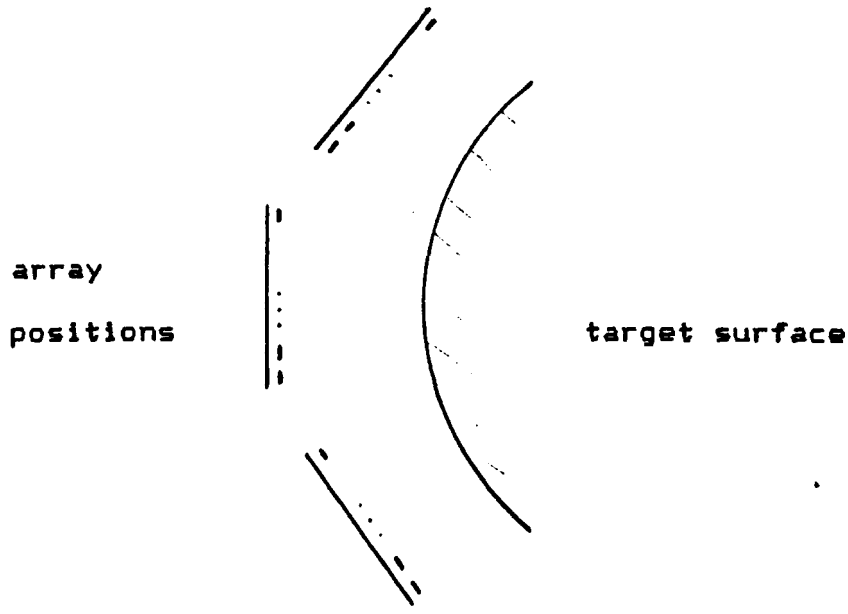

Fig. 6.14 Data acquisition from different positions

Additional advantages of spatial compounding are the improvements on image degradation due to other forms of artefacts such as grating lobes as well as due to aperture limitation. As a result of the limits in element directivity, the aperture in space over which a stationary array can detect and image is limited. Even within the aperture, all points are not seen by the array equally.

Looking from different positions enables the data acquisition system to see all points in the object plane, making it possible to image a much wider area with comparable definition for all points in the image.

Finally, two sets of simulated results (Figs. 6.16 and 6.17) are shown to demonstrate the effect of rotational compounding. For both sets of simulations, the array is assumed to be positioned at the bottom left hand corner of the target plane and subjected to rotational transformation. The relative arrangement of the array positions and target plane is outlined in Fig. 6.15.

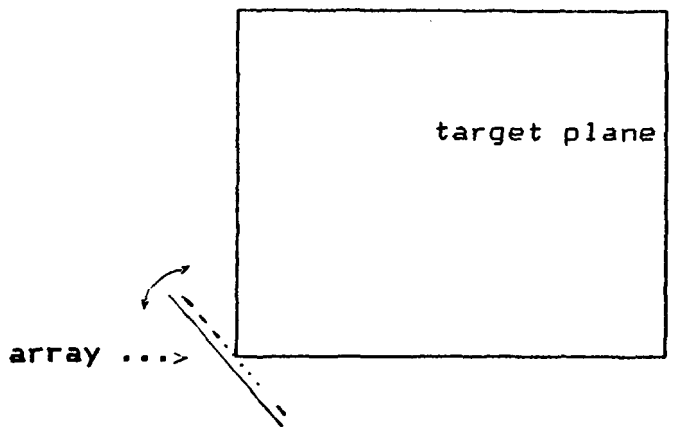

Fig. 6.15 Target plane and array position for simulated images shown in Fig. 6.16 and 6.17.

Figures 6.16a and 6.16b show the image of a point reflector using a 16 element array with single and multiple scans respectively. The multiple scans are performed using 3 x 15 degree rotations of the array around its centre. A reduction in the sidelobe levels as a result of compounding may be observed. The second set of simulations shows images of an ideal curved reflecting

surface. This surface, which is shown in Fig. 6.17a is assumed to comprise ideal point scatterers which reflect signals of equal amplitude to all elements in the sensor array. The focussed images of this surface for K=1 and for K=3 are shown in Figs. 6.17b and 6.17c respectively. As may be observed from these figures, the high intensity and wide distribution of the object caused artefacts appearing in the single scan image are significantly reduced in the compounded one.

6.3 IMAGING PERFORMANCE

This section reviews some standard image processing methods and presents sample experimental results which demonstrate the performance of the entire imaging unit. Most of the image data was acquired using a specially made 30 element transducer array with an element centre frequency of 1.48 MHz and an element centre to centre spacing corresponding to 1.3 times the wavelength in water (array #1). Two sample results using an array with a spacing of 0.7 of a wavelength (in water) are also shown (array #2). The constructional details and main parameters of both these arrays are discussed in APPENDIX D.

In order to represent a typically low SNR situation while at the same time having a known target configuration to allow verification of the results, target arrangements consisting of thin steel rods arranged in different patterns and a sector of a 2.5 cm radius metal rod were used. The steel rods had diameters of 2mm and 1mm, corresponding respectively to about 0.5 and 0.25 of a wavelength in steel, or 2 and 1 times a wavelength in water. These rods were found to reflect very weak echoes, totally undetectable at the receiver stage and barely so after multiple cycle processing. As for the metal sector, because of its specular nature most of the transmitted signals are reflected away, again resulting in low SNR in most of the array scan data. This is a situation often encountered in many imaging applications. (Photographs of

the targets may be found in APPENDIX F.)

For ease of implementation, all the experiments were performed in water. Also, the data acquisition was performed at a 12 MHz sampling rate and a 16 cycle averaging was used. In all cases, the images were formed using SAFT and a limited amount of image processing was carried out on some of them, with very good results being achieved. The images are displayed on an IBM-PC-AT using a display routine that reads 100 x 100 points of SAFT amplitude information and selectively zooms and displays the data in one or two colour grey scale intensities with up to 300 x 300 pixel points. Intermediate pixels in a zoomed display are filled by linear interpolation.

6.3.1 Some Applicable Image Processing Methods

Various image processing techniques exist for the enhancement of desired features within an image (or for the rejection of unwanted features). Extensive literature is available concerning processing methods for the improvement of image quality (for example, see [21,27]). Of particular interest in the present context (SAFT based ultrasonic pulse-echo imaging) are methods,

i. Which reduce the degree of background noise.

ii. Which detect and enhance edges.

iii. Which provide continuity where imaging artefacts result in defocussing effects.

The following two sections review some practical and

relatively simple techniques which may be used to achieve such improvements in the ultrasonic images formed using the present system. The reader should refer to the indicated references for a coverage of other complex and computationally intensive processing techniques.

(a) Noise reduction and image smoothing

In synthetically focussed images, in addition to other errors arising from sensor noise and channel errors as in alternative, for example, photographic images, there also exist artefacts generated by the focussing process. As discussed earlier the best way of reducing these is at source prior to image formation by using spatial averaging (see section 6.2.3).

Where this is not practical or where there still exists substantial level of random and isolated as well as coherent background noise within an image the methods outlined below may be applied.

(i) Selective thresholding

This operation involves rejecting image points above or below certain brightness levels to remain with only points possessing the desired intensities. Hence, in its use lies the inherent assumption that the intensity levels of the useful parts of an image are known and that they are clearly separated from those of the noise. A commonly used method for the determination of threshold levels is to utilise histograms of intensity versus number of pixels (Fig. 6.18) [27].

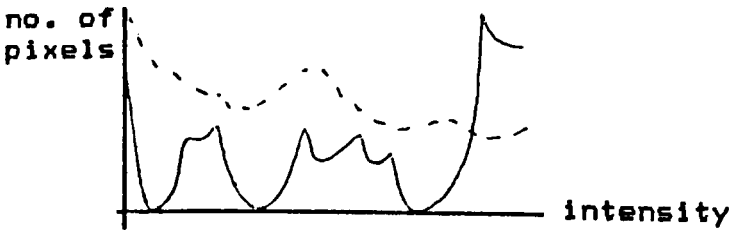

Fig. 6.18 Intensity histogram for threshold determination

Where there is a clear distinction between different levels, as shown with heavy line type in this figure, the nulls provide points where thresholds may be applied. Pixels with intensities below, above or in between such nulls may be rejected. This would be an objective approach which may be used in situations where the objects of interest are of reasonably uniform brightness placed against a background of differing brightness. However, in ultrasonic images, desired portions tend to consist of parts with similar intensity as undesired parts and the intensity histogram would appear as shown in dotted lines in Fig. 6.18. Hence, in practice, the choice of threshold may have to be a subjective trial and error process where one tries to minimise background noise without losing outlines of the objects.

In general, prior to any other operation on ultrasonic images, a limited thresholding on the focussed images is necessary to reduce low amplitude background clutter and artefacts. The histogram approach should always precede non-objective attempts of threshold level selection.

(ii) Pixel averaging

After thresholding, isolated random noise in an image may be eliminated by using so called 'averaging windows'. These are windows of 3 x 3 pixels (such as that shown in Fig. 6.19). The averaging operation involves replacing every pixel by the average value of the pixels around it so that abrupt image intensity variations are reduced. As random noise usually appears as isolated pixel variations within an image, averaging reduces its effect. The operation is outlined below. Consider adjacent pixels whose amplitudes are represented by a,b,c,d,o,f,g,h,i.

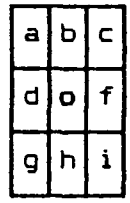

Fig. 6.19 A 3 x 3 averaging window.

Mathematically, the new value of o after averaging will be given by,

$$o' = \frac{1}{8} \Sigma a,b,c,d,f,g,h,i \qquad \ldots 6.13$$

The relative simplicity and hence processing speed of this algorithm makes it attractive for ultrasonic image processing. Removal of isolated noise is not its only application. Even in relatively noise free situations, as the averaging process tends to reduce amplitude differences, this technique may be used to provide continuity and uniformity of brightness in images. Its disadvantage is that it results in a degradation of

resolution as it reduces all abrupt amplitude changes, including those defined by object boundaries. One way of compensating for this may be succeeding the averaging by a second selective thresholding.

(iii) Logical smoothing

Logical smoothing is an operation which is primarily used to eliminate isolated noise from binary (two intensity level) images. It may also be applied to the general case by quantising pixel values to two levels. Then using a 3 x 3 window as that shown in Fig. 6.19 but with a,b,c,.. representing binary values, the new pixel value of the centre cell o will be given by,

$$o' = \bar{o}.(a.b.c.d.f.g.h.i) + o.(a+b+c+d+f+g+h+i) \quad ..6.14$$

Where, a+b denotes the logical 'a OR b' operation, a.b denotes the logical 'a AND b' operation and $\bar{o}$ denotes logical inversion. The new value o' is 1 if o is 0 and all its neighbours are one or if o is 1 and at least one of its neighbours is 1. The transformed binary pixel amplitudes are then multiplied by the original pixel amplitudes to recover the original image, less any isolated pixel variations. But care must be taken when using this technique with thresholding. In addition to deleting low amplitude background noise, thresholding may also remove low intensity parts of the useful image such that parts of the useful image would consist of loosely clustered pixels. Hence, if logical smoothing succeeds that operation, such portions consisting of loosely

clustered image points would also end up being totally deleted. Therefore, for ultrasonic images, logical smoothing may only be applied prior to thresholding. Consequently, it serves mainly to limit isolated noise that occurs due to channel errors. The relative advantage of this technique is that unlike pixel averaging, it does not degrade resolution as the amplitudes of the undeleted pixels remain unchanged.

(iv) Low pass spatial filtering

Noise in an image generally has a higher spatial frequency spectrum than do the normal image components [28]. Hence, another alternative for suppressing isolated pixel variations and providing smooth continuous images is two dimensional low pass filtering. The image data is Fourier transformed, passed through a suitable low pass frequency window function and inverse Fourier transformed to obtain the processed image data. Further, extensive discussion on two dimensional filtering may be found in references [21] and [27]. Low pass filtering is essentially a frequency domain implementation of the averaging operation described earlier and may be used interchangeably. However, it has the disadvantage of being slower. The need to repeatedly perform image intensity/ spatial frequency domain transformations necessitates a longer processing time. Its other disadvantage is that as in averaging, it leads to a limited loss of resolution.

The methods discussed here have been used for

processing the real, synthetically focussed images described in the next section with successful results. For simplicity and speed, selective thresholding and pixel averaging are the preferred techniques for noise reduction and image smoothing once the SAFT images have been formed. Logical smoothing may be used for noise reduction in unthresholded images and low pass filtering may be used where fast processing and high resolution are not essential. However, it should be emphasised that the best way of enhancing image SNR is to couple noise reduction with image reconstruction, instead of post-processing an already formed image. This involves enhancing the A-scan SNR prior to focussing (through matched filtering or simple averaging) and focussing with scans acquired from multiple positions of the sensor array (spatial compounding).

(b) Edge enhancement

In many ultrasonic imaging applications, notably in medical imaging it is often desired to extract feature outlines (object boundaries) from images consisting of target image, channel noise and focussing artefacts. Boundaries (such as, for example, organ outlines in medical imaging) are often distinguished by the relatively abrupt intensity variation they exhibit on images. But often these variations don't appear clearly distinct due to other high amplitude reflectors or artefacts in the

target plane which affect the image resolution. Additionally, in many ultrasonic testing applications, areas of interest may be located at specific regions on a continuous surface, such that if the surface is properly identified within an image, it may serve as a feedback to the transmit/receive/focus system to further localise the area of observation. For example, in NDE, corrosion monitoring may be facilitated if the surface where it occurs is properly identified. Similarly, in medical imaging proper identification of organ outlines will permit the improved localisation of regions of interest.

Edge detection employs a variety of algorithms to improve the definition of object boundaries in images. It essentially involves accentuating features that exhibit abrupt amplitude changes with specified orientations such that in later thresholding only outlines corresponding to edges will remain. Then depending on the application, the edge outlines may be superimposed on the original image to obtain an image with crispened object boundaries or alternatively the image of just the outlines may suffice.

In general, as edge detection essentially enhances amplitude variations in an image, its application will result in the amplification of all abrupt changes including those caused by noise. Hence, it is only applicable for low noise, low artefact images. Provided that this limitation is borne in mind, some of the methods discussed below may be used for edge detection in the

ultrasonic images formed using SAFT.

Consider an I x J image plane with pixel amplitudes F(i,j) where i and j represent the horizontal and vertical pixel coordinates respectively. A linear edge enhancement involves replacing pixel amplitudes by the difference of adjacent pixel amplitudes. Hence, for example, the operation described below of taking the difference of vertically adjacent pixels sharpens vertical edges.

$$F'(i,j)= F(i,j)-F(i,j+1) \qquad ...6.15$$

Similarly, taking the difference of horizontally adjacent pixels accentuates horizontal edges.

$$F'(i,j)= F(i,j)-F(i+1,j) \qquad ...6.16$$

The same method may be used to detect diagonally oriented edges.

$$F'(i,j)= F(i,j)-F(i+1,j+1) \qquad ...6.17$$

It is apparent from eqns. 6.15 to 6.17 that when these operations are applied, homogeneous sections of an image will result in low output and only those sections where large, abrupt changes occur will give high output. Hence, only boundaries will be enhanced.

Instead of taking just the difference of adjacent pixels the difference between slopes along a line may also be used. For example, the operation,

$$F'(i,j)= [F(i,j)-F(i,j-1)]-[F(i,j+1)-F(i,j)] \qquad ...6.18$$

enhances vertical edges.

If one thinks of these as differentiation operations, those described by eqns. 6.15 to 6.17 would be

first derivatives while that described by eqn. 6.18 would be a second derivative in the specified orientation. Hence, an operation as that described in eqn. 6.18 is more powerful in accentuating edges , but at the same time also more susceptible to noise.

Instead of taking simple differences, algorithms that utilise squared pixel differences and logarithmic pixel differences may also be used [27]. As in the case of taking second derivatives, squaring differences would provide better edge extraction but would also result in more noise amplification. In contrast, taking logarithms would show lower detection and lower noise.

Some non-linear two dimensional edge isolation methods are also available. For example, the so called Sobel edge detection utilises the algorithm described below for two dimensional edge accentuation [21,27]. Again consider the 3 x 3 pixel window shown in Fig. 6.19. For the determination of the new value for the centre cell **o**, firstly the total difference between vertical lines of pixels on both sides of **o**, followed by the total difference between the horizontally oriented ones are taken. In both dimensions, more weight is given to the differences of pixels directly in contact with **o** (b,d,f,h). Hence, the sum of horizontal differences will be given by, (refer to Fig. 6.19)

$$m = (a-c)+(2d-2f)+(g-i) \qquad \ldots 6.19a$$

Similarly, the sum of vertical differences will be

given by,

$$n = (a-g)+(2b-2h)+(c-i) \qquad \ldots 6.19b$$

Once the gradients in both dimensions are separately computed as shown, the overall magnitude is calculated to determine the new value of o. That is,

$$o' = \sqrt{m^2+n^2} \qquad \ldots 6.19c$$

The only disadvantage of this algorithm is its relative complexity (compared to those given by eqns. 6.15 to 6.18) and therefore lower processing speed.

Lastly, two dimensional edge enhancement may also be performed in spatial frequency domain using spatial high pass filtering [21,27]. This basically involves the two dimensional frequency domain transformation of the image plane, deletion of low frequency spectral components and inverse transformation to recover the image. Further discussions on the use of spatial filtering for the enhancement of feature outlines may be found in references [21] and [27]. As in the previously outlined techniques, since this approach essentially amplifies amplitude differences with any orientation, its use is limited only to high SNR images. Additionally, relative to the other techniques earlier, this method is slow and computationally intensive, mainly due to the transformation to and from spatial frequency domain.

SAFT images, such as those shown in the next section, invariably include focussing artefacts even in

external noise free conditions. Hence, for the present application, edge enhancement cannot precede thresholding and averaging. The choice of the actual method should be based on the consideration of susceptibility to noise in addition to algorithm simplicity and hence processing speed. The relatively simple algorithms given in eqns. 6.15 to 6.17 would best suit these requirements, provided that the level of noise has been minimised by the methods described in section (a).

Demonstrations of their use may be found in the simulated image of Fig. 6.17d and the real image from an arc sector shown in Fig. 6.28e.

6.3.2 Performance with small reflectors

This was investigated with 2 mm diameter steel rods placed in the far field of the array elements and 1 mm phantom rods in a perspex casing filled with water (also in the far field). Cross sectional sketches of the different target arrangements, their initial focussed images and the processed versions are presented in Figs. 6.21 to 6.27.

The 2mm rods were held in a grid of holes with a centre to centre spacing of 8mm. The array is positioned on top, looking down in a cross section. This is outlined in Fig. 6.20 below.

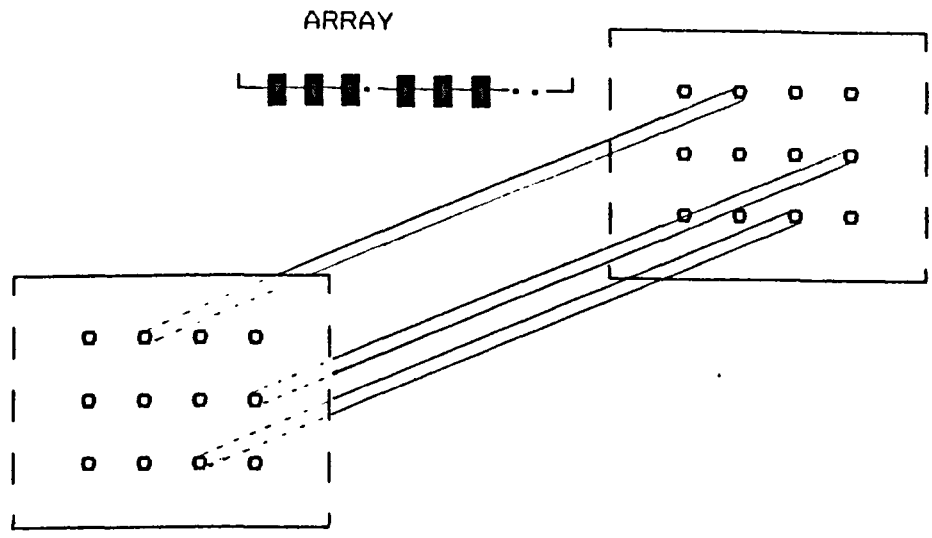

Fig. 6.20 Experimental set-up for imaging the 2mm rods.

The first target arrangement is shown in Fig. 6.21a. This is used to demonstrate the entire process and to compare the system with other pulse-echo imaging. The focussed image is shown in Fig. 6.21b. Although the rods may be identified, their resolution requires some improvement. Apart from the extremely low input scan SNR, another main reason for the relatively low image SNR is non-uniformity in the array element responses as described in APPENDIX D. Non-uniformity in pulse amplitudes are difficult to compensate by software techniques for situations where the data SNR is relatively low. This is because selective weighting of the scan data will also increase noise. The same problem is faced in correcting for ultrasound attenuation with depth as well as directivity effects.

It was then attempted to improve the original image by a combination of thresholding and averaging operations. For targets such as those in this arrangement where the dimensions and depth from the array of the scatterers are similar, with the likelihood of resulting in comparable amplitude images, an objective choice of thresholding level may be attempted. For this particular case the histogram of intensity versus number of pixels appears as shown in Fig. 6.21c. A 22% thresholding (the first low level on the histogram) was chosen here. However, as stated earlier, for ultrasonic images this choice is often subjective and is arrived at by a trial and error process in which it is attempted to minimise the background artefacts without losing the outlines of the scatterers. After thresholding, pixel averaging (eqn. 6.13) was applied to provide continuity in the rod images which after high thresholding appear as a cluster of isolated pixels. Low pass filtering may also be used for this purpose with the same effect. As the image has been passed through a high threshold level, logical smoothing is not applicable here. Finally, a second threshold is applied to limit the smearing (degradation of resolution) that occurs after pixel averaging or low pass filtering. The second threshold level is varied until the dimensions of the targets in the image correspond to their actual sizes (2mm). As shown in Fig. 6.21d, a very good improvement has been achieved by these relatively simple processing

methods. Although the rods in the processed image appear wider, a closer inspection reveals that these are in fact very close to the actual sizes (considering that the whole image plane represents a 4.4cm x 4.4cm target plane). The quality of the original focussed image may be appreciated by considering the situation without correlation reception. The array elements were excited by a single 5 volt pulse instead of the code burst and the digitised, receiver data was directly collected without any further processing. The resulting focussed image appears as shown in Fig. 6.21e. The very poor SNR is clearly evident. As this level of image SNR is occurring even after the averaging that occurs in the focussing process, it may give an indication of the severity of the poor SNR in the original scans. This example may also serve to demonstrate that it is really impossible to perform practical ultrasonic imaging at very low voltage excitation without additional, powerful signal to noise ratio enhancement techniques such as those developed in this work. As a further comparison, Fig. 6.21f shows the image of the same target arrangement obtained from a standard, commercial imaging unit utilising 200 volts excitation and linear array scanning with 400 elements. The image obtained using the low voltage system (Fig. 6.21d) is clearly as good as this one in terms of image quality and by far superior when one considers that it is operating at less than 2% of the excitation utilised in the commercial unit.

Attempts were made to image two more target configurations (with the 2mm rods) to further evaluate the focussing and processing methods used for the first arrangement. Details are not given here as it is exactly the same procedures that were applied. The outline of the second configuration, its focussed and processed images are shown in Figs. 6.22a, 6.22b, and 6.22c respectively. The performance is clearly as good as the earlier one. The same is true for the third arrangement shown in Figs. 6.23a to 6.23c.

To look at the effect of spatial addition another measurement was taken on the third arrangement by inverting the target set-up, ensuring proper alignment as before. This is equivalent to taking scan data of the same target plane, but with the array subjected to a reflection transformation about the centre of the plane. The image of the targets as seen from the second position is shown in Fig. 6.24. Now if this image is added to that of Fig. 6.23b, taking into account the reflection transformation, the result will be a compounded image (K=2) of the target plane. The result obtained by superimposing the two image data is shown in Fig. 6.25. The definition is clearly much better than in the single scan image shown earlier. A comparison of their intensity histograms shown in Fig.6.26 also demonstrates that the compounded image has a reduced level of low intensity pixels (hence, low background noise). Indeed, no additional processing is required.

Lastly, to see if any lesser input SNR is tolerated by the system it was attempted to image 1mm rods suspended in a perspex container filled with water (their distribution is shown in Fig. 6.27a, their photograph may be found in APPENDIX F). These are not only weak scatterers, but their size is at the limit of resolution that may be achieved for the particular transducer centre frequency being used. As shown in the focussed image of Fig. 6.27b, it was still possible to locate these rods, giving a good indication of the limits and potential of the system. Fig. 6.27c shows the image of the same rods obtained from the 200v commercial imaging unit used earlier. Here, the apparently superior image resolution of the commercial unit is only due to its higher frequency transducer array (3.5 MHz) and relatively wider array aperture. Considering that the image of Fig. 6.27b was obtained using a 30 element, 1.48 MHz array, it is clear that the low power system has the same potential.

6.3.3 Performance with a divergent specular reflector

Imaging near-specular reflectors is a problem often encountered in ultrasonic imaging. As most or all of the transmitted signal may reflect away from the receivers, the SNR in the array scan data is usually extremely poor. To investigate how the system behaves in such a situation, it was attempted to image a sector of a 5cm diameter steel rod positioned at a distance of 5cm from the array.

The original focussed images for two different focussing resolution and apperture sizes are shown in Figs. 6.28b and 6.28c respectively. The image shown in Fig. 6.28b covers a 4.4cm x 4.4cm target plane (100 x 100 pixels with 0.44mm resolution) while Fig. 6.28c represents a 2.5cm x 2.5cm plane (0.25mm resolution). Hence, while the former covers a wider area, the latter has a better resolution. Grating lobes may be seen in the relatively crude resolution image of Fig. 6.28b. Additionally, severe 'object focussing' effects appear in both images (as discussed in section 6.2.3). However, as the outer curved edge is clearly distinguishable in both images, a selection of processing operations were performed on them to obtain the much better defined images shown in Figs. 6.28d and 6.28e.

The processing used included the following.

Firstly, low thresholding (5 % of the peak) was applied to limit low amplitude background noise followed by pixel averaging (eqn. 6.13) to improve the amplitude uniformity within the image. After the averaging, a signed vertical edge extraction (eqn 6.15) was applied to detect the upper surface. 'Signed' refers to only considering positive pixel differences but setting negative ones to 0 or vice versa. It is necessary to use a signed approach because only considering magnitudes of differences would also detect all vertically oriented edges including the lower edge defined by the constructive interference of

the artefacts (see Fig. 6.28b and 6.28c). Lastly, low pass filtering was applied to smoothen the final image. As may be observed in Fig. 6.28d and 6.28e, the curve has been reasonably identified. It is believed that this example demonstrates that if succeeded by the appropriate image post-processing, the system developed in this work is also capable of imaging larger objects comprising specularly reflecting surfaces. Such surfaces are very common both in NDE and medical imaging applications.

6.3.4 Performance with small array

This section presents two more sample results to demonstrate that the system is also operational with smaller arrays. The array used to acquire the data (array #2) was a 32 element array with a nominal element centre frequency of 1.41 MHz and an element centre to centre spacing corresponding to 0.7 of a wavelength in water (corresponding to approximately half the spacing and the aperture size of array #1 which was used earlier). The experiments were conducted under identical conditions as those described in section 6.3.2. Here, only the focussed images without any further processing are presented. The first target was a 1 cm long, and 0.5mm wide sawblade placed 4 cm from the array. The cross sectional view of the target arrangement is outlined in Fig. 6.29a. In the focussed image which is shown in Fig. 6.29b, the sawblade may be clearly identified. The second set-up consisted of

the same rods used earlier with a thick glass block underneath (outline shown in Fig. 6.30a). Again, the focussed image is fairly good (Fig. 6.30b). The gaps that appear in the image of the glass reflector are acoustic shadows of the rods since they block the sound beam from the array from reaching parts of the glass reflector directly underneath.

Both the results of this section show performance as good as those obtained with the wider array used in section 6.3.2. Any irregularities in these images can only be attributed to the array non-uniformity (as detailed in APPENDIX D). If required, these may be improved further using the processing methods used in the previous section. Thus, it is concluded that the imaging system is also operational for different array configurations.

6.4 CONCLUSION

This chapter has looked at the image formation aspect of the present investigation. As the data acquisition hardware described earlier operates by multiplexing among array elements, a synthetic aperture reception focussing technique has to be used for image formation. The principles of this technique have been reviewed. Its dependence on the SNR of the original scan data and the improvements achieved by using correlation reception have been demonstrated using the Point Spread

Function (P.S.F.) as a comparison criteria. It was shown that the performance of SAFT depends on the target size or distribution and it was suggested that this could be improved upon by increasing the number of sensors, by using special array shapes and by spatially averaging the images.

In the second part of the chapter, some standard image processing methods which may be applicable to SAFT based ultrasonic imaging were reviewed. Finally, real focussed and processed images of various weakly reflecting target arrangements were shown, with excellent results. The system was shown to be operational for different array and target configurations. Additionally, it was shown to be superior to a system using conventional pulse-echo data acquisition at the same excitation level and to perform as good as a system using an excitation which is 50 times greater.

The processing methods that were considered included ways of reducing background noise (such as channel noise, coherent clutter and focussing artefacts) and edge detectors to extract feature outlines in high SNR images. It is useful to summarise some observations regarding these techniques.

Thresholding was recommended as an initial operation to limit low amplitude artefacts. However, it has also been noted that for most ultrasonic applications, the choice of the threshold level is largely subjective as

there usually is no clear distinction between error intensity levels and those of the useful parts of the image. Through the results, it has also been shown that pixel averaging and low pass filtering may be effectively used for ultrasonic images to provide continuity and reduce isolated intensity variations. If required, the limited resolution degradation due to these operations may be compensated for by additional thresholding. Finally, edge detection has been shown to be applicable, though it has been emphasised that it may only be used provided that the degree of noise has been sufficiently reduced by the techniques mentioned earlier. Among the unused but reviewed techniques are logical smoothing for random noise reduction and two dimensional high pass filtering for edge accentuation. The former is not recommended to be used after thresholding an ultrasonic image as it may reject desired parts as well as undesired ones, while the latter is not recommended for SAFT images unless the intensity of the useful sections is homogeneous and random noise as well as coherent artefacts are practically non-existent.

This demonstration of obtaining ultrasonic images from poor SNR input data and using very low voltage excitation concludes the present investigation. Further work in this line could involve the development of better quality arrays and the conduction of a thorough quantitative assessment of the imaging performance. Implementation and evaluation of the techniques proposed

for improving on object focussing effects in SAFT would provide interesting research areas. Finally, the possibility of expanding the system for real time imaging is worth pursuing.

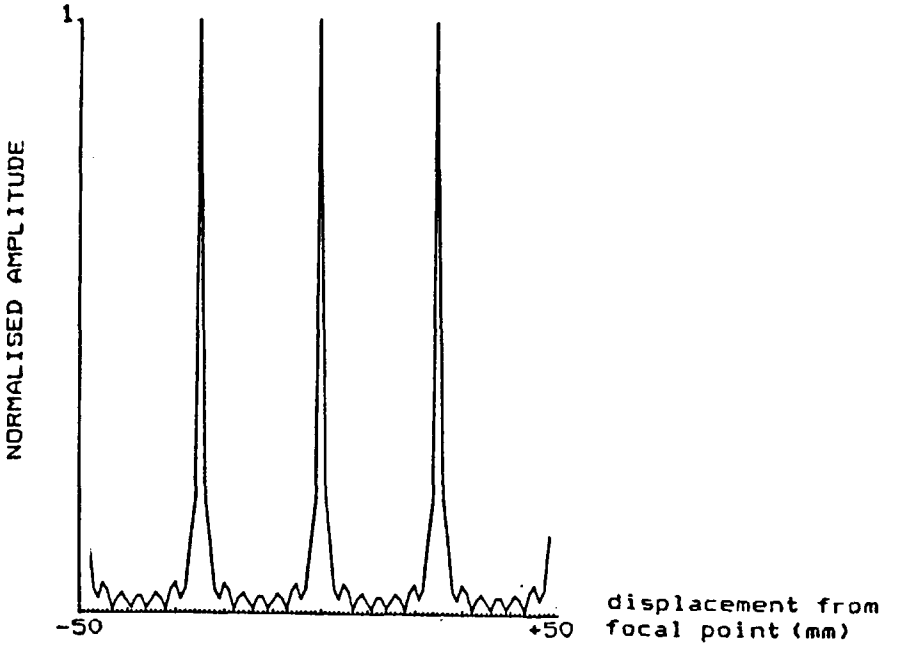

Fig. 6.3 Lateral P.S.F. magnitude for CW excitation, using a 32 element array with λ spacing.

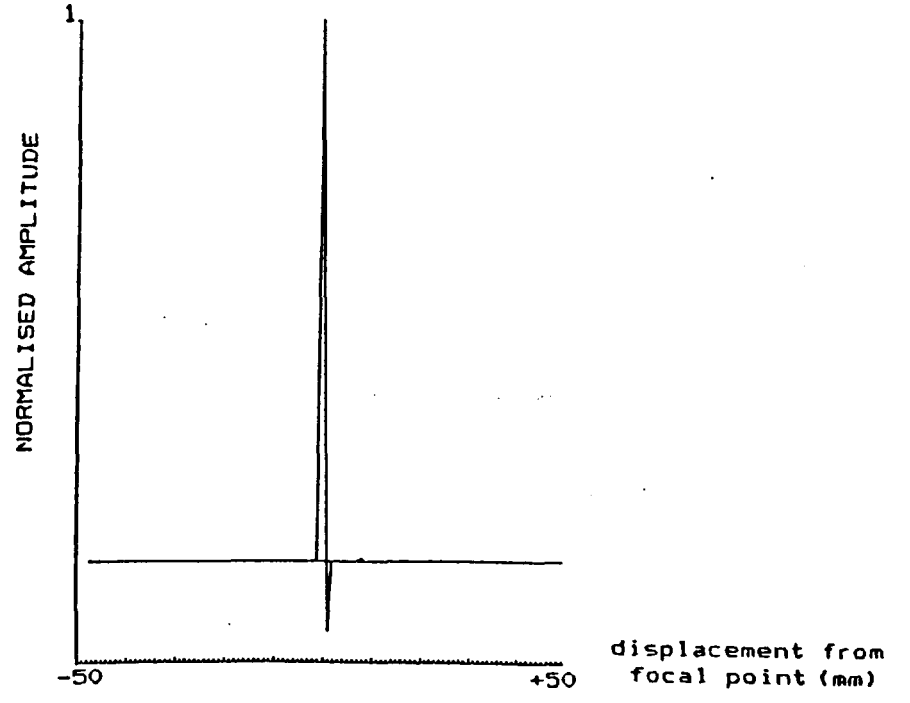

Fig 6.5a P.S.F. magnitude in the range direction using a 1.7MHz. wavelet, sampled at 12 MHz. Focussing performed using a 32 element array with λ spacing. No external noise assumed.

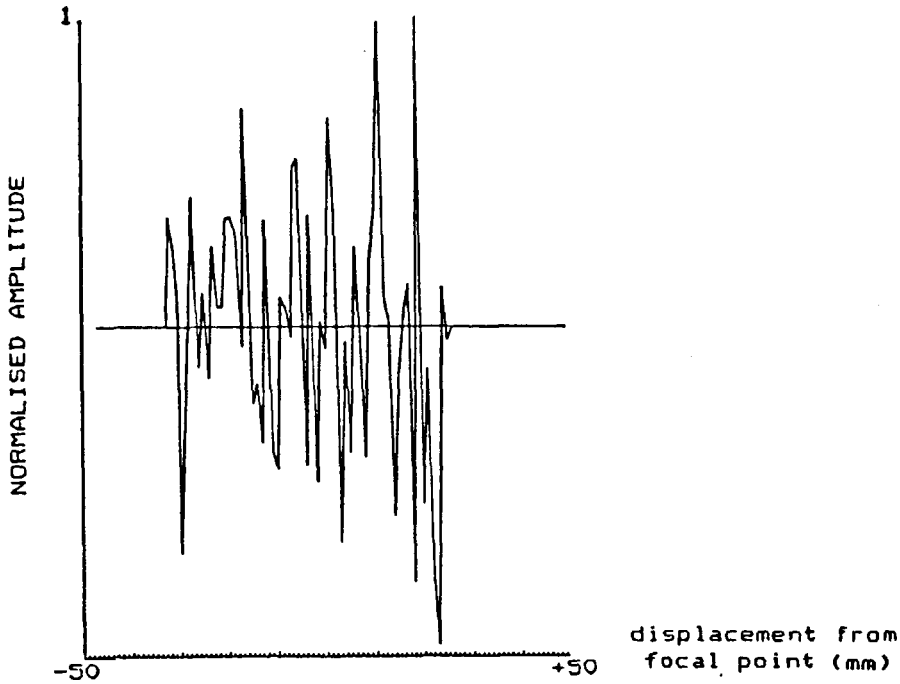

Fig. 6.5b P.S.F. of Fig. 6.5a when an external noise of σ_n =0.04 exists in the original scan data.

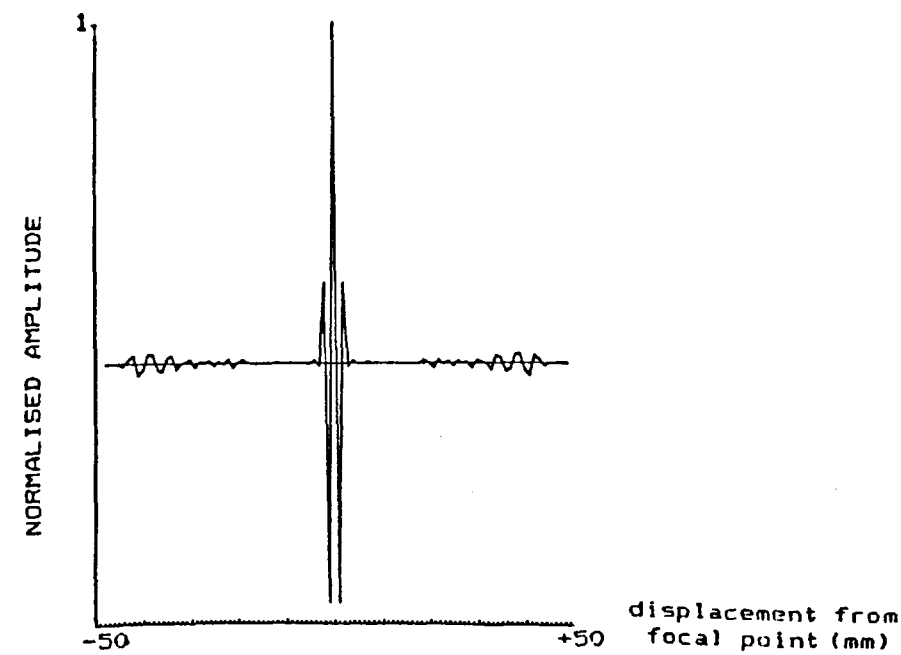

Fig 6.6a Lateral P.S.F. magnitude using a 1.7 MHz wavelet, sampled at 12 MHz. Focussing performed using a 32 element array with λ spacing. No external noise assumed.

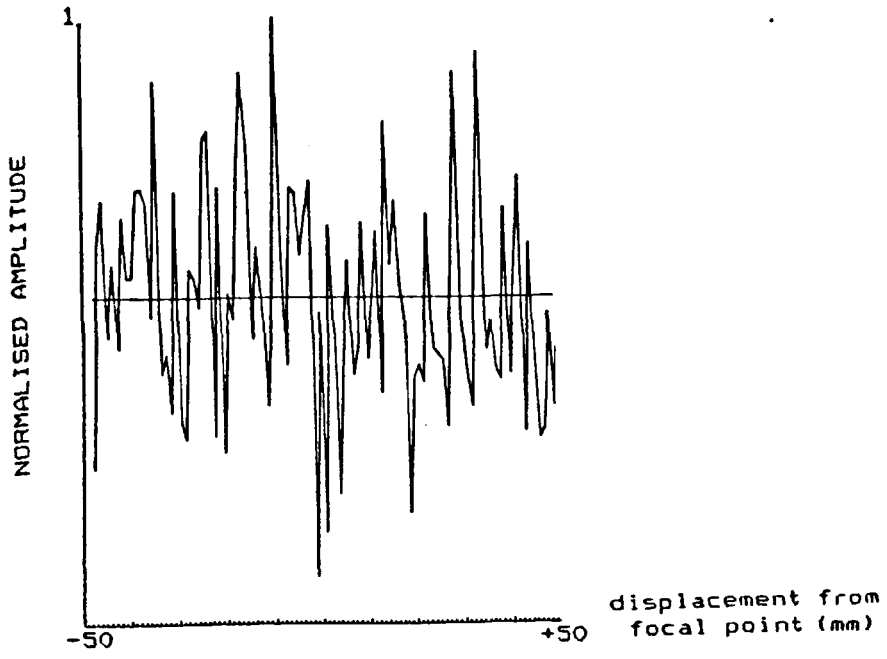

Fig 6.6b Lateral P.S.F. magnitude of Fig. 6.6a when an external noise of σ_n=0.04 exists in the original scans.

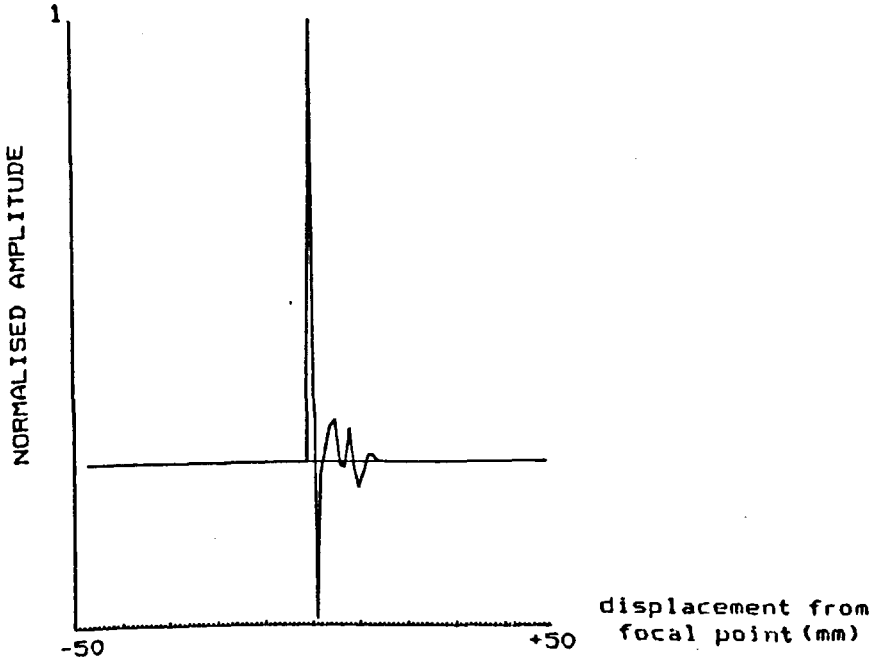

Fig.6.7a P.S.F. of Fig 6.5b, but using correlation reception. An external noise of σ_n=0.04 exists in the original data scan.

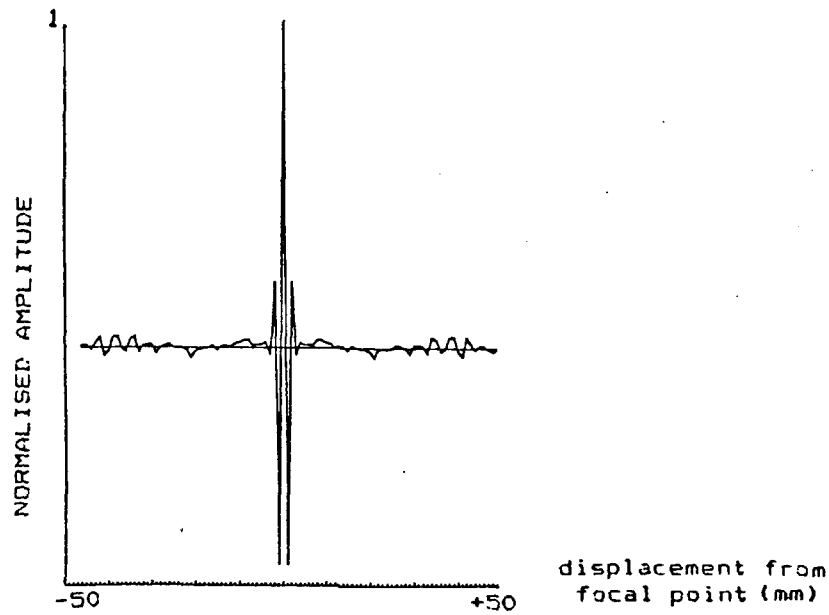

Fig. 6.7b P.S.F. of Fig 6.6b, but using correlation reception. An external noise of σ_n=0.04 exists in the original data scan.

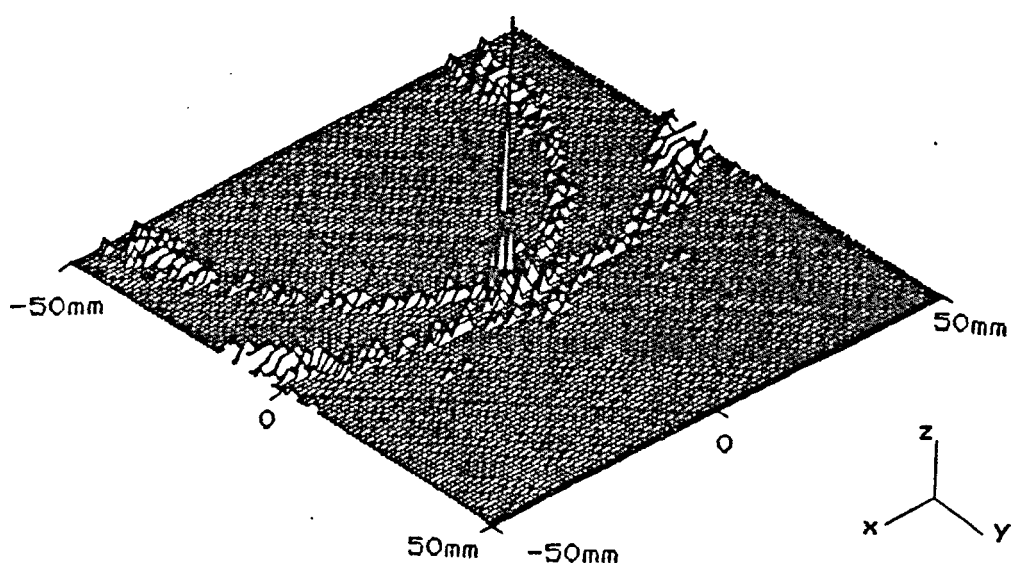

Fig 6.8 The combined P.S.F. magnitude in 2 dimensions. The x-y axes indicate the plane of focus while the z axis indicates normalised amplitudes of the image points. Correlation reception is used and scans are assumed to contain noise of σ_n=0.04.

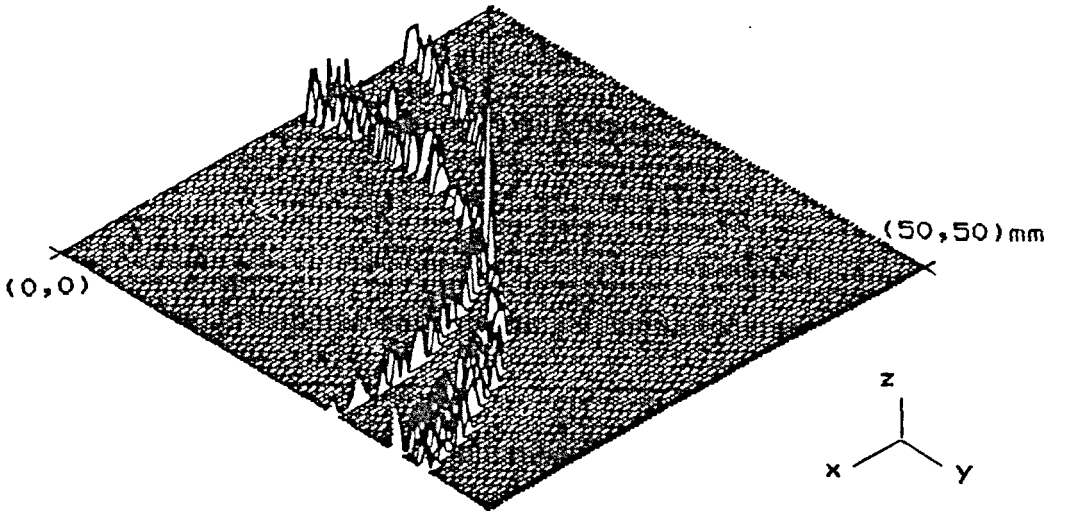

Fig. 6.16a Simulated image; point reflector using scans from a single position. A 16 element array is used.

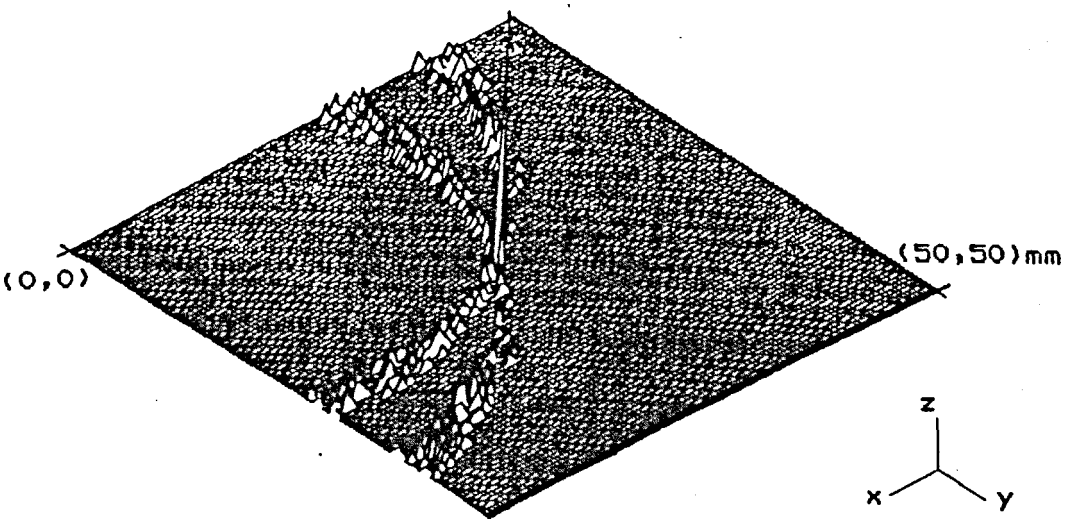

Fig 6.16b Simulated image of point reflector using scans from three rotational positions of array. (K=3 compounding). A 16 element array is used.

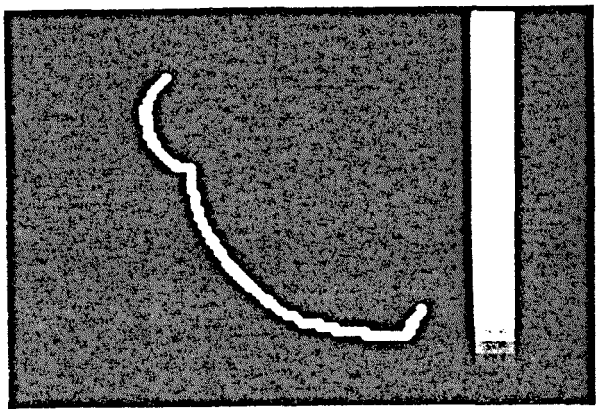

Fig. 6.17a A simulated, ideal reflecting surface.

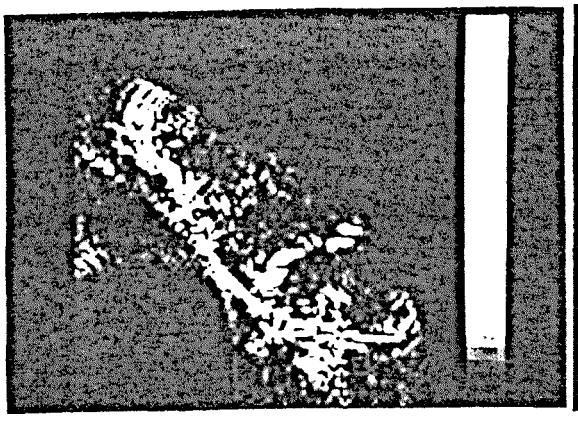

Fig. 6.17b
Simulated SAFT image
of 6.17a (K=1).

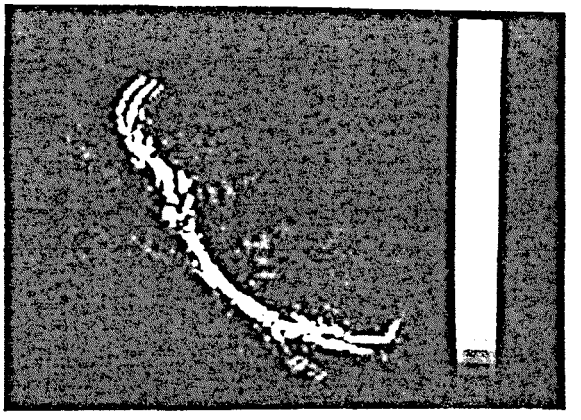

Fig. 6.17c
Simulated SAFT image
of 6.17a (K=3).

Fig. 6.17d Simulated SAFT image of 6.17c after thresholding (10%) and edge detection.

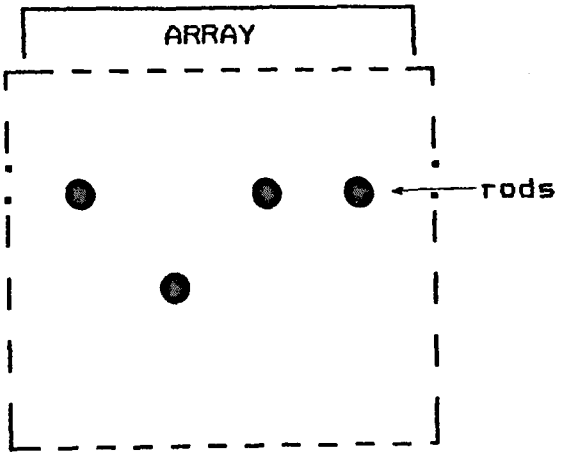

Fig. 6.21a Target arrangement #1. Rod sizes = 2mm
Horizontal and vertical separations=8.8mm

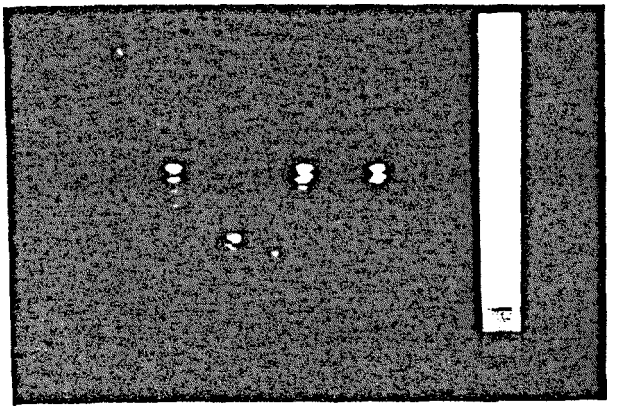

Fig. 6.21b Original SAFT image of #1.

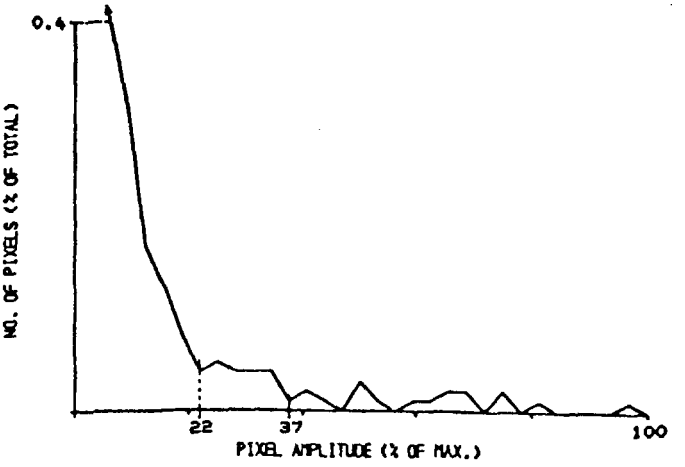

Fig. 6.21c Intensity histogram for image in Fig. 6.21b.

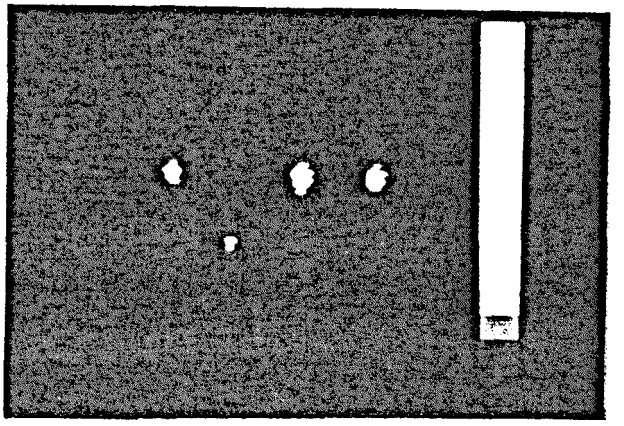

Fig. 6.21d Processed image of 6.21b.

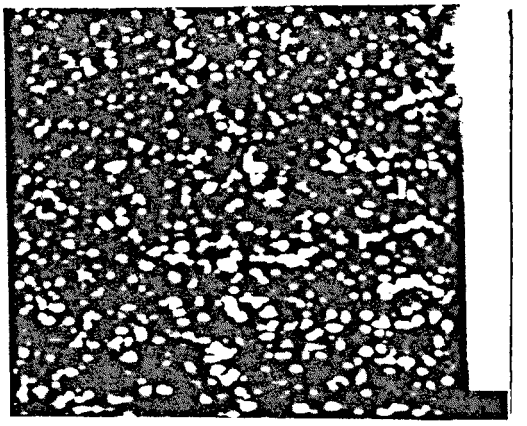

Fig. 6.21e SAFT image of #1 with 5 volt pulse excitation but without using correlation reception.

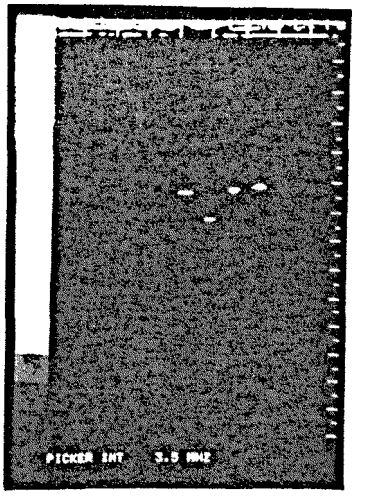

Fig. 6.21f Image of #1 using a 200v standard imaging unit.(400 element array, 3.5 MHz centre frequency)

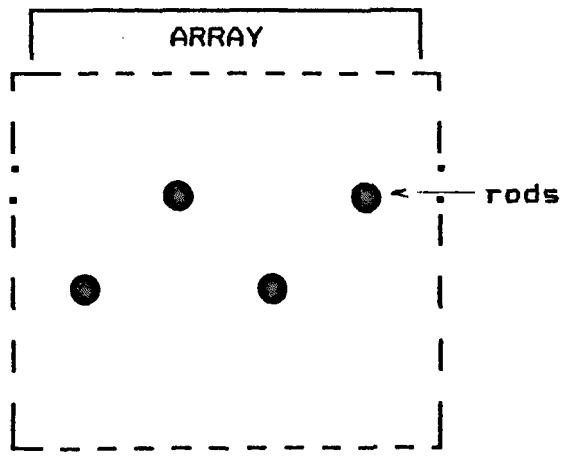

Fig. 6.22a Target arrangement #2. Rod sizes=2mm
Horizontal and vertical separations=8.8mm

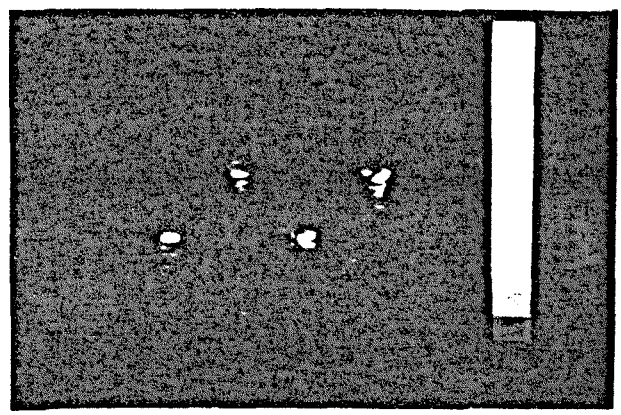

Fig. 6.22b Original SAFT image of #2.

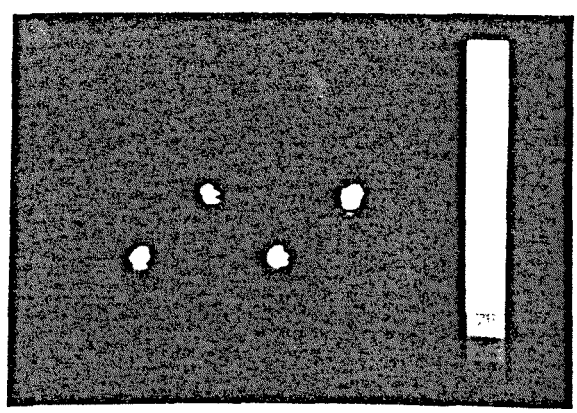

Fig. 6.22c Processed image of 6.22b.

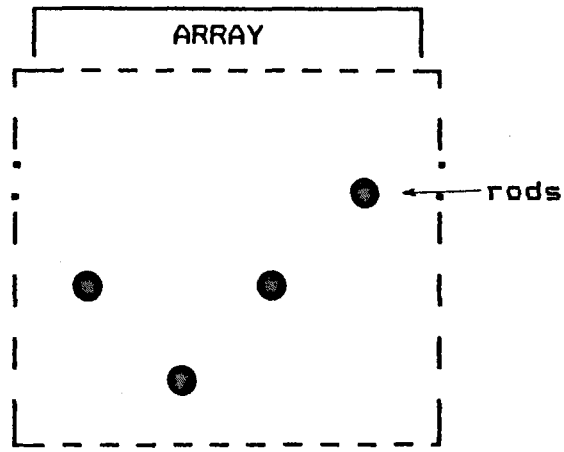

Fig. 6.23a Target arrangement #3. Rod sizes=2mm
Horizontal and vertical separations=8.8mm

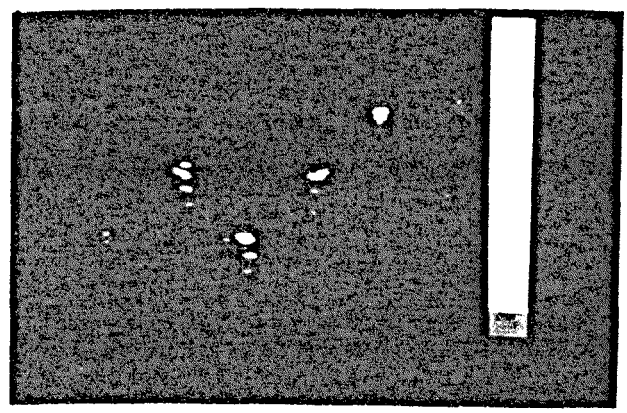

Fig. 6.23b Original SAFT image of #3.

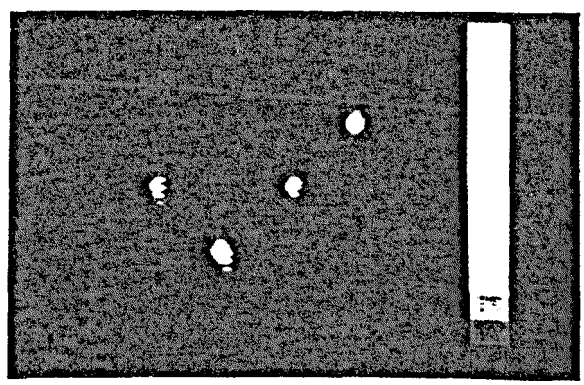

Fig. 6.23c Processed image of 6.23b.

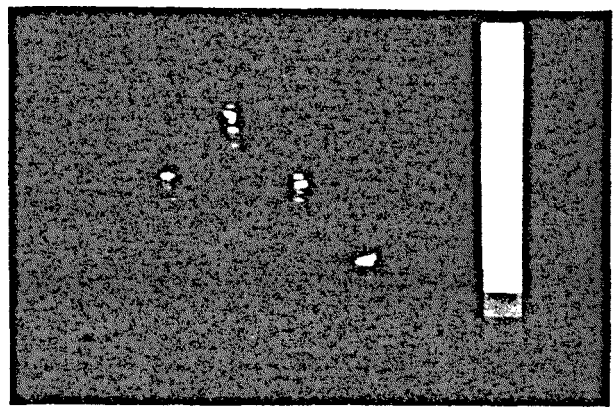

Fig. 6.24 SAFT image of #3 with the array positioned at the bottom of the target plane looking up.

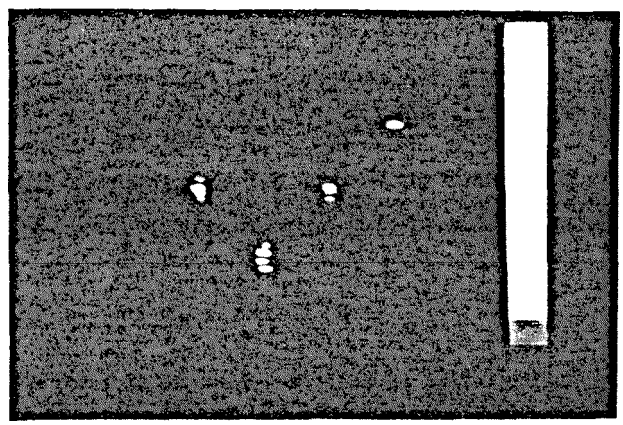

Fig. 6.25 Compounded image (K=2) of #3 obtained by adding 6.23b and 6.24 (reflected).(should be compared to the single scan image of 6.23b.)

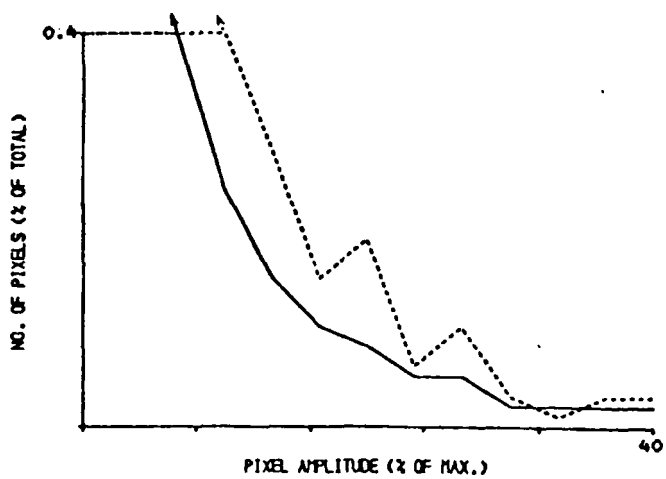

---- single scan ——— compounded

Fig. 6.26 Low intensity histograms for the single scan and compounded images of #3 (6.23b and 6.25).

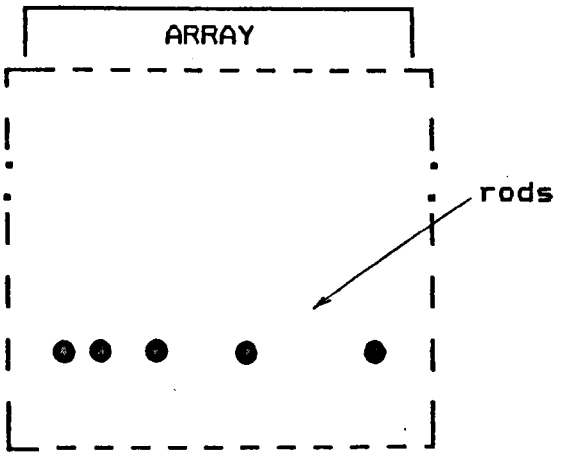

Fig 6.27a Target arrangement #4. 1mm rods in a perspex container.

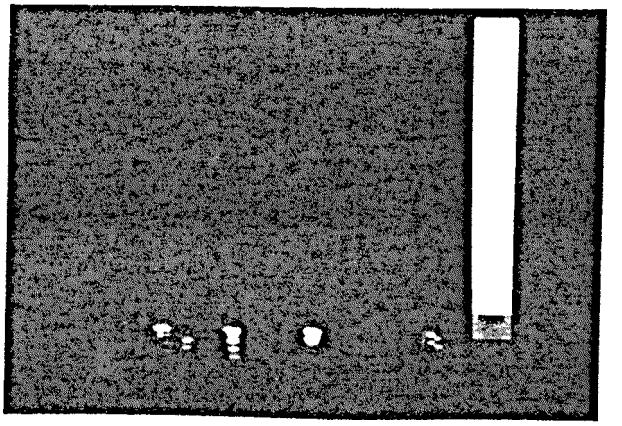

Fig. 6.27b SAFT image of #4

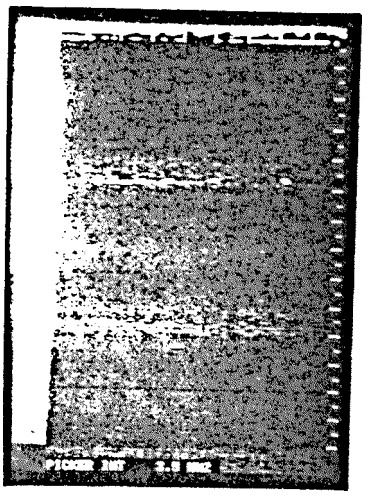

Fig. 6.27c Image of #4 obtained from a 200v standard imaging unit.(400 element array, 3.5 MHz centre frequency)

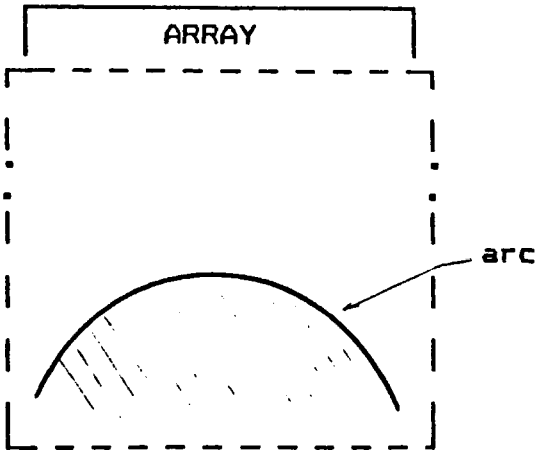

Fig. 6.28a Target arrangement #5. 2.5mm radius arc sector.

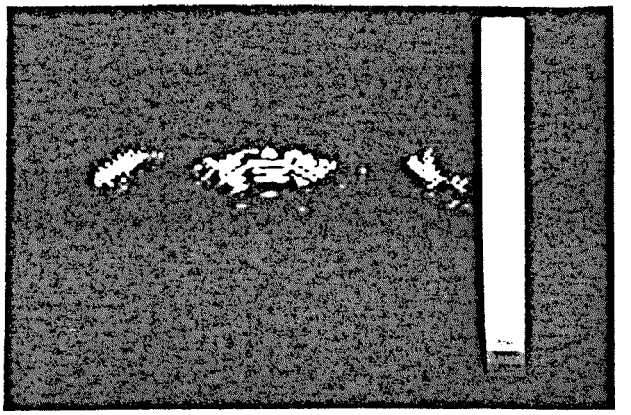

Fig. 6.28b Original SAFT image of #5 using a pixel resolution of 0.44mm.

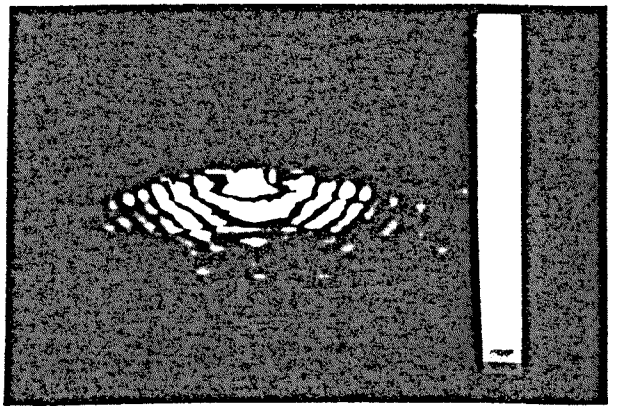

Fig. 6.28c Original SAFT image of #5 using a pixel resolution of 0.25mm.

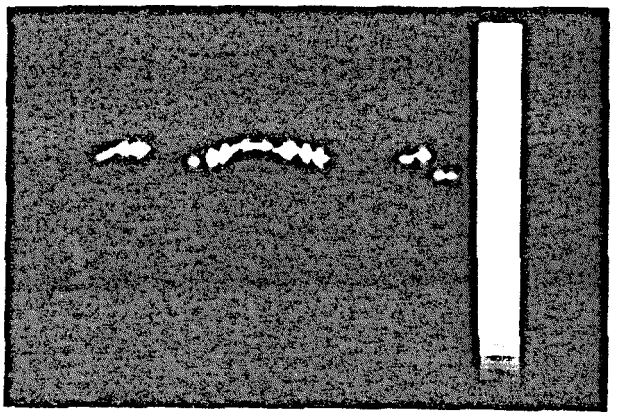

Fig. 6.28d Processed image of 6.28b.

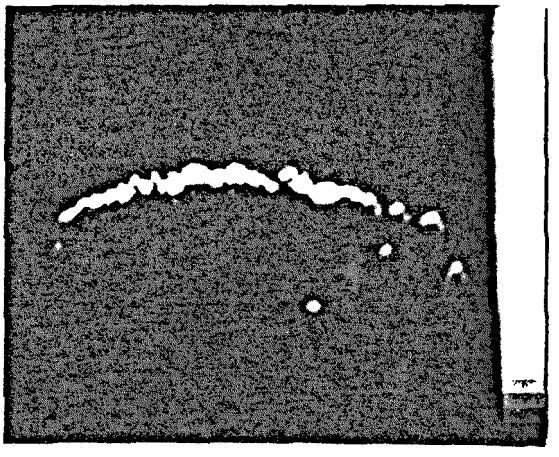

Fig. 6.28e Processed image of 6.28c.

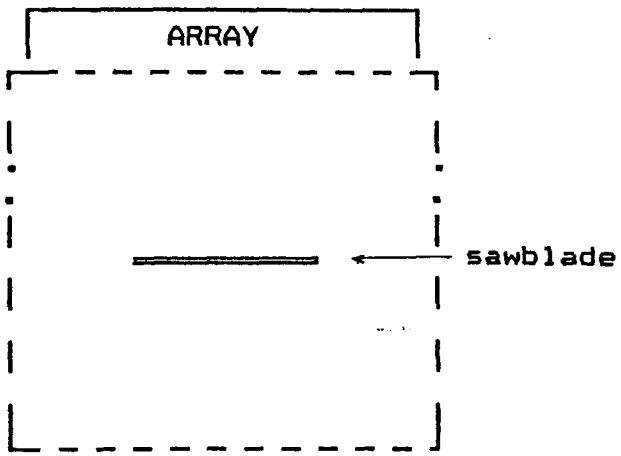

Fig. 6.29a Target #6. Used with array #2.

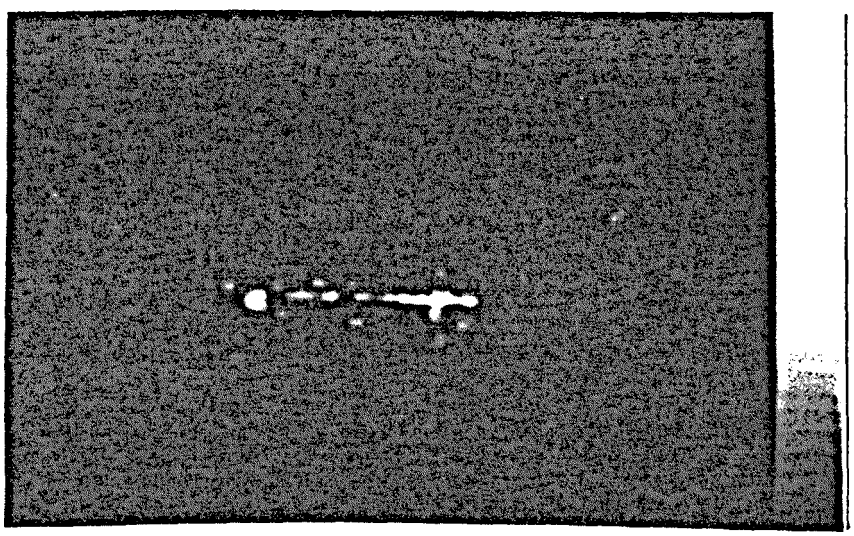

Fig. 6.29b SAFT image of #6.

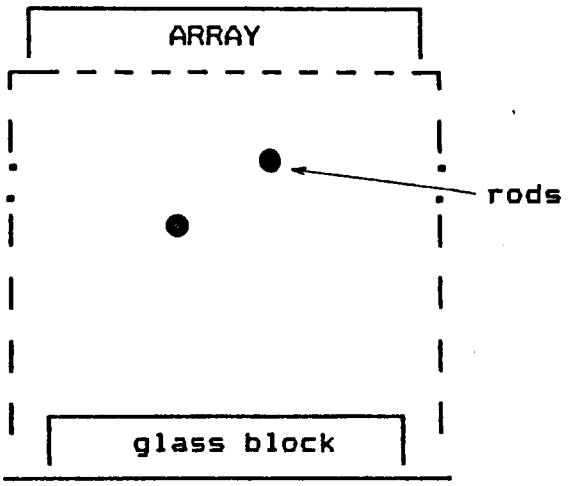

Fig. 6.30a Target #7. Used with array #2.

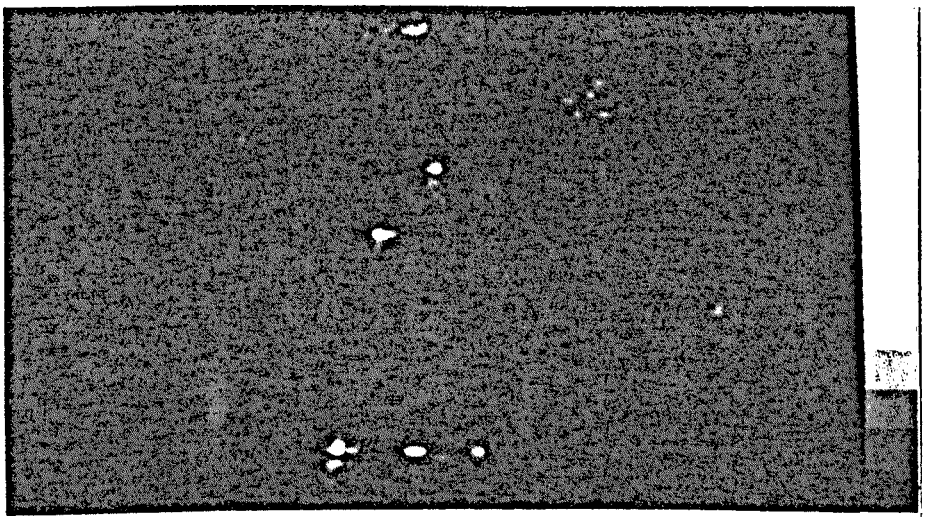

Fig. 6.30b SAFT image of #7.

CHAPTER 7

CHAPTER 7

CONCLUSION

7.1 SUMMARY

This work has presented the design rationale, computer and experimental evaluation of a new digital correlation ultrasonic imaging system which utilises dual Golay codes. The development of a dedicated special purpose system for ultrasonic applications has been traced from elementary theoretical considerations, through hardware development, image scan improvement and finally to good quality images. It has been demonstrated that ultrasonic imaging at less than 5 volt levels is feasible, pointing to a significant expansion of the application areas of ultrasonic NDE.

The system has been developed for ultrasonic imaging where low power but high SNR is required. NDE in power limited, explosive environments as well as medical imaging have been cited as potential application areas.

In the course of the system description, firstly, it was theoretically shown that the SNR of an ultrasonic pulse-echo system may be increased by using long duration pseudo-random binary sequences in transmission, followed by matched filtering to extract the resolution information from the received data.

Methods of implementing this technique were reviewed to justify the choice of a correlation implementation approach based on digital hardware.

A computer aided design study was conducted prior to engaging in hardware manufacture, which investigated quantisation effects, system excitation selection, system speed and SNR in a digital correlation system.

The design parameters derived in the design study were used for the development of dedicated TTL based data acquisition and processing hardware. The development of this dedicated hardware constituted a major part of the work. It was attempted to produce a relatively inexpensive, versatile system. The hardware system was shown to posses a number of original features including;

- o The use of 5 volt levels throughout.
- o The use of TTL devices for probe excitation.
- o The implementation of differential excitation and reception to optimise transmission and reception efficiency and SNR.
- o The use of dedicated digital correlation devices for ultrasonic pulse compression.
- o Incorporation of a direct memory interface for fast data transfer to a host computer.
- o The incorporation of facilities for use with a multi-element array.

Various simulated and experimental results were used to test the hardware performance and validate the theoretical study. Outstanding among the preliminary A-scan results was one demonstrating the SNR superiority of this 5 volt system over a 60 volt conventional

pulse-echo operation. The system's applicability for small array elements was also verified.

An alternative implementation based on a pre-filtering approach was suggested as a method of improving the system resolution while still maintaining the signal to noise ratio enhancement capability of the correlation technique. Accordingly, very good results were obtained in generating 8 bit Golay code sequences from a modelled disc probe. A four fold improvement in temporal resolution was demonstrated indicating the feasibility of the method for practical ultrasonic applications.

Finally, the present software based imaging section of the system was described. An imaging strategy based on the SAFT technique was reviewed and good quality results using the entire imaging unit were demonstrated.

To summarise, this work,

(a) has demonstrated the complete development of a specialised ultrasonic system, starting from computer aided theoretical evaluation, to extensive hardware development and experimental verification.

(b) has demonstrated that ultrasonic imaging at less than 5 volt system excitation is possible, without sacrificing SNR. As such, it is hoped that the findings shown here would widen the application areas of ultrasonic NDE, biomedicine and low power sonar.

(c) has demonstrated the use of direct TTL transmission and differential reception for ultrasonic data

acquisition, resulting in vastly reduced hardware complexity, improved flexibility and reduced cost.

(d) has demonstrated that pseudo-random codes may be generated from conventional probe structures by pre-filtering the excitation, creating the possibility of combining SNRE and resolution enhancement.

(e) has outlined an imaging strategy to be used in conjunction with such a low power data acquisition front end and demonstrated its effectiveness.

The following section proposes possible continuations of the areas investigated.

7.2 SUGGESTIONS FOR FURTHER INVESTIGATION

The following suggestions are given for continuation of the investigations covered in this work. The suggestions generally follow the order with which relevant sections appear in the thesis.

(a) Optimisation of the system excitation

Any investigation in this line should involve a complete survey of pseudo-random codes for direct sequencing applications, with transmission and reception efficiency being a deciding criteria. The codes used in the present work were selected primarily because they do not generate sidelobe artefacts and allow optimisation of speed and SNR. However, the code pair used here are not optimally matched to the transducers. Where one code exhibits high energy the complementary code does not,

resulting in differing transmission efficiencies. Hence, code selection based on efficiency should be investigated.

(b) Moving target detection

The use of a Golay code system for such application has been outlined in Chapter 3. As indicated in that section, the development of a velocity/flow measurement system which utilises Golay code properties may offer superior performance over existing methods. Implementation of such a system should prove to be a worthwhile investigation.

(c) Hardware integration

The correlation based data acquisition and processing hardware system has been sufficiently developed to allow consideration of integrating such a system into a single dedicated processor. At present, due to expense and hardware complexity, the system was multiplexed for use with multi-element arrays, ruling out the possibility of transmission focussing. Integration of the hardware may allow repetition of the system for all elements in an array, allowing transmission focussing if required. Alternatively, for single probe applications, a highly compact, highly sensitive but intrinsically safe test and measurement equipment may be developed as a result of a limited or complete hardware integration.

(d) Extension of system for real time imaging

Although the SAFT approach is used here, the repetition rate is sufficient to allow the expansion of

the back end of the system into a real time image formation/display unit. At present this aspect is performed purely in software, resulting in a generally long period from the data acquisition to the image display. Considering the excellent performance of the front end, limiting its use to simple A-scan enhancement and slow imaging is an under-utilisation. The additional hardware required for real time imaging may involve:

(i) A large signal memory bank to store the scan data from all elements.

(ii) A focus memory unit, where time delay information to each point in the image plane may be stored and used to address the signal memory during the image formation.

(iii) A summer to add the selected signal samples for each image point (capable of adding 32, 16 bit words at a time).

(iv) A digital to analogue converter to convert the summed values into voltages for controlling image intensity.

(v) A raster scan display.

(vi) A controller unit to control and synchronise the X-Y beam deflections of the display unit with the data acquisition and processing section.

Real time imaging using the SAFT approach has been demonstrated before [20]. Hence, the feasibility has been established. The novelty in implementing it with the present system would be, as stated earlier, the

significantly higher SNR and the markedly reduced peak excitation.

Thus, extension of the hardware to this end is a logical continuation of the present work and is therefore strongly recommended.

(f) Development of a repeatable array manufacturing technique

The sensor end of the system still requires to be optimised. As stated in Chapter 6, a uniform sensor is imperative to get good images as software compensation for non-uniformity in element response is not possible for low SNR data acquisition. The manufacturing technique suggested here requires specialised arrays with individual return lines, further complicating the manufacture process especially for high centre frequency transducers. An investigation of optimal array backing material, optimal ways of bonding ceramic with backing and making the appropriate individual connections for this particular application is still required. Utilising monolithic arrays with the present system also needs to be investigated, as such array manufacture is more reliable and repeatable [30].

(g) Quantitative assessment of imaging performance

As a continuation of the present work, a detailed quantitative study of the imaging section would be beneficial to complete the evaluation of such a low power

imaging unit.

(h) System extension for multiple position data acquisition

The design of an interface for a motor drive system to allow the data acquisition hardware to be used for on line data acquisition from automatically adjusted sensor positions is recommended. This would enable an accurate implementation of the spatially compounded image formation suggested in Chapter 6.

(i) Optimisation of pre-filtering techniques

The results achieved in this line, though satisfactory for the short code lengths do not guarantee that the method holds for long duration sequences. As shown earlier, the SNRE offered by the correlation system is proportional to the transmitted sequence duration. Hence, to combine the pre-filtering and correlation approaches, it must be possible to generate long sequences. To this end, it is first necessary to optimise the generation of lower order codes and to devise processing means of correcting for imperfect generation. Two possibilities are envisaged. Firstly, instead of attempting to directly generate the high frequency profiles, it may be more effective to generate a profile better matched to the transducer characteristics. This may involve generation of a modulated profile followed by a demodulation on reception. Alternatively, if direct generation is desired, the addition of extra correction

bits in the generation sequence may allow better recovery of the binary waveform on reception. A study of pre-filter performance vs. transmission power levels would also establish the applicability of the technique for low power data acquisition.

ACKNOWLEDGEMENTS

Firstly, I would like to thank Dr.G.Hayward of the Department of Electronic and Electrical Engineering at the University of Strathclyde for his active and very enthusiastic supervision of this work.

Thanks are due to Professor T.S.Duranni, for providing all the necessary assistance as Chairman of the Department. The advice and assistance provided by past and present members of the Ultrasonics Group at Strathclyde is also appreciated. Particularly, special thanks are due to Mr.W.Galbraith, Dr.J.E.Lewis, Mr.J.Hossack and Mr.D.Riley.

I am very grateful to the Advanced Studies and Scholarship Committee of the University of Strathclyde and to the Faculty of Technology of the Addis Ababa University for providing the necessary financial support. I am also grateful to Professor D.J.Tedford, the Vice Principal of Strathclyde, for helping me get the opportunity to compete for the available scholarships and join the University of Strathclyde.

Finally, I would like to express my gratitude to my parents Mrs. Saba Temtem and Mr. Gorfu G.Medhin for their support and encouragement.

REFERENCES

[1] R.E.Apfel, "Possibility of microcavitation from diagnostic ultrasound", IEEE Trans. on UFFC, vol.UFFC-33(2), pp. 139-143, 1986.

[2] D.R.Gaunt, "Standards and certification in Europe", Control and Instrumentation, pp. 31-33, May 1981.

[3] R.Slater, "Guide to instrumentation in explosive atmospheres", Control and Instrumentation, pp. 64-65, April 1982.

[4] A.Chatterjee, P.K.Das and L.B.Milstein, " The use of SAW convolvers in spread-spectrum and other signal-processing applications", IEEE Trans.Sonics Ultrason., vol.SU-32(5), pp. 745-760, 1985.

[5] J.Dunlop and D.G.Smith, "Telecommunications Engineering", U.K., Van Nostrand Reinhold Co., 1984, Chapter 3.

[6] C.M.Elias, "An ultrasonic pseudorandom signal correlation system", IEEE Trans.Sonics Ultrason., vol.SU-27, pp.1-7, 1980.

[7] E.S.Furgason et al, "Application of random signal correlation techniques to ultrasonic flaw detection", Ultrasonics, pp. 11-17, January 1975.

[8] M.J.Golay, "Complementary series", IRE Trans. Info.Theory, vol. IT-7(4), pp. 82-87,1961.

[9] Y.Gorfu and G.Hayward, "A hardware correlation scheme for ultrasonic non-destructive testing in explosive

environments", Proc. IEEE Ultrasonics Symposium, pp.573-577, 1986.

[10] G.Hayward and Y.Gorfu, "A digital hardware correlation system for fast ultrasonic data acquisition in peak power limited applications", accepted for publication in IEEE Trans. on UFFC, 1987.

[11] G.Hayward and Y.Gorfu, "On line correlation techniques for NDT in attenuating or power limited environments", 4th European NDT Conference, London, September 1985.

[12] F.K.Lam and M.S.Hui, "An ultrasonic pulse compression system using maximal length sequences", Ultrasonics, vol. 20, no. 3, pp. 107-112, 1982.

[13] B.B.Lee and E.S.Furgason, "An evaluation of ultrasound NDE correlation flaw detection systems", IEEE Trans. Sonics and Ultrason., vol. SU-29, pp.359-369, 1982.

[14] B.B.Lee and E.S.Furgason, "High speed digital Golay Code flaw detection system", Ultrasonics, vol. 21, no. 4, pp. 153-161, 1983.

[15] D.Nahmoo and A.C.Kak, "Ultrasonic echo imaging with pseudo-random and pulsed sources", Ultrasonic Imaging, vol. 3, pp. 1-36, 1981.

[16] V.L.Newhouse et al, " Flaw-to-grain echo enhancement by split spectrum processing", Ultrasonics, vol.20(2), pp. 59-68, 1982.

[17] M.I. Skolnik, "Introduction to Radar Systems", Tokyo,

McGraw-Hill Inc., 1981, Chapter 10.

[18] F.G. Stremler, "Introduction to Communication Systems", Phillipines, Addison-Wesley Publishing Co., 1977 , Chapters 7-9.

[19] K.M.Sung, "Piezoelectric multilayer transducers for ultrasonic pulse compression", Ultrasonics, pp. 61-84, March 1984.

[20] P.D. Corl et al, "A digital synthetic focus acoustic imaging system", Acoustical Imaging, vol. 8, pp. 39-53, 1978.

[21] R.O.Duda and P.E.Hart, "Pattern Classification and Scene Analysis", New York, Wiley, 1973.

[22] K.Liang et al, "A 50 MHz synthetic focus system", Acoustical Imaging, vol. 11, pp. 625-645, 1981.

[23] M.Nikoonahad, "Synthetic focussed image reconstruction in the presence of a finite delay noise", Proc.IEEE Ultrasonics Symposium, pp. 819-825, 1986.

[24] G.E.Trahey et al, "Speckle SNR vs lateral resolution in ultrasonic imaging", Proc. IEEE Ultrasonics Symposium, pp. 811-813, 1986.

[25] D.K.Peterson and G.S.Kino, "Real-time digital reconstruction; a description of imaging hardware and an analysis of quantization errors", IEEE Trans. Sonics and Ultrason., vol. SU-31(4), pp. 337-357, 1984.

[26] D.K.Peterson et al, "Quantitative evaluation of real-time synthetic aperture acoustic images", in "A Review of Progress in Quantitative Nondestructive Evaluation", New York, Plenum Press, 1982.

[27] W.K.Pratt, "Digital Image Processing", New York, John Wiley and Sons, 1978.

[28] C.F.Schueler et al, "Fundamentals of digital ultrasonic imaging", vol. SU-31(4), pp. 195-217, 1984.

[29] R.N.Thomson, "Transverse and longitudinal resolution of synthetic aperture focussing technique", Ultrasonics, pp. 9-15, January 1985.

[30] M.A.Campbell, "An Evaluation of Monolithic Arrays for Non-Destructive Testing", Ph.D. Thesis, University of Strathclyde, U.K., 1986.

[31] G.Hayward and M.N.Jackson, "A lattice model of the thickness mode piezoelectric transducer", IEEE Trans. on UFFC, vol. UFFC-33(1), pp. 41-50, 1986.

[32] D.Gillies, "Linear Systems Modelling of Two-Dimensional Piezoelectric Structures", Ph.D. Thesis, University of Strathclyde, U.K., 1986.

[33] G.Hayward, "The influence of pulser parameters on the transmission response of piezoelectric transducers", Ultrasonics, pp.103-112, May 1985.

[34] C.Chassaignon and J.F. de Belleval, "Input signal optimisation of ultrasonic transducers for non-

destructive testing", Proc. Ultrasonics International 85, pp. 557-562, 1985.

[35] G.Hayward and J.E.Lewis, "A theoretical approach for inverse filter design in ultrasonic applications", submitted for publication, IEEE Trans. UFFC, 1988.

[36] J.E.Lewis, "A Study of the One Dimensional Inverse Problem in Ultrasonic Systems", Ph.D Thesis, University of Strathclyde, U.K., 1987.

[37] P.J.t'Hoen, "Design of ultrasonographic linear arrays", Acta Electronica, vol.25(4), pp. 301-310, 1983.

[38] P.Horowitz and W.Hill, "The Art of Electronics", Cambridge, Cambridge Univ. Press, 1980.

[39] P.L.Meyer, "Introduction to Probability and Statistical Applications", Massachusetts, Addison Wesley, 1966.

[40] EG&G Reticon, "Analog Signal Processing Integrated Circuits", 1985.

[41] Fairchild, "Fast Data Book", 1985.

[42] IBM Corp., "Technical Reference", vol. 1 and 3, 1984.

[43] IBM Corp., "Macro Assembler Reference", 1984.

[44] IBM Corp., "Professional Fortran Reference", 1984.

[45] IBM Corp,. "Graphical Kernel System", vol. 1-3, 1984.

[46] Intel, "Microsystems Components Handbook", vol. 2, 1985.

[47] Siliconix Inc., "Integrated Circuits Data Book",1985.

[48] Texas Inst., "The TTL Data Book for Design Engineers", vol. 1 and 2, 1984.

[49] TRW Inc., "TRW LSI Products", 1984.

APPENDICES

APPENDIX A

Major Hardware System Specifications

Some major specifications are given below with an explanation where it was felt appropriate.

1. Number of transducers: maximum - 32

This is only a current limit. As elements are fired sequentially, the number can be extended by modifying the multiplexing and demultiplexing facilities.

2. Samples processed: 1024

This gives scan packets of up to 8 cm. in water (at a sampling rate of 10 MHz). But the scan can be offset to capture data from any cross section. More hardware is required in the timing unit and output memory if it is desired to handle a wider scan.

3. Output size: maximum - 1024 x 16 bits
minimum - 1024 x 12 bits

The output of a single correlation cycle is extended from 7 to 12 bits by the weighting stage. Averaging over 16 cycles extends the width by an additional 4 bits($\log_2 16$).

4. Processing speed:

1 cycle, 1 element:

transmit: 2codes/cycle . 32bits/code . 100ns/bit = 6.4μs

delay(min): 2delays/cycle . 3200ns/delay = 6.4μs

processing: 2codes/cycle . 1024samples/code . 50ns/sample =102.4μs

output : 1024samples . 50ns/sample = 51.2μs

TOTAL =166.4μs

16 cycles, 1 element: ..... TOTAL = 1.894ms

16 cycles, 32 elements:..... TOTAL = 60.6ms

For multiple cycles or elements all but the output rate are proportionally multiplied.

5. Signal to noise ratio enhancement:

For a 20 MHz rate and 32x100ns codes : 8.06dB to 20.10dB

For a 10 MHz rate and 32x200ns codes: 11.07dB to 23.11dB

Values are evaluated using eqn. 2.2 of Chapter 2, with an assumed transducer -3 dB bandwidth of 1 MHz. The minimum values are for one cycle and the maximum for sixteen cycles.

6. Components:

correlators	: TDC 1023 (TRW)
transmitters	: 74F241
receiver	: RS 1612, NE592, LH0004
A/D	: TDC 1014 (TRW)
code memory	: 74S289 & TMS 2532
output memory	: UPD2149, HM6168
summers	: 74F283
counters	: 74ALS193
multiplexer	: DG 526 (Siliconix)
other interfaces	: S,AS & ALS family TTL

APPENDIX B

Functions and Flowchart of Digital Correlation Simulation Package

The inputs, outputs, options and operations of the digital correlation simulation package are outlined below.

1. External Input (to be supplied by user):
   - i. Transducer impulse response data.
   - ii. Data size.
   - iii. Data sampling rate.
2. Selectable Options (for internally generated factors)
   - i. Excitation sequence length and bit width.
   - ii. Additive noise mean and standard deviation.
   - iii. Level of quantisation.
   - iv. Indication of required plots or output data.
3. Processing:
   - i. Convolution of transducer response and excitation codes.
   - ii. Noise addition and signal quantisation.
   - iii. Cross correlation of quantised data and codes.
   - iv. Summation and averaging.
   - v. FFT of signal at selected stages.
4. Outputs (user selectable):

   Time and frequency domain plots or data files of:
   - i. Transducer impulse response.
   - ii. Excitation codes.
   - iii. Additive noise.
   - iv. Receiver signal.
   - v. Digitised signal.

vi. Processed result for one or two codes.

vii. Averaged result.

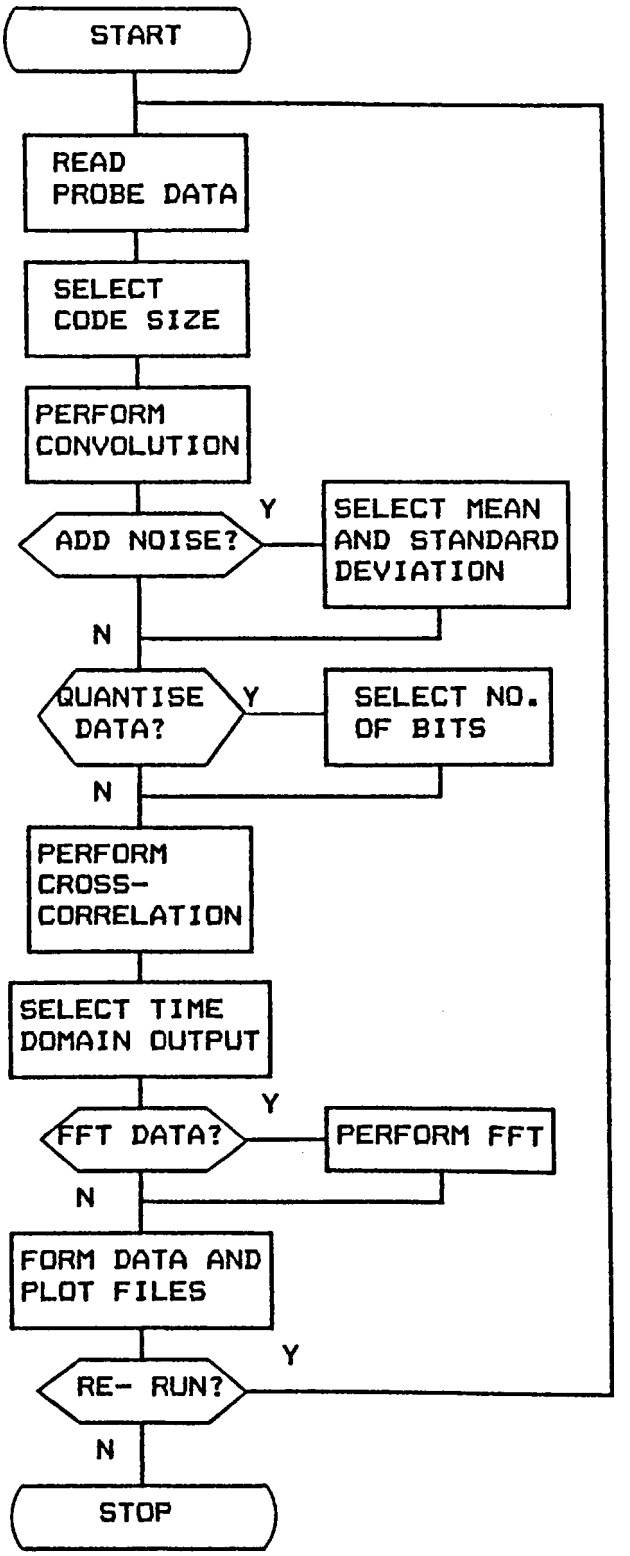

APPENDIX C

Main Electromechanical Parameters of Probes

The probes are those used in Chapters 4 and 5.

C.1 Transducer #1 (disc transducer)

The layout is shown in Fig. C1.

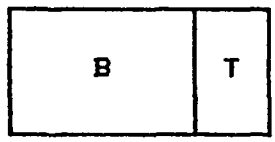

Fig. C1

B	backing layer tungsten+epoxy	acoustic impedance = 10MRayls
T	transducer Lead-metaniobate	mechanical resonance = 1.07MHz static capacitance = 1.24nF piezoelectric constant= 1.56e9 N/C relative permittivity = 325.3 acoustic impedance = 21.7MRayls diameter = 30.06mm thickness = 1.65mm
F	transmission medium(water)	acoustic impedance = 1.48MRayls

Table C1

C.2 Transducers #2 and #3 (small array elements)

		Transducer #2	Transducer #3
Transducer	material thickness width length fo	PZT 5A 1.5mm 0.75mm 48.0 mm 1.0 MHz	PZT 5A 0.99mm 0.48mm 20.0 mm 1.7 MHz
Backing	material impedance	Epoxy 2.2 MRayls	Devcon Aluminium 5 MRayls
Sides	material	Epoxy	Epoxy
Front layer	material thickness	--	Epoxy 150 μm
Propagation medium		Water	Water

Table C2

C.3 Transducer #4 (disc transducer)

The layout is the same as that shown in Fig. C1

B	backing layer Devcon Aluminium	acoustic impedance = 5 MRayls
T	transducer PZT 5A	mechanical resonance = 1.16 MHz static capacitance = 2.9 nF piezoelectric constant= 2.02e9 N/C relative permittivity = 830 acoustic impedance = 36.6MRayls diameter = 30mm thickness = 1.97mm
F	transmission medium(water)	acoustic impedance = 1.48MRayls

Table C3

APPENDIX D

Array Manufacture

This section outlines the manufacturing process of transducer arrays used in the present application and summarises the main parameters of those used in Chapter 6. As indicated in Chapter 7, further investigation is recommended to see if better, more repeatable techniques can be developed.

D.1 Ceramic and Electrodes

A standard PZT-5A ceramic slab with thickness corresponding to the frequency of operation may be used. However, an optional, slight modification in the electroplating process is introduced. The top and bottom edges are slightly rounded off and the front and back electrodes are extended over the two edges as shown in Fig. D1. This 'wrap round' technique is chosen,

(a) to simplify connection to the back electrodes which would be largely covered by a backing material.

(b) to avoid problems in casting a front matching layer which would arise if electrical connections extend over the front surface.

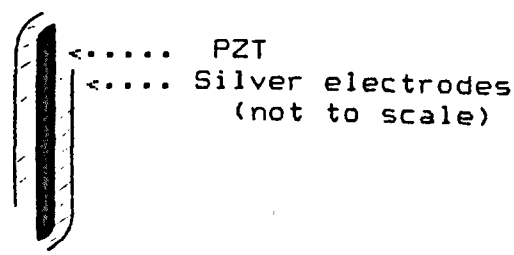

Fig. D1 Side cross sectional view of PZT and electrodes.

D.2 Backing

In order to obtain a wide band response, the PZT should be backed by a lossy material with high acoustic impedance. Additionally, in the present application the total electrical isolation of each array element is required to allow differential excitation and reception. Hence, the backing must not be electrically conducting. A tungsten and araldite mixture with a weight ratio of 6 to 1 has been found to be ideal for this purpose, exhibiting an acoustic impedance of 10 MRayls and practically no electrical conductivity. Although higher acoustic impedances may be obtained by increasing the tungsten portion, the mixture begins to be electrically conducting with increasing parts of tungsten.

The backing may be cast in a specially made mould, polished and bonded under pressure to the PZT with epoxy. Alternatively, it may be cast on the ceramic itself by using the ceramic as one side of the casting mould. The bonded ceramic and backing appear as shown in Fig. D2a and D2b.

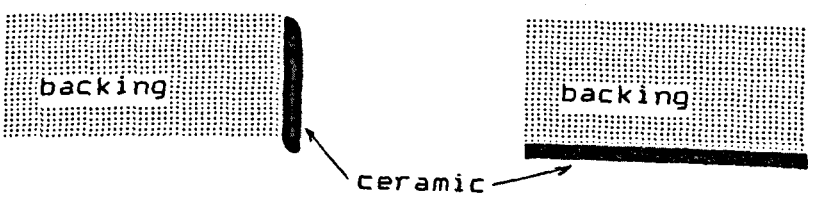

(a) side view (b) top view

Fig. D.2 Cross sectional view of ceramic and backing.

D.3 Electrical Connection and Extension

As it is inconvenient to directly connect electrical extension cables to individual array elements, a specially

designed printed circuit board (PCB) is used to provide the necessary intermediate connection. On one side, the PCB has closely arranged tracks with spacing corresponding to the array element spacing (see next section), while on the other three sides it has widely dispersed cable connection points (see Fig. D3). The PCB is glued to the top and bottom of the backing block with the sides having closely spaced tracks making contact to the front and back electrodes of the ceramic as shown below. The connection between the PCB tracks and ceramic is made either by using low melting point solder or silver loaded epoxy.

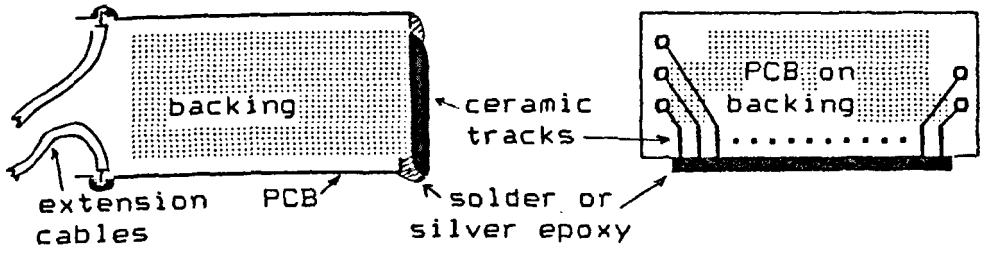

(a) side view **(b) top or bottom view**

Fig. D3 Cross sectional view of electrical connection.

D.4 Cutting Individual Elements

After making the electrical connection between the PCB's and ceramic, the whole ceramic/backing/PCB assembly is mounted on a diamond wire saw unit and the ceramic is cut into individual elements.

Some considerations in the choice of element spacing and width when using this manufacturing technique and the associated problems are summarised below.

To ensure that the element vibrates mainly in the thickness mode, it is necessary for the element width to be equal to less or equal to half the thickness of the

ceramic [32]. For a PZT with a 2 MHz resonance frequency the thickness is normally about 1mm so that an element cut out from such size of ceramic will need to have a width of 0.5mm. As higher frequency ceramics have correspondingly smaller thickness, the width of array elements that may be cut out from them becomes thinner and thinner. The thinner the elements the more fragile they become. They break very easily or are disengaged from their backing during the cutting process. For this reason, it has not been possible to construct arrays with transducers of greater than 2 MHz resonance frequency using this technique.

The choice of spacing is based on the consideration of the required aperture size and the significance or otherwise of grating lobes (see Chapter 6). Grating lobes are artefacts that arise due to inadequate spatial sampling of an array. To totally avoid grating lobes from occurring within an image, it is necessary to choose an array with inter-element spacing equal to or less than half a wavelength in the medium of operation. Thus for a 2 MHz array operating in water, a spacing of 0.375mm would be required. For the present application, the width was set at 0.5mm minimum (for the reasons indicated earlier) and the smallest available cutting wire size was 0.2mm so that the minimum spacing was 0.7mm (nearly equal to one wavelength at 2 MHz). However, when a 2 MHz PZT plate is cut into 0.5mm wide elements, the centre frequency shifts down to about 1.5 MHz so that a spacing of 0.7mm will actually correspond to 0.7 of a wavelength in water.

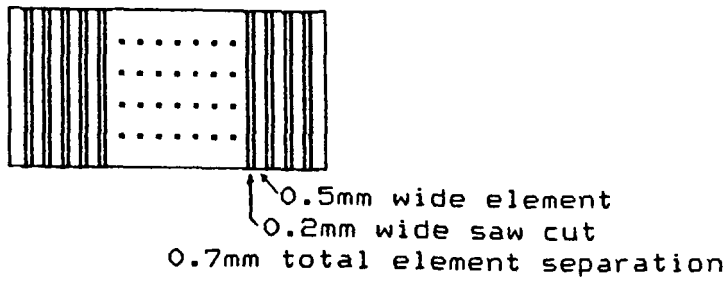

Fig. D4 Front view of ceramic cut into individual elements.

The total number of elements is determined by consideration of other processing hardware complexity as indicated in APPENDIX A.

For the present application, as the maximum number of elements is set at 32, the minimum aperture size (for 0.7mm spacing) is 2.24cm. As such an aperture is too narrow, an array with a wider aperture of 4cm (requiring a spacing of about 1.3mm) was also constructed and used for most of the experiments in Chapter 6. As shown in that Chapter, grating lobes do arise in images formed using an array with such spacing. However, as indicated in the same Chapter, they could be minimised by spatially averaging the images. It is also known that the relative amplitudes of grating lobes are reduced with shorter pulse length. This could be achieved by using heavy backing for the arrays.

D.5 Front Matching Layer and Potting

For better matching to water, low viscosity epoxy resin with an acoustic impedance of 3 MRayls (the optimal for matching is 7 MRayls) is separately cast and bonded to the front face of the array. A thickness equal to a quarter wavelength in epoxy is used.

Finally, to pot the entire assembly, it is placed in a specially made metallic casting mould which is filled with low viscosity epoxy. When the epoxy is set, the casting mould is removed. The cross section of the casting mould and array assembly appears as shown in Fig. D5.

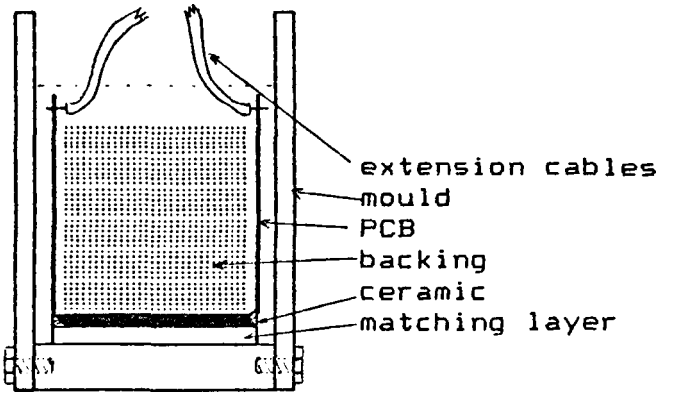

Fig. D5 Cross section of array assembly and mould.

D.6 Parameters of Arrays Used in Chapter 6

Fig. D.6a and D.6b show the directivities of the centre elements of array #1 and #2 used in Chapter 6.

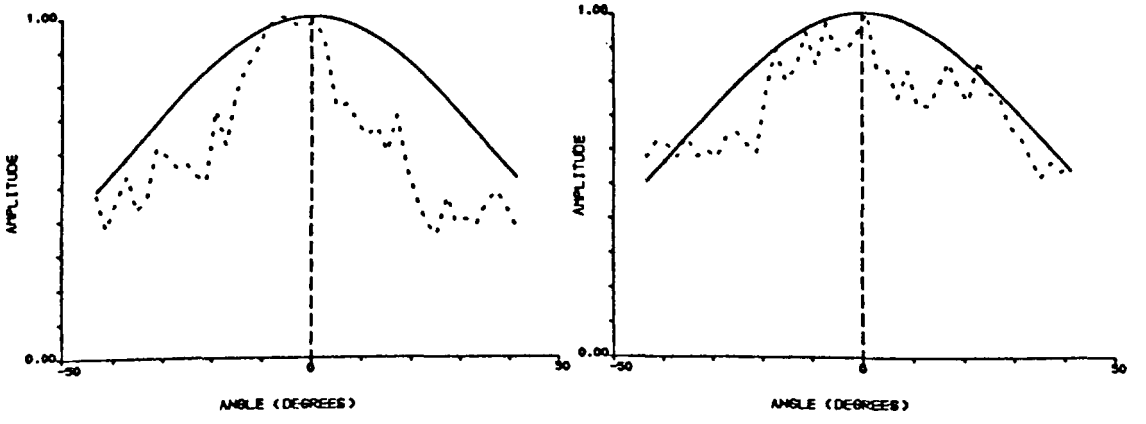

(a) ARRAY #1 (b) ARRAY #2

Fig. D6 Transmission directivities of centre elements.
----- measured, ——— theoretical

Other important parameters are tabulated next.

TABLE D1	ARRAY #1	ARRAY #2
Transducer	PZT-5A	PZT-5A
Backing	tungsten/araldite	tungsten/araldite
Matching layer	λ/4 epoxy	none
No.of elements, spacing and width	30 @1.3mm spacing and 0.5mm width	32 @0.7mm spacing and 0.5mm width

N	fe (MHz)	Z(fe) (Ω)	fm (MHz)	eff%
1	1.40	739	1.84	69
2	1.41	787	1.82	67
3	1.43	829	1.81	65
4	1.50	862	1.81	60
5	1.52	846	1.81	58
6	1.46	844	1.82	64
7	1.49	813	1.83	62
8	1.46	804	1.81	63
9	1.47	797	1.83	63
10	1.51	803	1.85	62
11	1.48	852	1.84	63
12	1.49	820	1.85	63
13	1.51	803	1.86	62
14	1.49	830	1.85	63
15	1.48	832	1.86	64
16	1.52	807	1.89	63
17	1.51	809	1.89	64
18	1.51	804	1.87	63
19	1.50	820	1.87	64
20	1.50	873	1.85	62
21	1.48	841	1.86	64
22	1.48	826	1.85	64
23	1.49	773	1.82	61
24	1.50	793	1.82	61
25	1.50	795	1.85	62
26	1.49	783	1.85	63
27	1.49	764	1.86	64
28	1.50	786	1.86	63
29	1.48	823	1.87	65
30	1.51	685	1.89	64
mean	1.48	808	1.84	63

Table D2 ARRAY #1

N	fe (MHz)	Z(fe) (Ω)	fm (MHz)	eff%
1	1.35	742	1.90	74
2	1.39	743	1.89	71
3	1.40	740	1.94	73
4	1.42	743	1.85	68
5	1.42	820	1.86	68
6	*	*	*	*
7	1.34	741	1.87	73
8	1.40	746	1.88	70
9	1.48	750	1.94	68
10	1.38	747	1.88	72
11	*	*	*	*
12	1.41	713	1.90	71
13	1.41	734	1.91	71
14	1.42	726	1.88	69
15	1.47	700	1.93	69
16	1.41	697	1.86	69
17	1.46	729	1.91	68
18	1.41	657	1.88	70
19	1.46	684	1.89	67
20	1.45	727	1.86	66
21	1.38	730	1.87	71
22	1.38	729	1.89	72
23	1.42	721	1.89	70
24	1.42	748	1.89	70
25	1.42	746	1.92	71
26	1.40	770	1.91	72
27	1.46	802	1.96	70
28	1.36	729	1.84	71
29	1.42	741	1.90	70
30	1.39	801	1.91	72
31	1.40	746	1.91	72
32	1.39	831	1.88	71
mean	1.41	741	1.89	71

Table D3 ARRAY #2

* unused faulty elements

fe, fm: electrical and mechanical resonance frequencies.

Z(fe): impedance at electrical resonance.

eff%: efficiency.

APPENDIX E

Listing of IBM DMA Set-up Program

This program sets up the various registers of the DMA controller of the IBM PC and prepares the system for a 32K data transfer. It is written using the assembly language of the 80286 microprocessor [42].

```
;Program DMA7.ASM
;32k transfer outside dseg. hardware or software
;request-----------------------------------YG JULY 1986
 DM_5    EQU     0C4H     ;CH5 base address
 DM_R    EQU     0D0H     ;DM registers start address
 PG_5    EQU     08BH     ;CH5 page
 PG_R    EQU     08FH     ;Refresh page reg.
;-------------------------------------------------------
 DSEG    SEGMENT PARA PUBLIC 'DATA'
 TRN     DW 1 DUP(?)
 DSEG    ENDS
;--------------------------------------
 CSEG    SEGMENT PARA PUBLIC 'CODE'
         ASSUME CS:CSEG,SS:STASEG
 BEGIN   PROC FAR
         PUSH DS
         XOR AX,AX
         PUSH AX
         MOV AX,DSEG      ;load seg. ID into a general reg.
         MOV DS,AX        ;put seg ID into data seg. reg.
         ASSUME DS:DSEG   ;tell assem. that DS has seg.ID of
                          ;data seg.
;-------------------------------------------------------
         CLI
;REGISTERS INITIALIZATION
         MOV AL,7H        ;clear data
         OUT DM_R+0AH,AL  ;write master clear
;
;1 MODE REGISTERS
         MOV DX,DM_R+6    ;MOD reg, all channels
         MOV AL,10000101B;CH5 mode,write,no
                          ;autoinitialize,block tran.
         OUT DX,AL        ;write mode reg.
;
;2 BASE REGISTERS and PAGE REGISTERS
         XOR AX,AX
         MOV DX,DM_5      ;CH5 base
         OUT DX,AL        ;write base reg.lsb
         JMP $+2
         MOV AL,AH
         OUT DX,AL        ;msb
;
```

```
        MOV BL,4
        MOV DX,PG_5       ;CH5 page
        MOV AL,BL
        OUT DX,AL         ;write page reg.
;
        MOV DX,PG_R       ;refresh page
        OUT DX,AL
        XOR CX,CX         ;start point of record is
                          ;4000:0000
;3. MASK
 rep:   MOV DX,0DEH
        MOV AL,1101B      ;unmask channel 5
        OUT DX,AL
;
;4. WORD COUNT REGISTER
        MOV DX,DM_5+2     ;CH5 word
        MOV AX,1023       ;1024,16 bit words to
                          ;transfer/channel
        OUT DX,AL         ;write word count lsb
        JMP $+2
        MOV AL,AH         ;
        OUT DX,AL         ;msb
;
;
;temporary loop, waiting for hardware request
 chk:   IN AX,DX
        CMP AX,0FFFFh     ;check if count is complete
        JE cont
        JMP chk
;
;-------------------------------------------------
;5 REQUEST REGISTER (only for software request)
;       MOV DX,DM_R+2     ;REQUEST reg, all channels
;       MOV AL,101B       ;CH5 request
;b1:    OUT DX,AL         ;write request reg.
;       MOV DX,DM_5       ;check current address
;       IN AX,DX
;       MOV DX,PG_5       ;check current word count
;       IN AX,DX
;-------------------------------------------------
 cont:  INC CX            ;increment count
        CMP CX,32         ;check if all channels are
                          ;finished
        JNE rep           ;proceed to next channel
 fin:   MOV AL,7H         ;clear data
        OUT DM_R+0AH,AL   ;write master clear
        MOV DX,DM_R       ;disable controller
        MOV AL,100b
        OUT DX,AL
        MOV DX,70h        ;nmi on
        MOV AL,0FFh
        OUT DX,AL
;
        RET               ;return to DOS
;
 BEGIN  ENDP
```

```
CSEG    ENDS
;-------------------------------------------------------
STASEG SEGMENT PARA STACK 'STACK'
        DB  64 DUP("STACK...") ;256 word stack area
STASEG ENDS
;-------------------------------------------------------
        END BEGIN
```

APPENDIX F

Selected Photographs

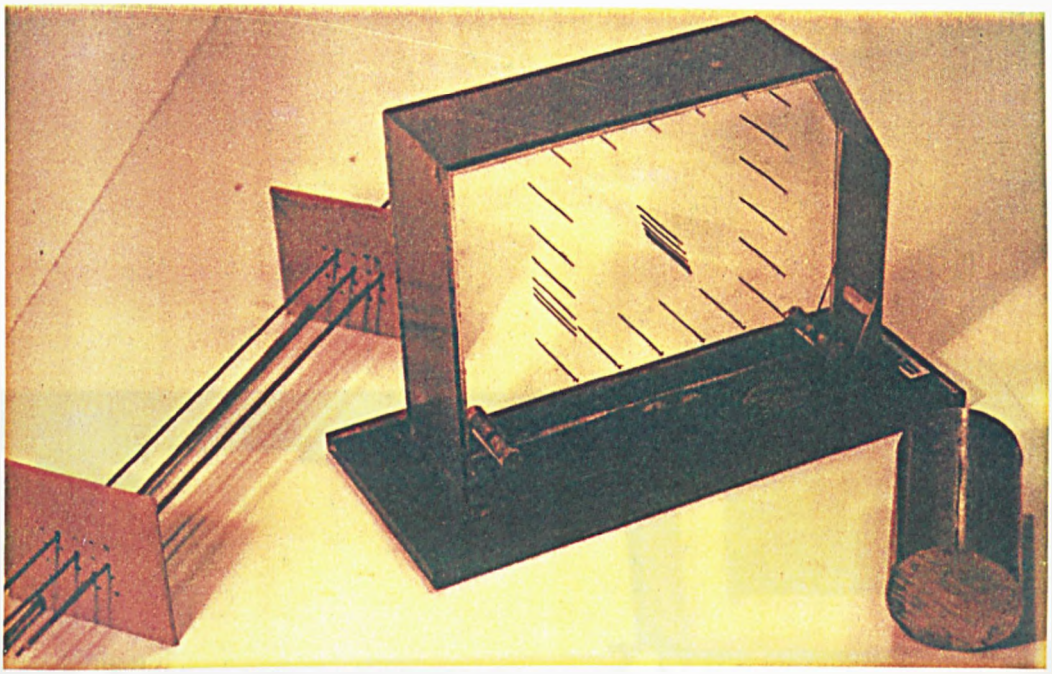

Fig. F1 Targets used in imaging experiments (Chapter 6). Left to right: 2mm steel rods, 1mm steel rods in a perspex container and a 2.5cm radius rod.

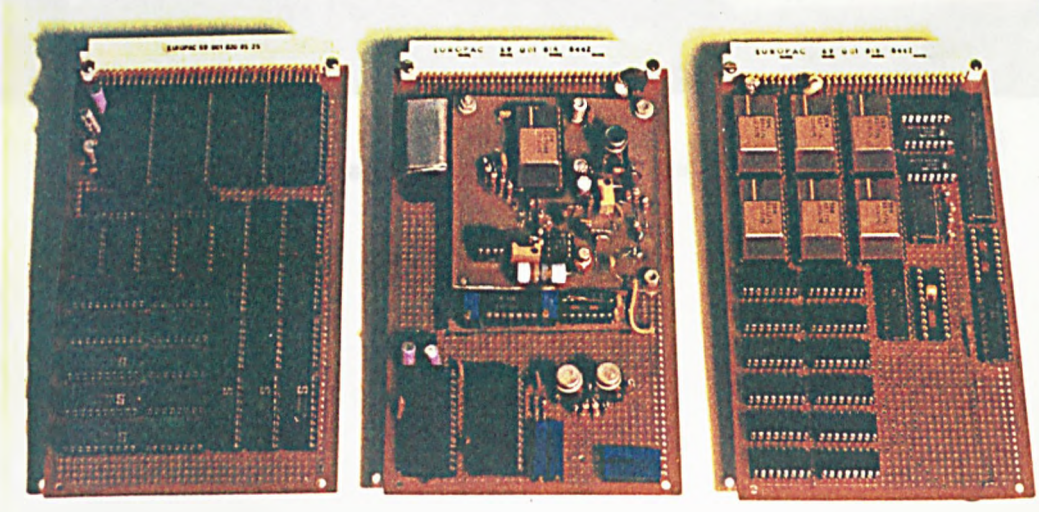

Fig. F2 Boards from the data acquisition hardware. Left to right: Transmission, reception and processing modules.

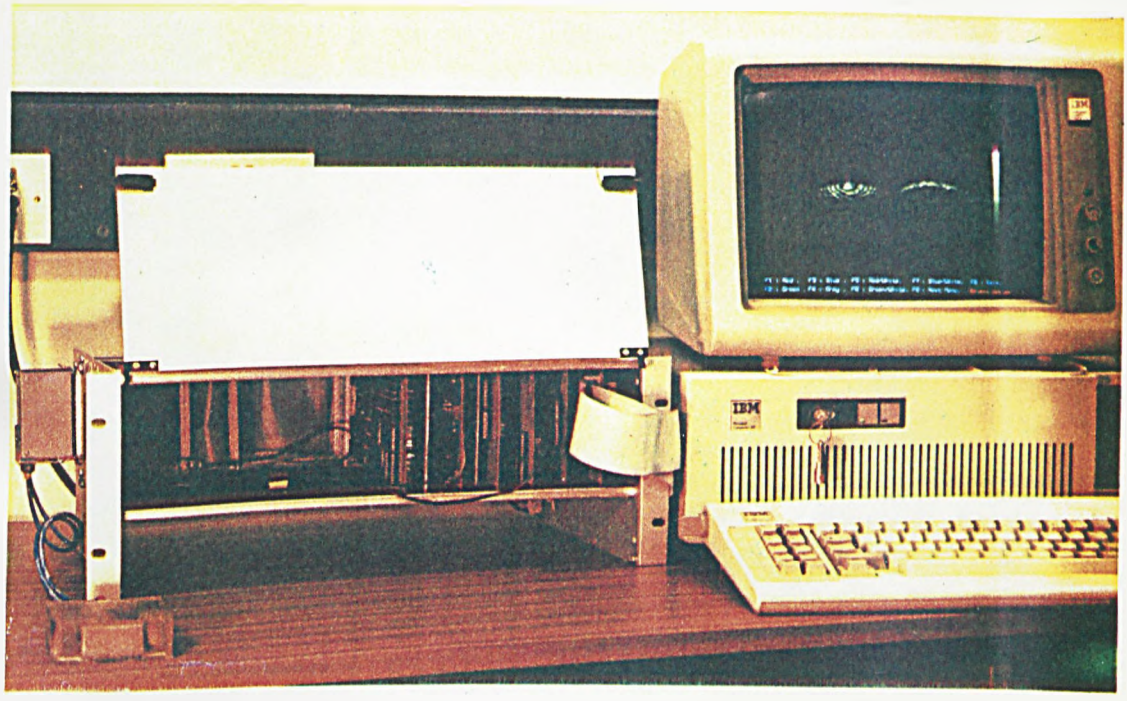

Fig. F3 The data acquisition and imaging system.